UNIVERSITÀ DEGLI STUDI DI MILANO

Scuola di Dottorato in Scienze Biologiche e Molecolari

XXIV Ciclo

STRUCTURAL CHARACTERIZATION OF THE EARLY STAGES OF THE β-2 MICROGLOBULIN AMYLOIDOSIS

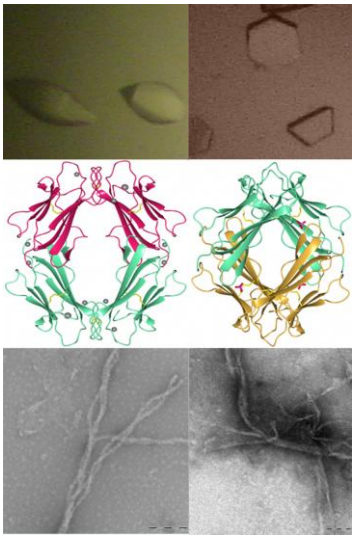

Matteo Colombo (R08209)

Coordinatore: Prof. Martino Bolognesi

Tutor: Dott. Stefano Ricagno

Anno Accademico 2010-2011

ABSTRACT.

Background. β-2 microglobulin (β2m) is an amyloidogenic protein responsible for dialysis related amyloidosis in man, which result in the deposition of β2m amyloid fibrils at a skeletal level. β2m is a 99 residue protein formed by two β-sheets linked by a disulphide bond. In the early stages of fibril formation, β2m associate into dimers and higher order oligomers that are structurally poorly characterized due to their transient nature. Furthermore, the aggregation properties of β2m are affected by its fold-stability. In particular, the DE loop region, which connect the D- and the E- strands, has been reported to be crucial for the β2m fold-stability.

Results. Four monomeric β2m cysteine mutants (S20C, E50C, W60C and S88C) were produced and their correspondent disulphide-linked homodimers were prepared (DIMC20, DIMC50, DIMC60 and DIMC88). The aggregation properties, the crystallogenesis and the oligomerisation state in solution were tested for each β2m homodimer. DIMC20, DIMC50 and DIMC88 form amyloid fibrils, crystals and display a varying mixtures of dimeric and tetrameric species in solution, while DIMC60 is not amyloidogenic and is purely dimeric in solution. DIMC20 and DIMC50 X-ray structures (2.45 Å and 2.7 Å resolution, respectively) shared a non-covalent D-D strand interface that mediate the formation of a tetrameric assembly in both DIMC20 and DIMC50. Moreover, DIMC20 and DIMC50 in solution can catalyse the w.t. β2m fibrils formation in the absence of fibril seeds at pH 7.4, strongly suggesting that the D-D strand interface is involved in the early stages of β2m amyloid aggregation.

In order to further characterize the role of the DE loop in β2m fold-stability, a K58P-W60G β2m mutant was produced and purified. The K58P-W60G β2m mutant showed improved thermal and chemical stability and a faster folding compared to the w.t. β2m. The crystal structure of the K58P-W60G β2m mutant (1.25 Å resolution) showed that the internal disulphide bond was severed as reported by Electrospray ionization-mass spectrometry spectra, which display that a fraction of the K58P-W60G β2m mutant has a reduced disulphide bond. These data suggest a stabilizing role of Pro58 and stress the importance of the DE loop on the biophysical properties of the β2m.

PUBLICATION INCLUDED IN THE THESIS:

1) **Colombo M**, Ricagno S, Barbiroli A, Santambrogio C, Giorgetti S, Raimondi S, Bonomi F, Grandori R, Bellotti V & Bolognesi M (2011) The effects of an ideal beta-turn on beta-2 microglobulin fold stability. *J Biochem* **150**, 39-47.

MANUSCRIPT:

1) **Colombo M.,** De Rosa M., Bellotti V., Ricagno S. and Bolognesi M. (2011). A recurrent D-strand association interface is observed in β2m oligomers. *FEBS J., Under Review*.

PUBLICATIONS NOT INCLUDED IN THE THESIS:

1) S. Ricagno, **M. Colombo**, M. de Rosa, E. Sangiovanni, S. Giorgetti, S. Raimondi, V. Bellotti and M. Bolognesi (2008). "DE loop mutations affect β-2 microglobulin stability and amyloid aggregation." Biochem Biophys Res Commun **377**(1): 146-50.

2) C. Santambrogio, S. Ricagno, **M. Colombo**, A. Barbiroli, F. Bonomi, V.Bellotti, M. Bolognesi and R.Grandori (2010). "DE-loop mutations affect β-2 microglobulin stability, oligomerization, and the low-pH unfolded form." Protein Sci **19**(7): 1386-94.

3) Santambrogio C, Ricagno S, Sobott F, **Colombo M**, Bolognesi M & Grandori R Characterization of beta2-microglobulin conformational intermediates associated to different fibrillation conditions. (2011) *J Mass Spectrom* **46**, 734-741.

4) Azinas S, **Colombo M**, Barbiroli A, Santambrogio C, Giorgetti S, Raimondi S, Bonomi F, Grandori R, Bellotti V, Ricagno S & Bolognesi M (2011) D-strand perturbation and amyloid propensity in beta-2 microglobulin. *FEBS J* **278**, 2349-2358.

INDEX:

ABBREVIATIONS:

NMR	Nuclear Magnetic Resonance
ANS	1-Anilino-8- Naphtalene Sulphonate
β2m	Beta-2 microglobulin
BD	2,3 Butandeione
BSH	Beta-mercaptoethanol
CD	Circular dichroism
CR	Congo Red
D59P	Asp59→ Pro59 β2m mutant
DEPC	Diethylpyrocarbonate
DRA	Dialysis Related Amyloidosis
DTNB	5,5'-dithiobis-(2-nitrobenzoic acid)
E50C	Glu50→ Cys50 β2m mutant
ESI-MS	Electrospray Ionisation Mass Spectrometry
H13F	His13→ Phe13 β2m mutant
IMS-MS	Ion mobility mass spectrometry-mass spectrometry
K58P-W60G	Asp58→Pro58 and Trp60→Gly60 β2m mutant
MHC-I	Major hystocompatibility complex class I
NHSA	Sulfo-N-hydroxysuccinimide acetate
P32A	Pro32→ Ala32 β2m mutant
P32G	Pro32→ Gly32 β2m mutant
P32V	Pro32→ Val32 β2m mutant
S20C	Ser20→ Cys20 β2m mutant
S88C	Ser88→ Cys88 β2m mutant
SEC	Size Exclusion chromatography
SSNMR	Solid State NMR
TEM	Transmission Electron Microscopy
TFE	2,2,2 Trifluoroethanol
ThT	Thioflavine T
W60C	Trp60→ Cys60 β2m mutant

W60G Trp60→ Gly60 β2m mutant

1. STATE OF THE ART

1.1 *A protein misfolding disease: β-2 microglobulin causes Dialysis Related Amyloidosis.*

Protein misfolding arises from the failure of proteins to fold correctly or to keep their native state. Protein misfolding can result in the extracellular or intracellular deposition of aggregates such as amyloid fibrils. The causes of protein misfolding can be genetic (*e.g*. Huntington's disease), environmental (*e.g*. Alzheimer's disease) or transmitted by infection (prion's disease) [1]. Although the pathogenesis of each protein misfolding disease is different, the formation of fibrillar aggregates is a hallmark of the amyloid related diseases. Amyloidosis can result from the conversion of a soluble folded protein into amyloid aggregates that in turn deposit extracellularly in a variety of organs such as heart, brain, kidneys and skeletal system. Amyloidosis can be divided in three major groups: neurodegenerative associated, localized non-neuropathic and systemic non-neuropathic. Alzheimer's and Parkinson's diseases belong to the first group involving the extracellular accumulation of amyloid fibrils formed by $A\beta_{1-40}$/ $A\beta_{1-42}$ peptides and α-synuclein respectively, which trigger the neuronal degeneration. Cataract is a localized non-neuropathic amyloidosis and it is caused by the aggregation of γ-crystalline in the retina. Dialysis related amyloidosis (DRA) pertains the third group and affects joints and tendons due to the accumulation of β-2 microglobulin (β2m) converted into amyloid fibrils (Fig. 1). β2m is a 99 residue protein and it is recognized as a molecular archetype for the study of folding and amyloid transition processes. β2m tendency to aggregate is the focus of this thesis.

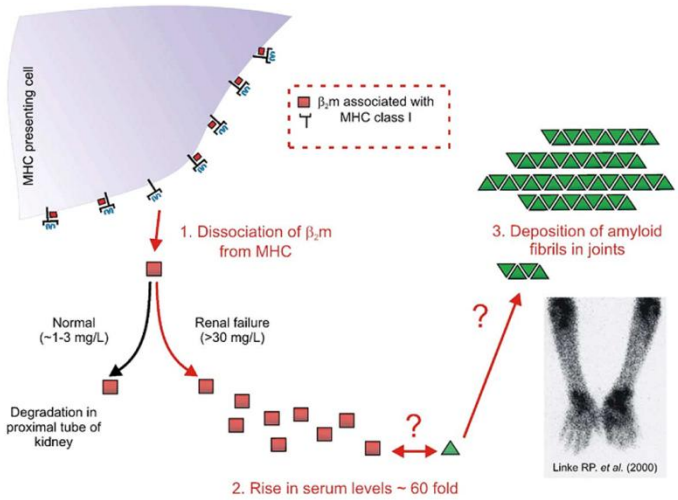

Figure 1. Schematic view of the Dialysis Related Amyloidosis etiology (see text) [2].

β2m is the light chain of the class-I major histocompatibility complex (MHC-I) [3] and stabilize MHC-I allowing its expression on the cell surface. β2m was first isolated by Berggard and Bearn from the urine of patients suffering tubular proteinuria [4]. During the catabolic cycle of MHC-I, β2m dissociates and enters blood circulation as a monomer [5]. Then, β2m is filtered by the glomerules in the kidneys and it is reabsorbed and destroyed by proximal tubular cells [6]. In patients with renal disorders and undergoing dialysis, β2m is not cleared and it starts to accumulate in the serum where its concentration increased up to 60-fold [7,8]. Long-term hemodialysed patients keeping the high concentration of β2m for 3-5 years start to accumulate amyloid fibrils in the synovium, cartilage and bones developing DRA. This pathology is characterized by carpal tunnel syndrome, bone cysts and chronic invalidating arthralgias resulting in bone fractures [5]. Although many efforts, there are several features of the mechanism of the β2m amyloid fibrils formation that need to be depicted. Indeed, β2m maintains a monomeric state in solution up to milliMolar concentration and many factors such as metal ions, glycosaminoglycanes and proteases were suggested as β2m folding destabilization

promotors [9,10]. Furthermore, very little is known about the early stages of the β2m aggregation and in particular the interactions that mediate the formation of the β2m oligomeric interfaces. In the next paragraphs I am going to summarize the main steps that lead to the formation of β2m amyloid fibrils: the amyloidogenic intermediate formation, the amyloidogenic regions of the β2m molecule and the data available on the structure of β2m amyloid fibrils.

1.2 *The relation between the β-2 microglobulin folding and an amyloidogenic intermediate.*

Protein folding is a spontaneous process and the funnel folding theory describes it as a progressive reduction of the free energy of the polypeptide chain from the unfolded state till the native state [11,12] (Fig. 2).

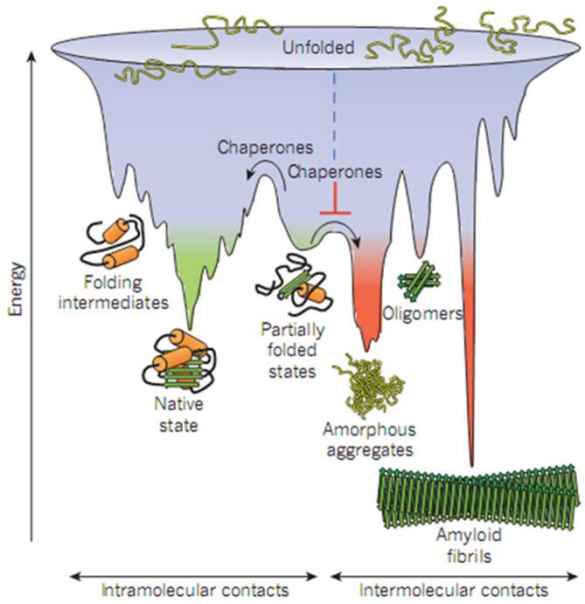

Figure 2. A graphical representation of the funnel folding theory. A competition between intramolecular and intermolecular interactions during the protein folding [13].

To reach the native state, unfolded β2m molecules have to cross a series of free-energy barriers that correspond to partially folded species with a different degree of stability.

In order to identify the β2m species that are on the folding pathway, kinetics studies were performed [14-16]. In particular, the β2m folding process was studied by circular dichroism, double-jump experiments, intrinsic fluorescence and NMR [14,16,17]. β2m folding revealed three different phases: a burst-phase, a fast phase and a slow phase [15]. During the burst phase (sub-milliseconds time-scale) unfolded β2m molecules are converted into partially folded conformers (I_1) with a significant level of secondary structure and a disordered hydrophobic core as revealed by far-UV circular dichroism and ANS binding. The fast phase (millisecond time-scale) converts I_1 into I_2. This latter represents a population of partially folded conformers with a more compact hydrophobic core than I_1 and a level of secondary structure similar to I_1. I_2 is then converted into the β2m native state through a slow-phase [16] (Fig. 3).

Figure 3. Schematic representation of the proposed β2m folding reactions. U, unfolded; I_1, first intermediate; I_2, second intermediate; N, native state [15].

The slow phase of folding has been observed *in vitro* in many proteins such as Rnase A, Ribonuclease T1 and thioredoxin [18-20] and it has been related to the *trans-cis* prolyl isomerization, which is an obligate step to achieve the final conformational state for many proteins [21]. In the non-prolyl peptide bond the *trans* isomer is favored over the *cis* isomer by a factor of 100-1000 [22]. The case of proline is different because the nitrogen of the amide is bound to the δ-carbon of the prolyl side chain, forming an iminoacid. In the imine the *trans* and *cis* isomers

are more equally distributed with a 30% of the *cis* isomers and a 70% of the *trans* isomers [18]. This could be due to the comparable steric hindrance of the two proline isomers. β2m has five proline residues (Pro5, Pro14, Pro32, Pro72, Pro90), but Pro32 is unique in adopting a *cis* conformation in the native folded state. Kameda *et al.* [16] demonstrate that Pro32 *trans*→*cis* isomerization is responsible for the β2m slow-phase of folding by site-directed mutagenesis. In the P32V β2m mutant, the valine adopts a *trans* orientation, and its kinetic refolding monitored by both circular dichroism and 1D ^{1}H NMR, showed the absence of the slow-phase due to the removal of the *trans*→*cis* isomerization. The prolyl-isomerization is also affected by the proline preceding residue. Indeed, NMR measurements of different peptides containing a histidine residue before a proline show a rate-isomerization dependence [23,24]. In particular, the rate of prolyl-isomerization increased up to 10 fold by changing the pH from basic to acid, when the proline preceding residue is a histidine [23]. Moreover, at pH>7, histidine favors the increment of the *cis* proline isomer content suggesting an intramolecular mechanism that induce prolyl-isomerization [23]. The slow-phase of folding implies the presence of a β2m intermediate in which Pro32 displays a *trans* conformation, but the secondary structures and the hydrophobic core are well defined. It has been suggested that the *trans* orientation of Pro32 is a hallmark of the β2m aggregation prone species [16,25]. Moreover, NMR experiments suggested that the *trans* orientation of Pro32 is accompanied by a general perturbation of the flanking residues and in particular of the FG loop and N-*terminus* [16]. In addition, P32G β2m mutant, in which the glycine adopted a *trans* conformation, displays enhanced aggregation propensity compared to the w.t. β2m [26] and an increased amount of the amyloidogenic intermediate I_2. Moreover, the level of I_2 is correlated with the rate of the β2m fibril formation suggesting that the *cis* Pro32 isomer in the native state can be the limiting step of the β2m amyloid aggregation.

1.3 *β-2 microglobulin amyloid fibril formation.*

A full understanding of the mechanism of the amyloid fibril formation requires the elucidation of every species that are on pathway. Interestingly, dependent from the ionic strength of the buffer, different amyloid fibrils can be obtained. Indeed, it has been shown that at pH 3.6 and at a concentration >100 mM NaCl, worm-like (WL) amyloid fibrils were obtained [27,28]. Conversely, at pH 2.5 and at a concentration <100 mM NaCl, long-straight (LS) amyloid fibrils grew [28]. Interestingly, LS amyloid fibrils grown at pH 2.5 and at pH 7.4 display a similar β-sheet architecture compared to the *ex-vivo* β2m amyloid fibrils [27]. Recently, it has been shown that WL fibrils follow a non-nucleated mechanism for the fibrils formation, while LS amyloid fibrils are formed by a nucleation dependent mechanism [29]; because LS fibrils were shown to be similar to the *ex-vivo* β2m amyloid fibrils, this thesis will be focused on the nucleation mechanism of the β2m amyloid fibril formation. β2m amyloid fibrils formed by a nucleation-dependent mechanism revealed a first-order kinetic reaction that is characterized by two main phases called lag phase and log phase. During the lag phase β2m molecules associate to form *nuclei* which in turn act as a scaffold for the elongation of the β2m amyloid fibrils by subsequently monomers or oligomers addition that lead to the formation of amyloid fibrils (log phase) (Fig. 4) [1]. The lag phase can be overcome by adding seeds, which are fragments of sonicated mature amyloid fibrils. The lag phase is currently extensively studied, due to recent evidences that suggest that oligomeric species are the most toxic species in protein misfolding diseases such as Alzheimer and Parkinson [1,30]. β2m oligomers are very difficult to isolate due to their rapid exchanging equilibrium. Recent data indicate that the first β2m oligomer formed is the dimer that in turn associate to form tetramers and higher order oligomers [31]. Finally, cryo-electron microscopy on β2m amyloid fibrils grown at pH 2.5 revealed that a dimeric species of β2m can be the building block of the amyloid fibrils [32].

The final product of the β2m aggregation process are the amyloid fibrils. β2m *ex-vivo* amyloid fibrils have been found associated with heparin and type I collagen [33,34]. Indeed, β2m amyloid fibrils are stabilized by glycosaminoglycanes such as heparin that has been shown to inhibit depolymerization of β2m fibrils *in vitro* [35]. In order to mimic the environmental conditions that occur *in vivo* and that leads to the β2m amyloid fibrils, different approaches were used *in vitro*. Among different conditions the most used are the acidic pH (from pH 2.5 to pH 4.0) and the neutral pH with the addition of 20% TFE or stoichiometric amounts of Cu^{2+} [9,36,37]; the other *in vitro* conditions are listed in Table I. In general, the amyloid fibrils derived by different polypeptides display proteinase-resistance and measures ~10 nm diameter. Furthermore, amyloid fibrils bind Thioflavine T and they display a green birefringence, at the cross-polarized light microscopy, when they are bound to the Congo Red fluorescent dye [38,39].

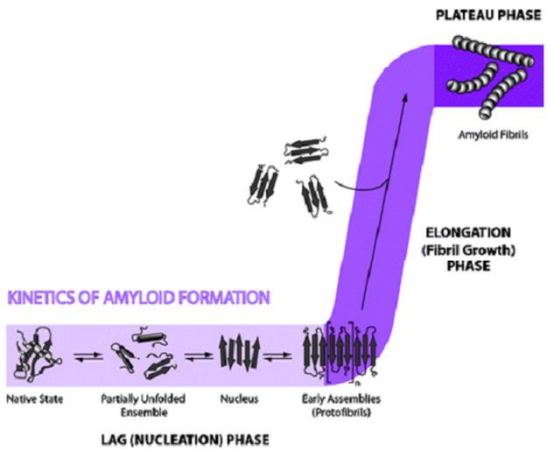

Figure 4. Phases of amyloidosis: lag phase, log phase and plateau phase.

In the next paragraph will be summarized the unveiled structural features of the β2m amyloid fibrils.

Table I. β2m amyloid fibril formation *in vitro*.

Conditions for extension	Seeds
Acidic pH with varying ionic strength[28,40]	/
Dialysis with pH 7.4 buffer containing 200 µg mL^{-1} [41]	/
Dialysis against deionised water and subsequent evaporation of solvent[42]	/
pH 7.4, 150mM KCl, 1M urea with 200 µM Cu^{2+}[9]	/
Extension of seeds during refolding experiments[14]	Ex-vivo β2m amyloid fibrils
Extension of seeds in the presence of SDS 0.5 mM, pH 7.5[43]	Ex-vivo β2m amyloid fibrils
Extension of seeds in the presence of TFE 20%, pH 7.4[35]	Ex-vivo β2m amyloid fibrils

1.4 *β2m amyloid fibril structure.*

The amyloid fibril structure derived by different polypeptides has been studied by X-ray diffraction revealing a common core structure with a cross-β architecture, where the β-sheets are oriented parallel to the long axis of the fibril and the β-strand are perpendicular to the fibril long axis [44].

To date, the high resolution structure of the β2m amyloid fibrils is not available. However, Hydrogen/deuterium exchange (H/D exchange) experiments performed on β2m fibrils grown at pH 2.5 revealed that the main regions protected in the β2m amyloid fibrils were the D-strand, the DE loop, the E-strand, the BC loop, the C-strand and partially the B-strand [45]. In agreement with Hoshino *et al.* [45], a recent SSNMR work reported that the structure of the β2m amyloid fibrils is built by native-like β2m monomers in which the major rearrangements occur in the loop regions such as AB loop (Ala15) and EF loop (Thr71 and Thr73) [46].

Conversely, a parallel SSNMR study proposed that the structure of the β2m monomers that form the amyloid fibril are not native-like showing an increase in the β-structure content (a longer D-strand, a β-character for the native DE loop)

[47,48]. Although the high resolution structure of the β2m amyloid fibrils represents the major challenge, there are evidences that the toxicity in amyloid diseases such as Alzheimer and Parkinson is mediated by oligomeric species more than amyloid filaments [1] underlying the importance of the structural characterization of the β2m oligomers.

1.5 *β-2 microglobulin native structure.*

β2m is the light chain of MHC-I and its physiological role is to drive the correct folding of the MHC-I for antigen presentation [49]. β2m adopts an immunoglobulin-like fold and is formed by two β-sheets linked by a disulphide bond. One β-sheet is formed by four β-strands (A, B, D, E) while the facing β-sheet has three β-strands (F, G, C). The disulphide bond link the two β-sheets by Cys25 (strand B) and Cys80 (strand F) (PDB 1LDS) (Fig. 5) [50]. The disulphide bond is fundamental for the formation of amyloid fibrils; indeed, its reduction resulted in the abrogation of β2m amyloid fibrils formation [51]. In the last decade, four main regions of β2m were indicated to affect the overall protein stability: the N-*terminus*, the D-strand, the DE loop and the BC loop (Fig. 5).

1.5.1 *The role of β2m N-terminus.*

The *ex-vivo* β2m amyloid fibrils are formed by 30% of ΔN6-β2m variant, which lack the first six residues [52,53]. ΔN6-β2m variant displayed a less compact fold with respect to the w.t. β2m [53]. Moreover, circular dichroism experiments showed a decreased content of secondary structure and an altered tertiary structure of the ΔN6-β2m variant compared to the w.t. β2m [53]. ΔN6-β2m variant resulted less stable compared to the w.t. in terms of chemical stability ($C_{m\ \Delta N6}$= 1.65 M *vs* $C_{m\ w.t.}$= 2.23 M) [53]. Importantly, ΔN6-β2m aggregates into amyloid fibrils at pH 7.0 without the addition of seeds, which are commonly used to bypass the lag phase [53,54]. Furthermore, a recently NMR structure of the ΔN6-β2m variant displays a

trans conformation of the Pro32 and it shows the property to convert the w.t. β2m into an amyloidogenic intermediate forming amyloid fibrils [55].

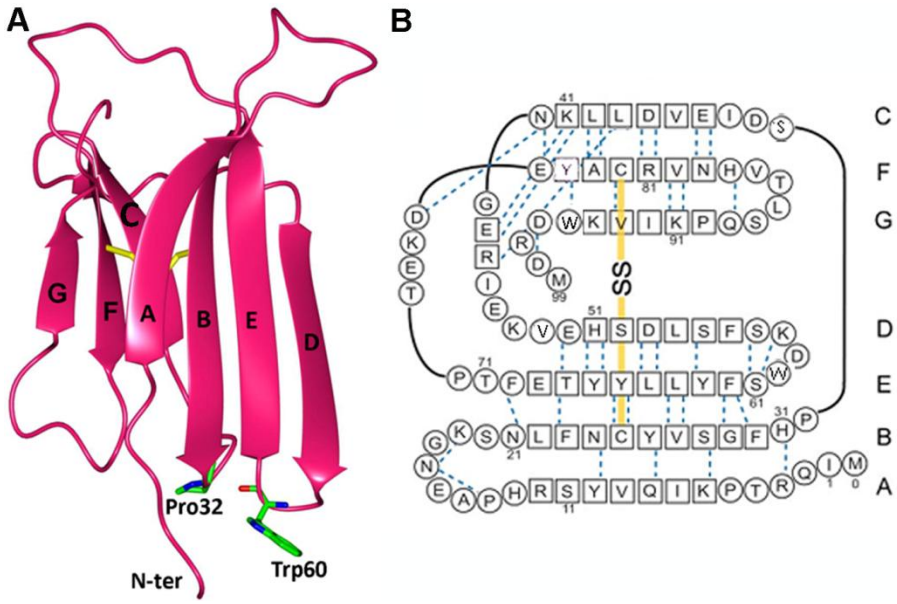

Figure 5. A) Ribbon representation of the β2m fold. Residues Pro32, Trp60 highlight BC loop and DE loop, respectively. **B)** Primary sequence of β2m combined with its secondary structure. Circle represent residues that are located on loops, square represent residues forming β-structure (the scheme is taken from [56]).

ΔN6-β2m showed an increased propensity to oligomerize and in particular it has been suggested a ΔN6-β2m dimerization interface through the BC and DE loops based on the chemical shifts of residues 25-34 and 51-66 [55].

1.5.2 *The role of the β2m DE loop and of the D-strand.*

The DE loop is formed by Ser57-Lys58-Asp59-Trp60 residues and it deeply affects the β2m folding stability and aggregation properties. The substitution of Trp60 with a glycine resulted in an increased thermal and chemical stability of the β2m [57]. Indeed, Trp60 is conserved among the vertebrates due to its interchain hydrogen-

bonding with the Asp122 of the MHC-I [58]. The increased stability of W60G β2m mutant was translated in the total abrogation of amyloid fibrils propensity at neutral pH in the presence of seeds [57]. Conversely, the substitution of Asp59 with a proline decreases the thermal and chemical stability of the β2m which result in an enhanced tendency to aggregate [59]. Moreover, ESI-MS experiments showed a lower propensity to establish protein-protein interactions of the W60G β2m compared to the w.t. β2m at neutral pH, under native conditions [60]. All these data suggest that the DE loop geometry affects the folding stability of β2m and consequently its aggregation propensity [59].

The DE loop is preceded by the D-strand, which has been repeatedly reported to be involved in the β2m fibrillogenesis [50,61,62]. In this regard, NMR studies suggest that the D-strand adopts a number of conformations in solution and its flexibility could result as a favoring feature for the β2m aggregation.

1.5.3 *The role of the β2m BC loop and the copper binding.*

The BC loop contains the Pro32 residue, which is responsible for the slow-phase of β2m folding and that adopts a *trans* orientation in the β2m amyloidogenic intermediate. To date, the mechanism of the Pro32 *cis-trans* conversion is still unclear. However, His31 is a key residue in the Pro32 isomerization. Indeed, His31 is the favorite copper binding site to β2m [16,36]. A role of metal ions has been proposed for several amyloid diseases such as Parkinson, Alzheimer and prions [63-65]. In particular, Cu^{2+} often resulted the most effective metal ion in promoting amyloid fibrils formation; This feature may be due to the open shell system electron configuration of Cu^{2+} [66]. Regarding β2m, a mechanism for Pro32 isomerization mediated by copper has been proposed [62]. The copper binding can induce a protonation of the His31 imidazole nitrogen. The charged histidine determines a repulsion of the adjacent N-*terminus*, due to the positive charge on the

Arg3 side chain. The N-*terminus* is displaced and the Pro32 isomerization can occur. Interestingly, the same effect on the protonation of the His31 could be mediated by the acidic pH (pKa His31 = 5.4 [62]); indeed β2m forms fibrils at acidic pH faster compared to the neutral pH.

1.6 *β2m oligomers.*

Oligomeric β2m species are formed during the early steps of fibrillogenesis in the so-called lag phase. Due to their transient nature, their structural characterization is difficult. To date, β2m oligomers have been structurally characterized by ESI-MS and X-ray crystallography. The ESI-MS used a covalent labeling technique which allow to follow protein-protein interactions by measuring the differential reactivity of the amino acid side chains with specific compounds [67]. This method was applied *in vitro* to β2m that was mixed with a fibrillogenesis buffer containing copper to study the dimeric and tetrameric species of the β2m [68,69]. The side chains of the amino acids were covalently modified at different time points in order to identify the amino acids involved in intermolecular β2m interactions (dimer and tetramer formation). The degree of covalent labeling would be as low as the amino acids sensible to modification are involved in the dimer ad tetramer surfaces of interaction. The side chains sensible to covalent labeling are lysine and asparagine by acetylation (with NHSA), the side chains of histidine, serine and threonine that are carboethoxylated (by DEPC) and the side chains of arginine which are modified with butanedione (by BD) [68]. Mendoza *et al.* [68] showed that the residues involved in the β2m dimer formation are located on the N-*terminus*, A-strand, AB loop and E strand, while D-strand, DE loop and G-strand mediate the tetrameric interface of the β2m (Fig.5A) [69]. Recently, a new mass-spectrometry device was coupled to the ESI-MS, the ion mobility spectrometry (IMS), to study β2m oligomeric assemblies. IMS-MS has the capability of separating ions of the same *m/z* ratio but with

different collision cross-sections (Ω) and/or charge states by monitoring the mobility of an ion in a gaseous atmosphere under the influence of an electric field [70]. Interestingly, ESI-IMS-MS on β2m oligomers produced under both low (on pathway for the worm-like fibrils) and high ionic strength (on pathway for the long-straight fibrils) at acidic pH, revealed β2m oligomers with different Ω which reflected a globular organization for the WL oligomers and an elongated conformation for the LS oligomers [71].

Higher resolution data were obtained using X-ray crystallography. This technique needs high monodispersed samples in order to obtain protein crystals of good diffracting quality, and the nature of the oligomers seems to be in contrast. However, mutant design and protein engineering together with the use of antibodies or ligands (such as metal ions) can increase the stability of the oligomeric species allowing us to get insights in the early β2m protein-protein interactions.

Indeed, the engineered P32A β2m mutant crystallized as a dimer and its X-ray structure revealed a surface of interaction mediated by two straight antiparallel D-strand (PDB 2F8O) [25] (Fig. 6A). However, P32A β2m mutant does not form dimeric species in solution and it is not amyloidogenic.

Recently, the X-ray structure of the ΔN6-β2m variant was determined in complex with a specific camelide monoclonal antibody (PDB 2X89). Interestingly, the X-ray structure displays a swapped dimer of the ΔN6-β2m variant, which is formed by two ΔN6-β2m monomers formed by six β-strands each (A, B, E, C, D, F) and with the G strand that is exchanged one to the other [72].

The interactions between the monomers are mediated by residues 83-89 (F-strand) which formed a new β-sheet (Fig.6B). Interestingly, an isolated β2m peptide formed by residues 83-89 is amyloidogenic, suggesting that this region has an intrinsic propensity to aggregate [74].

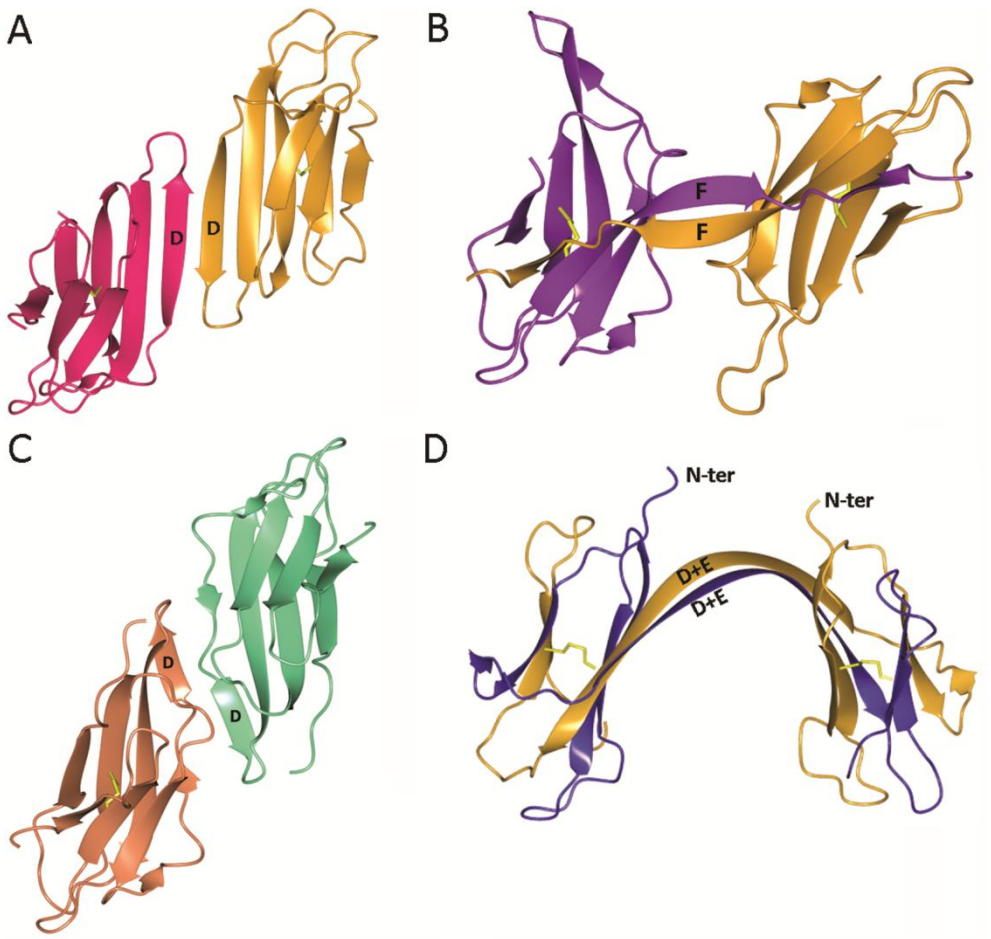

Figure 6. Four β2m interfaces. **A)** Crystallographic dimer of the P32A β2m mutant. **B)** Swapped dimer of the ΔN6-β2m variant. **C)** D-D strand interface of the hexameric β2m of the H13F β2m mutant. **D)** Swapped dimer of the full-length β2m [25,61,72,73].

Another recent X-ray structure of dimeric β2m based on domain-swapping was reported by Eisenberg and co-workers (PDB 3LOW) [73]. In this case, the β2m swapped-dimer was isolated during the refolding step of β2m purification in the presence of BSH. The X-ray structure of the β2m domain-swapped dimer showed an open interface and a closed interface.

The former is mediated by an antiparallel β-sheet between the D strand and the E strand of the two β2m subunits. The latter is based on the rearrangement of the internal β2m disulfide that is mediated by Cys25 of one subunit and Cys80 of the facing subunit resulting in the formation of an intermolecular disulphide bond that in turn determined the exchange of the β-strand E, F and G between the two subunits.

The H13F β2m mutant form a hexamer in solution in the presence of stoichiometric amounts of Cu^{2+} [61]. Moreover, the X-ray structure of the H13F β2m mutant revealed a hexamer which build two surfaces of interaction (PDB 3CIQ). One interface is mediated by the D strand, the BC loop and the E strand of two adjacent chains, while a second interface involves the stacking of the two ABED sheets of two adjacent β2m chains. The first interface is mainly mediated by His31, Asp34, His51, Phe56 and Trp60 and cover 700 $Å^2$, while the second interface mainly involves stacking interaction between Tyr63, Tyr26 and Tyr10 of two adjacent chains [61] (Fig. 6C). Among the four oligomeric high resolution structures reported to date, the only amyloidogenic mutant is the swapped dimer ΔN6-β2m.

2. AIM OF THE THESIS

β2m is an amyloidogenic protein that is responsible for dialysis related amyloidosis. One million people worldwide undergoing dialysis for 3-5 years are at risk of systemic amyloidosis due to β2m aggregation [75]. The mechanism underlying β2m aggregation is not completely understood. Indeed, soluble β2m is converted into insoluble amyloid fibrils through a dynamic process that involves many transient species, from intermediates with a native-like conformation to dimeric, tetrameric and higher oligomeric species which in turn aggregate into amyloid fibrils. It has been recently reported that the oligomers, that are on pathway for the formation of the amyloid fibrils, are the most toxic species in protein misfolding disease (Alzheimer's disease, Parkinson's disease and prion's disease) stressing the importance to provide structural insights in the early protein-protein interactions. Due to the low thermodynamic stability of these oligomers, it is very challenging to characterize their structural features to high resolution. Understand the interactions that occur at the early stages of β2m amyloidosis at a molecular level is fundamental to develop chemical compounds to treat DRA. This thesis is focused on two major points I) to isolate and characterize at atomic resolution β2m oligomeric species. II) to determine the β2m structural determinants that are correlated to the β2m aggregation propensity. The main approaches used are X-ray crystallography, fluorescence spectroscopy and circular dichroism.

3. MAIN RESULTS:

3.1 A recurrent D-strand association interface is observed in β2m oligomers.

3.1.1 *β2m cysteine mutants design (S20C, E50C, W60C and S88C).*

In order to map the β2m protein-protein interactions that are important for the β2m fibrillogenesis, four β2m cysteine mutants were designed (S20C, E50C, W60C and S88C). The residues mutated are distributed on the overall structure of the β2m (Fig. 7). In particular Ser20 is located on the AB loop that adopt an inward conformation when β2m is bound to the MHC-I while it adopts an outward conformation when β2m is monomeric in solution [45,46,50]. Glu50 and Trp60 lay on the N-termini and C-termini respectively, of the D-strand. This latter has been reported to be involved in the amyloid fibrils formation [50,62]. Indeed, it has been hypothesized that a straight conformation of the D-strand would favor the aggregation of the β2m while the presence of a β-bulge at the residue 53 would impair the β2m cross-β arrangement [50].

Residue 60 is very conserved among vertebrates because it is fundamental for the binding between β2m and MHC-I in the cell [58]. Furthermore, Trp60 is located on the DE loop which has been recently shown to affect the stability of the β2m [59,76]. Residue 88 lies on the FG loop. This region was previously indicated as the central β-spine of the amyloid fibril [74].

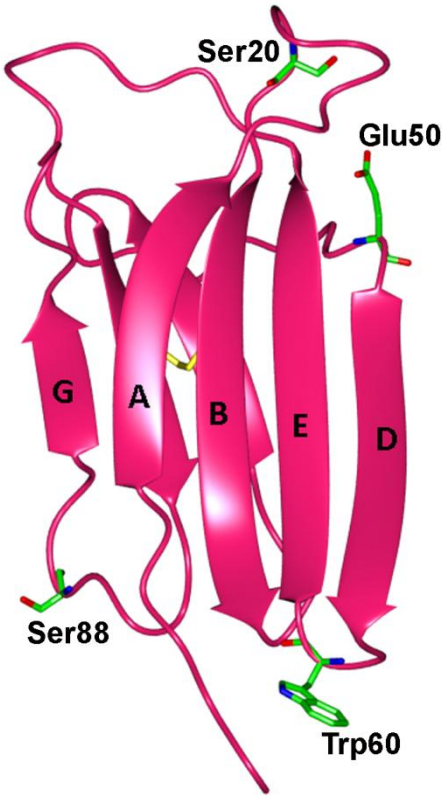

Figure 7. β2m cysteine mutants design. Sticks highlight the mutation sites.

3.1.2 *β2m disulphide-linked homodimers aggregation properties.*

The preparation of the disulphide-linked homodimers started by mixing each monomeric β2m cysteine mutant at a concentration of ~1660 μM with H_2O_2 at a molar ratio of 2:1 (see material and methods of manuscript I for details).

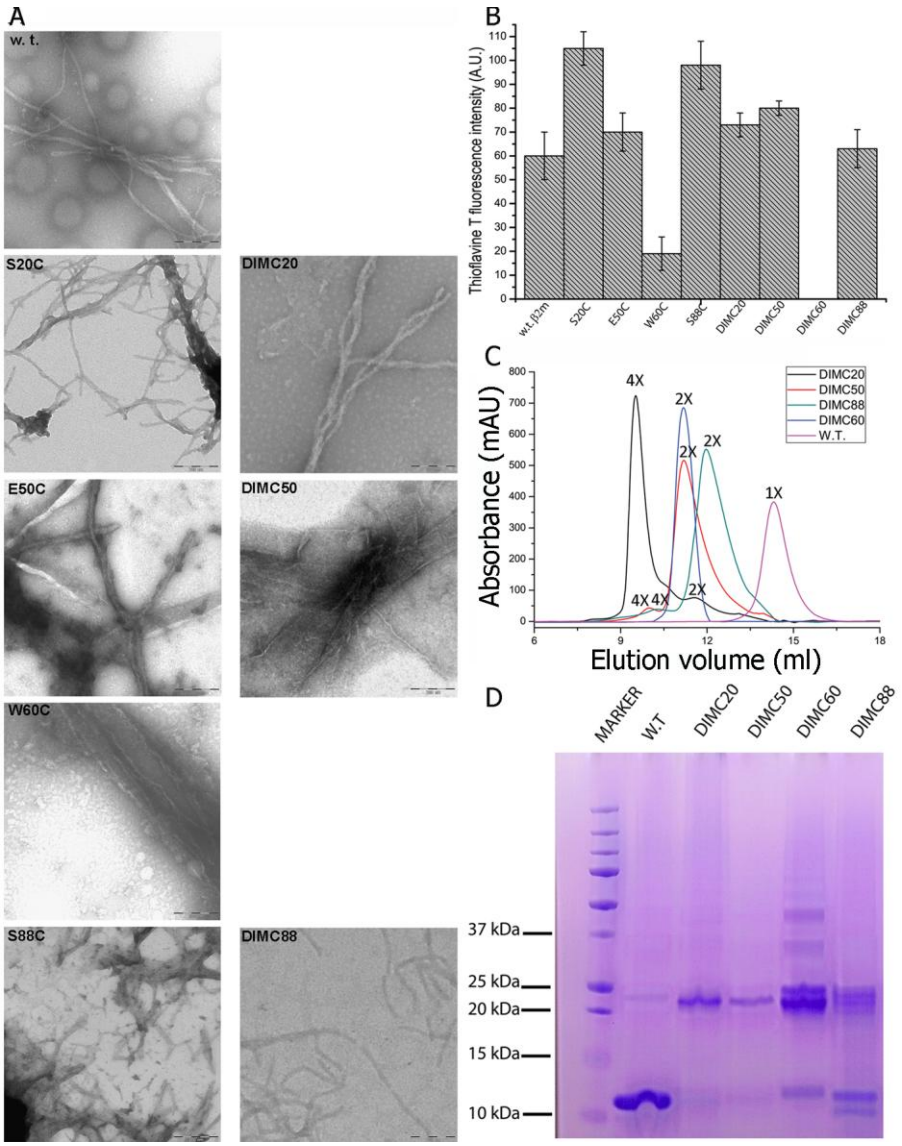

Figure 8. A) TEM Negative-stained amyloid fibrils of w.t., S20C/E50C/W60C/S88C β2m monomeric mutants and DIMC20/DIMC50/DIMC88 β2m mutants. **B)** ThT values for each β2m mutant at the plateau phase of fibrillogenesis. **C)** SEC profiles of each β2m homodimer. 1X indicates monomer, 2X dimer and 4X tetramer. **D)** SDS-PAGE of the fibrillogenesis samples of each β2m dimeric mutant dissolved into SDS 10%.

The mix was loaded on a Superdex75 column in order to separate the various species based on their hydrodynamic radius. The elution profiles of each mix displayed the presence of the expected dimeric species (Fig. 8 C). The aggregation

properties of each homodimer were tested in solution and under amyloid conditions. By observing the elution profile of the preparative SEC, it is noteworthy that DIMC20, DIMC50 and DIMC88 showed an additional tetrameric species, referred to a single β2m molecule, while DIMC60 revealed only dimeric species.

The dimeric species of the DIMC20, DIMC50 and DIMC60 were eluted at the same volume while DIMC88 is eluted later, revealing a more compact structure with respect to the other dimers. Furthermore, the amyloid propensity of each β2m homodimer were tested; indeed, DIMC20, DIMC50, DIMC60 and DIMC88 were mixed independently with the fibrillogenesis buffer (final concentration 100μM) and incubated at 37°C for 1 week. DIMC20, DIMC50 and DIMC88 showed positive values to ThT (Fig. 8 B) and Congo Red binding. Furthermore, TEM images displayed the presence of amyloid fibrils (Fig. 8 A). Conversely, DIMC60 does not bind ThT nor Congo Red and TEM images do not display any amyloid fibrils. Recently, Eisenberg *et al.*[73] showed that β2m can form oligomers by a domain-swapped mechanism that involved a reorganization of the β2m internal disulphide bond showing a characteristic ladder of bands on the SDS-PAGE. In order to exclude a domain-swapped mechanism, the amyloid fibrils of DIMC20, DIMC50 and DIMC88 were dissolved in 10% SDS for 10 minutes and loaded on a SDS-PAGE (Fig. 8 D). The gel displayed that each of the amyloid fibrils sample showed a higher fraction for the dimeric species and only traces for the other oligomers, suggesting that the intermolecular-disulphide introduced does not react with the internal β2m disulphide bond and no domain-swapping occur in our samples.

3.1.3 *Crystallogenesis of the β2m homodimers.*

In order to investigate the structure of the β2m homodimers, crystallization trials were performed using commercial crystal screens kits for each of the β2m homodimer. DIMC20, DIMC50 and DIMC88 protein crystals grew with different sizes and geometries, while DIMC60 failed to form protein crystals in any of the conditions screened. DIMC20 and DIMC50 crystals diffracted at a good resolution (2.45 Å and 2.7 Å, respectively) allowing to determine the protein structure, while DIMC88 crystals diffracted poorly (Fig. 9).

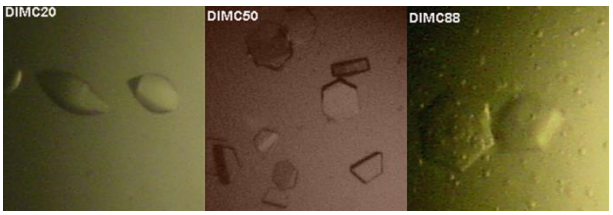

Figure 9. Crystals of the DIMC20, DIMC50 and DIMC88 β2m mutants.

3.1.4 *DIMC20 X-ray crystal structure.*

DIMC20 was concentrated to 6 mg/ml in milli-Q water and protein crystals were grown by the sitting drop technique using Greiner 96-wells plates prepared by Oryx8 crystallization robot. DIMC20 was found to crystallize into Hepes 0.1 M pH 7.7, $CdSO_4$ 0.12 M, sodium acetate 2.4 M, at T=293 K. Details of the DIMC20 X-ray structure data reduction and refinement can be found in the manuscript I. In the unit cell of the crystal, the electron density revealed a tetrameric assembly, formed by a non-covalent interface between two DIMC20 molecules (Fig. 10 A). For the sake of the clarity, the terms tetrameric, dimeric and monomeric will be referred to a single β2m molecule. Each β2m monomer displayed a clear electron density for residues 0-99. Moreover, the ($2F_o$-F_c) map showed the presence of the intermolecular disulphide bond between the two engineered cysteine residues at

position 20 that form the DIMC20 molecule. Interestingly, the two DIMC20 molecules that form the tetramer are not identical (r. m. s. d. 1.53 Å over 200 Cα pairs) and indeed display two somewhat different β2m chain conformations (r. m. s. d. 1.44 Å over 100 Cα pairs). Although they shared the same conformation of the AB loop, which adopts the inward orientation of the β2m in complex with MHC-I, they display a different conformation of the D-strand. Indeed, while one DIMC20 molecule is formed by two β2m chains displaying a D-strand with a β-bulge at the residue 53 reflecting the same conformation of the D-strand of the β2m in complex with MHC-I, the second DIMC20 molecule β2m chains showed a D-strand in which the residues 52-55 adopt a less regular conformation. Nevertheless, all the β2m chains in the DIMC20 crystal structure matched β2m from the MHC-I complex (PDB 3I6G, r.m.s.d. 0.9 Å and 1.6 Å over 100 Cα for each β2m chain configuration). The quaternary structure revealed an antiparallel non-covalent interface (hereafter called D-D strand interface) of ~600 $Å^2$ between the two DIMC20 molecules that is mediated by the D-strand, the DE loop, the BC loop, the E-strand and by a Cd^{2+} ion which was present in the crystallization buffer (Fig. 10 C). In particular, His31 and Met0 of one chain and Asp34 of the adjacent chain coordinate a Cd^{2+} ion together with a water molecule, while Pro32 adopts a *cis* orientation.

Besides, Trp60 of one chain is wedged in a hydrophobic pocket formed by Leu54, Leu64 and Tyr66 and formed stacking interaction with the aliphatic chain of Asp34. His51 of one chain established stacking interactions with Phe56 at one side giving rise to a hydrophobic pattern formed by residues Asp34, Trp60, Phe56 and His51. The region surrounding the intermolecular disulphide bond involves residues 12, 13 (A-strand), 18-22 (AB loop), 47 (CD loop), 52-54 (D-strand), 67-71 (E-strand) and cover ~400 $Å^2$. A residual electron density located among residues His13, Glu47, Glu69 was modeled as a Cd^{2+} ion.

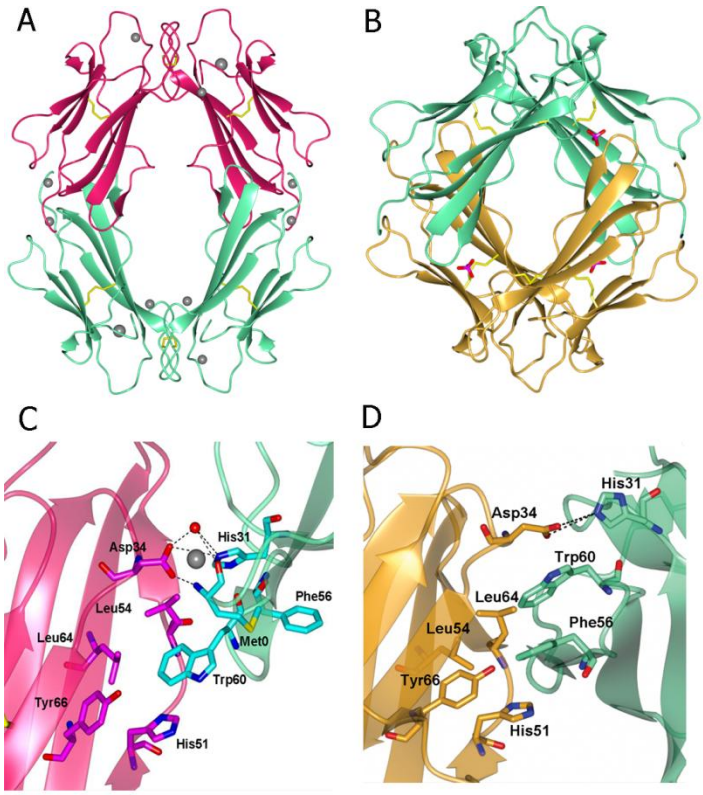

Figure 10. A) Tetrameric assembly of DIMC20 formed by two disulphide-linked homodimers molecules (cyan and magenta). Grey spheres are cadmium ions. **B)** Tetrameric assembly of DIMC50 formed by two disulphide-linked homodimers molecules (cyan and gold). Magenta sticks represent phosphate ions. **C)** D-D strand interface of DIMC20. Dashed lines highlight hydrogen bonds and red sphere is a water molecule. **D)** D-D strand interface of DIMC50. Dashed lines highlight hydrogen bonds.

3.1.5 *DIMC50 X-ray crystal structure.*

DIMC50 was dissolved in milli-Q water at a final concentration of 9 mg/ml. The protein crystals were grown by sitting-drop technique in a Greiner 96 well plate prepared by Oryx8 crystallization robot. The optimum conditions of crystallogenesis resulted in imidazole-malate 0.2 M, pH 5.5, PEG 600 24% solution (Stura crystal screen MD1-20, condition 2) at T=293 K. The details of data

reduction and structure refinement are reported in the manuscript I. The DIMC50 crystal diffracted at a resolution up to 2.7 Å. The asymmetric unit contains four molecules of DIMC50 assembled in two tight tetramers (one tetramer is shown in Fig. 10 B). For the sake of the clarity the terms tetrameric, dimeric and monomeric are always referring to a β2m chain. Residues 0-97 are clearly traced in the electron density calculated and all of the β2m chains are identical (r. m. s. d of 0.46 Å over 98 Cα). Moreover, the four covalent dimers and the two tetramers are identical (r. m. s. d. of 0.78 Å over all the 196 Cα and a r. m. s. d of 0.62 Å over all the 392 Cα, respectively). Each β2m chain matches well the β2m in complex with MHC-I (PDB 3I6G, average over 98 Cα r. m. s. d 1.07 Å) displaying the same conformation of the AB loop and showing the β-bulge at the residue 53 on the D-strand. The tetramer displays two non-covalent interfaces. One interface closely resemble the D-D strand interface observed in the DIMC20 X-ray structure and cover 570 $Å^2$ (Fig. 10 D). Indeed, the D-D strand interface of DIMC50 involves a H-bond network established between Asp34 of one chain with the His31 of the adjacent chain. Moreover, Trp60 is inserted in a hydrophobic pocket formed by Leu54, Leu64 and Tyr66. Trp60 formed stacking interaction with the aliphatic side chain atoms of Asp34 of the adjacent chain as well as with Phe56 of the same chain that in turn establish stacking interaction with His51 of the opposite chain. Trp60, Asp34, His51 and Phe56 form a hydrophobic pattern that stabilize the interface as observed in the DIMC20 D-D strand interface.

The second non-covalent interface is smaller and cover ~150 $Å^2$. It is mediated by two chains that are disposed in an anti-parallel orientation and the main interactions occur between A and D strands. The interface contains a phosphate ion that is coordinated by Arg12 and His13 of one chain and by Lys58 of the opposite chain.

The region surrounding the intermolecular disulphide bond includes residues 45-52 of the CD loop and residues 67-69 located at the end of the E-strand.

3.1.6 *DIMC20 and DIMC50 promote the w.t. β2m amyloid aggregation.*

Finally in order to shed light on the fibrillogenic properties of DIMC20 and DIMC50, unseeded fibrillogenesis tests have been performed using a mixture of DIMC20 or DIMC50 with w.t. β2m in a ratio of 1:3, respectively. As controls, in the same conditions unseeded reactions of w.t. β2m and of the mixture DIMC60/w.t. β2m (ratio 1:3) have been also carried out. As shown in Fig. 11A, DIMC20 and DIMC50 are able to trigger amyloid formation without seeds while the mixture of DIMC60/w.t. β2m and w.t. β2m alone do not aggregate (see Table I). In order to check that the amyloid fibrils of the DIMC20-w.t. and DIMC50-w.t. mixtures were formed by both the homodimers and w.t. β2m, the amyloid fibrils of each mixture were dissolved in SDS 10% and loaded on SDS-PAGE. The samples corresponding to DIMC20/DIMC50 together with the w.t β2m indicate that both species are aggregating. As controls, fibrils of w.t. β2m, DIMC20 and DIMC50 alone were also analyzed by SDS-PAGE, displaying only one species, confirming that the two bands present in the mixed samples are indeed w.t. β2m and a disulphide-linked dimer (Fig. 11B).

Taking all these data together, the DIMC20 and DIMC50 are highly amyloidogenic and can act as seeds for w.t. β2m.

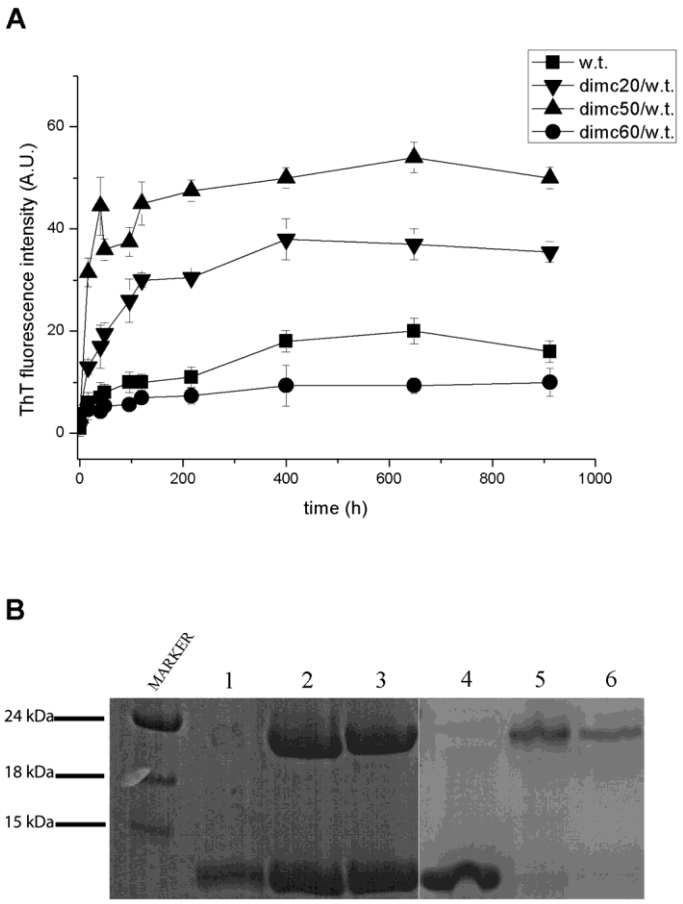

Figure 11. A) Kinetics of the amyloid fibrils formation of the following unseeded reactions: w.t. β2m (■) and the mixtures of DIMC20-w.t. β2m (1:3 ratio) (▼), DIMC50-w.t. β2m (1:3 ratio) (▲), DIMC60-w.t. β2m (1:3 ratio) (●). Bars represents standard deviations. **B)** SDS-PAGE showing soluble w.t. β2m (lane 1), then solubilised samples of DIMC20-w.t. amyloid fibrils (lane 2), DIMC50-w.t. amyloid fibrils (lane 3), amyloid fibrils of w.t. β2m (lane 4), amyloid fibrils of DIMC20 (lane 5), amyloid fibrils of DIMC50 (lane 6).

3.1.7 *The D-D strand interface is involved in the early steps of the amyloidosis.*

DIMC20 and DIMC50 tetramers shared a common D-D strand interface, although their engineered disulphide bonds are located in two different regions in β2m structures. Interestingly, a modeling of the DIMC88 structure shows that the intermolecular disulphide bond would not impair the formation of a D-D strand interface. According to these considerations, DIMC20, DIMC50 and DIMC88 display tetrameric species in solution and they are amyloidogenic, while DIMC60 does not form tetrameric species in solution nor amyloid fibrils. Importantly, DIMC20 and DIMC50 resulted capable in promoting w.t. β2m amyloid aggregation in the absence of fibril seeds. This result implies that DIMC20 and DIMC50 share a compatible aggregation pathway with respect to the w.t. β2m. Recently, it has been reported that the ΔN6-β2m variant can catalyse the w.t. β2m amyloid aggregation in the absence of fibrils seeds [55]. In the same article it has been reported that a D-D strand interface similar to the one reported in this thesis is observed at high concentration of the ΔN6-β2m variant. By observing the D-D strand interface, it is noteworthy that Trp60 is located in the middle of the interface, where it forms an hydrophobic pattern together with the aliphatic side chain of Asp34, Phe56 and His51; by inserting a disulphide at residue 60, the D-D strand interface would be impaired and the results here reported demonstrate that the three dimers (DIMC20, DIMC50 and DIMC88) that can form the D-D strand interface are amyloidogenic and oligomerize in solution, while DIMC60 failed. Moreover, DIMC60 does not induce a w.t. β2m amyloid aggregation. Another important feature emerging from the D-D strand interface is the involvement of residues His31 and Asp34. His31 is a key residue for the isomerization of the Pro32; indeed it has been proposed that His31 protonation triggers the *cis-trans* conversion of the Pro32 [62].

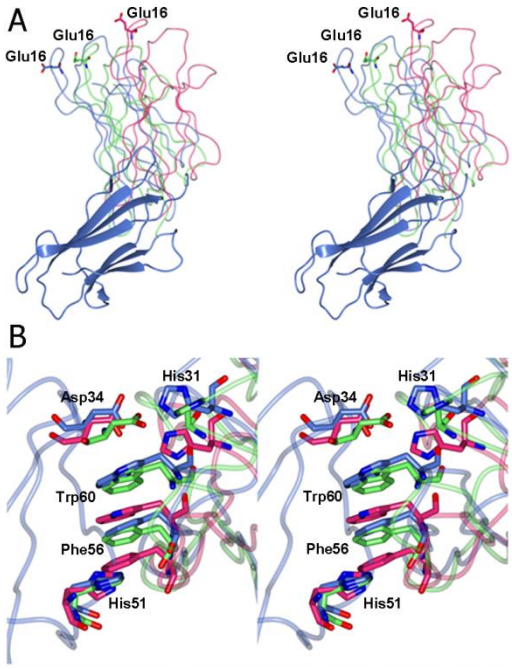

Figure 12. **A)** Stereo-view of the superimposition among the D-D strand interfaces of H13F β2m (green), DIMC20 (magenta) and DIMC50 (light blue). For clarity, only the DIMC50 backbone is shown as ribbon (light blue). As a reference, three Glu16 residues are drawn as stick models. **B)** Stereo-view of the superimposition of the residues involved in the D-D strand interfaces shown in **A)**.

Interestingly, a hexameric structure of the H13F β2m mutant contained a D-D strand interface, involving the same residues (His31, Asp34, His51, Phe56, Trp60) and with a high degree of similarity (r. m. s. d. values of 3.3/2.0 Å calculated over the whole Cα backbones of dimers built across the D-D strand interfaces of DIMC20 and DIMC50, respectively) (Fig. 12). In the D-D strand interface of the DIMC20 a cadmium ion is coordinated by His31 of one chain and Asp34 of the facing subunit, with the Pro32 adopting a *cis* conformation.

In the H13F β2m mutant hexameric structure, His31 participated to the coordination of a copper ion but the Pro32 adopted a *trans* conformation. The superimposition of the two metal binding sites shed light on the mechanism of the Pro32 isomerization mediated by metal ions (Fig. 13).

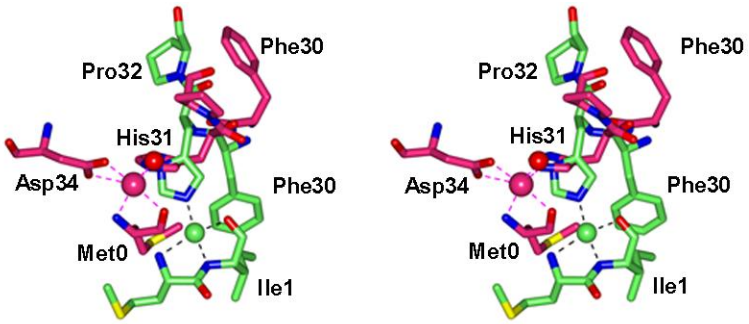

Figure 13. Stereo-view of the superimposition of the metal-binding site of DIMC20 (magenta) and H13F β2m mutant (green). Red sphere is water, green sphere is copper and magenta cadmium ion.

Protonated His31 may be repulsed by Gln2 and Arg3 on the N-*terminus* that in turn is displaced. The N-*terminus* movement allows the Pro32 *cis-trans* isomerization and consequently the 180° rotation of Phe30 [62] (Fig. 13). Moreover, NMR spectra of the amyloidogenic intermediate with Pro32 in a *trans* orientation showed that the regions adjacent to the BC loop, (DE loop and the N-*terminus*) are perturbed and poorly structured [16]. Interestingly, these three regions are involved in the D-D strand interface, suggesting a cooperative role of the BC loop, the DE loop and the N-*terminus* in the β2m early steps of aggregation.

3.2 Unpublished Results

3.2.1 *β2m-cys mutants fibrillogenesis monitored by acrylodan fluorescence.*

In order to evaluate the role of the residues in position 20, 50, 60 and 88 and of the adjacent regions during fibrillogenesis, the four monomeric β2m-cys mutants were labeled with acrylodan [77]. This latter is a fluorescent dye, which reacts specifically with cysteine residue. Acrylodan fluorescence varies the emission maximum (λ_{MAX}) upon change in solvent accessibility, allowing to follow local protein conformational changes. Each labeled β2m-cys mutants was mixed with the fibrillogenesis buffer and the amyloid fibrils formation was monitored by λ_{MAX}. Fluorescence spectra were recorded sequentially every 20 mins for each β2m-cys mutants. λ_{MAX} of each fluorescence spectra were plotted against time for each of the β2m-cys mutants (Fig. 14 E). The curves of the labeled S20C, E50C and S88C β2m-cys mutants were fitted with a single exponential equation $y=y_0+A*(e^{R0t})$ and data were summarized in Fig. 14 F, while the labeled W60C β2m mutant does not follow an exponential function. Moreover, labeled W60C does not form fibrils with the same amount of the other mutants. The degree of burial is indicated by the parameter A, which represents the slope of the curve. Results display that residue 88 is more buried in the amyloid fibrils (A_{S88C}= 23 nm) compared to the residues 20 and 50 (A_{S20C}= 19 nm and A_{E50C}= 19 nm), that in turn showed a similar degree of burial.

From the exponential equation $y=y_0+A*(e^{R0t})$ the rate constant R_0 for each β2m-cys mutant was calculated (Fig. 15 F). Residue 88 displays a R_{S88C} that is ≈ 2 times R_{S20C} and $R_{E50C.}$ These values would suggest that the region around residue 88 is involved primarily in the fibrillogenesis process.

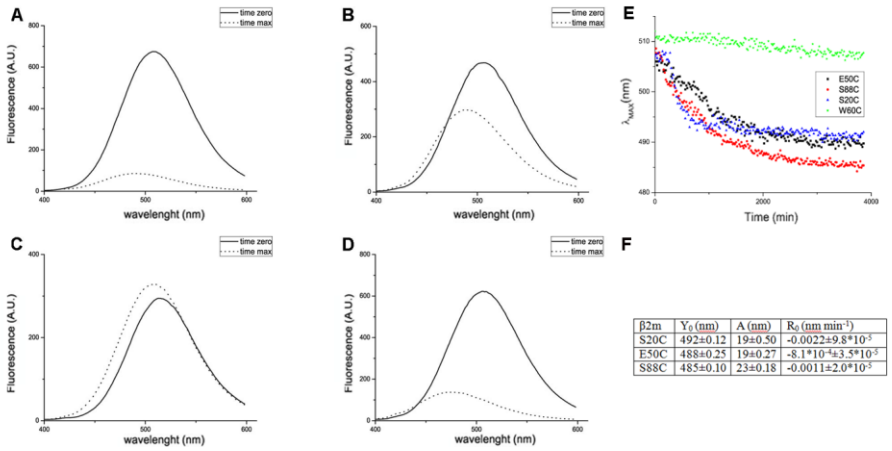

β2m	Y_0 (nm)	A (nm)	R_0 (nm min^{-1})
S20C	492±0.12	19±0.50	-0.0022±9.8*10^{-5}
E50C	488±0.25	19±0.27	-8.1*10^{-4}±3.5*10^{-5}
S88C	485±0.10	23±0.18	-0.0011±2.0*10^{-5}

Figure 14. A-D) Initial and final fluorescence spectra (solid line and dotted line respectively) of the fibrillogenesis of each labeled β2m-cys mutant S20C (A), E50C (B), W60C (C), S88C (D). **E)** λ_{MAX} variation over time for each labeled β2m-cys mutant. **F)** Fitting data of the curves shown in **E)** with the exponential equation $y=y_0+A*(e^{R0t})$. W60C does not follow the exponential equation.

3.2.2 *Material and methods.*

Acrylodan labelling of the β2m Cys-mutants.

Each monomeric β2m Cys-mutant and acrylodan were mixed in sodium phosphate 10mM pH 7.4 in a 1:5 molar ratio and stirred O/N at room temperature. Samples were centrifuged at 10000 rpm for 8 mins, and the supernatant was collected. The degree of labeling has been calculated using the following equation: $(A_{ACRY}/\varepsilon_{ACRY})*(MW_{\beta2m\text{-}cys}/mg/ml_{\beta2m\text{-}cys}) = mol_{ACRY}/mol_{\beta2m\text{-}cys}$ (provided by Invitrogen), where A_{ACRY} is the absorbance of acrylodan at λ=420 nm, ε_{ACRY}= 16400 M^{-1}, $MW_{\beta2m\text{-}cys}$=11862 Da. Each cys-mutant yielded a good degree of labeling ranging from 50 M^{-1} to 90 M^{-1}. The labeled β2m Cys-mutant was loaded on a Hitrap Desalting column in order to remove the acrylodan excess.

Fluorescence monitoring of labeled β2m Cys-mutants fibrillogenesis.

Each labeled β2m Cys-mutant was mixed with Sodium phosphate 50 mM pH 7.4, TFE 20%, NaCl 0.1M and seeds wt β2m 2.5 μg/ml (hereafter referred as fibrillogenesis buffer) at a final concentration of 100 μM in a quartz cuvette, under shaking and incubated at 37 °C. Labeled β2m Cys-mutants fluorescent spectra were recorded every 20 minutes over ≈64 h using a Cary Eclipse fluorescent spectrophotometer (VARIAN). The excitation wavelength was set at 372 nm and the emission spectra were detected in the range 380-600 (nm). Acrylodan itself exhibits only a very low fluorescence quantum yield, while thiols adducts of acrylodan are brightly fluorescent and resulting in a fluorescence emission maximum (λ_{MAX}) of ≈530nm when it is completely exposed to polar solvents [77]. Initial λ_{MAX} for all the four labeled β2m-Cys mutants is lower than expected for a completely exposed acrylodan. This is due to the presence of TFE in the fibrillogenesis buffer (controlled with β-mercaptoethanol, data not shown).

The kinetic curves were calculated using the equation $y=y_0+A*(e^{R0t})$ by ORIGIN version 8.1. The estimation of the error is based on the standard error (*SE*) $SE = s/\sqrt{n}$, where *s* is the standard deviation of the samples and *n* is the number of observations of each sample.

3.3 The effects of an ideal β-turn on the β2m fold.

3.3.1 *Design of the K58P-W60G β2m mutant.*

The second part of this thesis is focused on the structural determinants of β2m primarily related to its aggregation propensity. Recently, the geometrical strain of the DE loop has been reported to affect the overall stability of β2m. Indeed, the substitution of Trp60 with Gly confers a relaxed DE loop conformation which is translated with an increased thermal and chemical stability [57]. Conversely, the substitution of Asp59 with Pro increases the strain of the DE loop that resulted in a diminished thermal and chemical stability of the β2m [59]. Moreover, W60G and D59P display different aggregation properties; W60G does not form amyloid fibrils at neutral pH while D59P form amyloid fibrils faster than the w.t. β2m and a most abundant yield either at neutral pH and acidic pH. The K58P-W60G β2m mutant was designed to increase the β2m stability, because proline and glycine residues at positions 58 and 60 respectively, are considered the most favored residues to obtain a perfect type I β-turn (DE loop) that can further increase the β2m fold stability [78].

3.3.2 *Fold stability and folding kinetics.*

The conformational stability of the K58P-W60G β2m mutant has been assessed by means of chemical and thermal stability. Chemical stability was measured by guanidium hydrochloride equilibrium unfolding and it showed that the K58P-W60G β2m mutant is more stable with respect to w.t. β2m ($C_{m\ K58P\text{-}W60G}$ = 2.7 M GdHCl vs. $_{Cm\ w.t.}$= 1.7 M GdHCl, while $\Delta G°_{K58P\text{-}W60G\ (H2O)}$ = 7.6 kcal mol^{-1} vs $\Delta G°_{w.t.\ (H2O)}$= 5.5 kcal mol^{-1}). Thermal stability was measured by circular dichroism (Far-UV and Near-UV) and by intrinsic fluorescence. Near-UV and intrinsic fluorescence spectra revealed a higher stable tertiary structure of the K58P-W60G β2m mutant relative to the w.t. and comparable to that of the W60G β2m mutant.

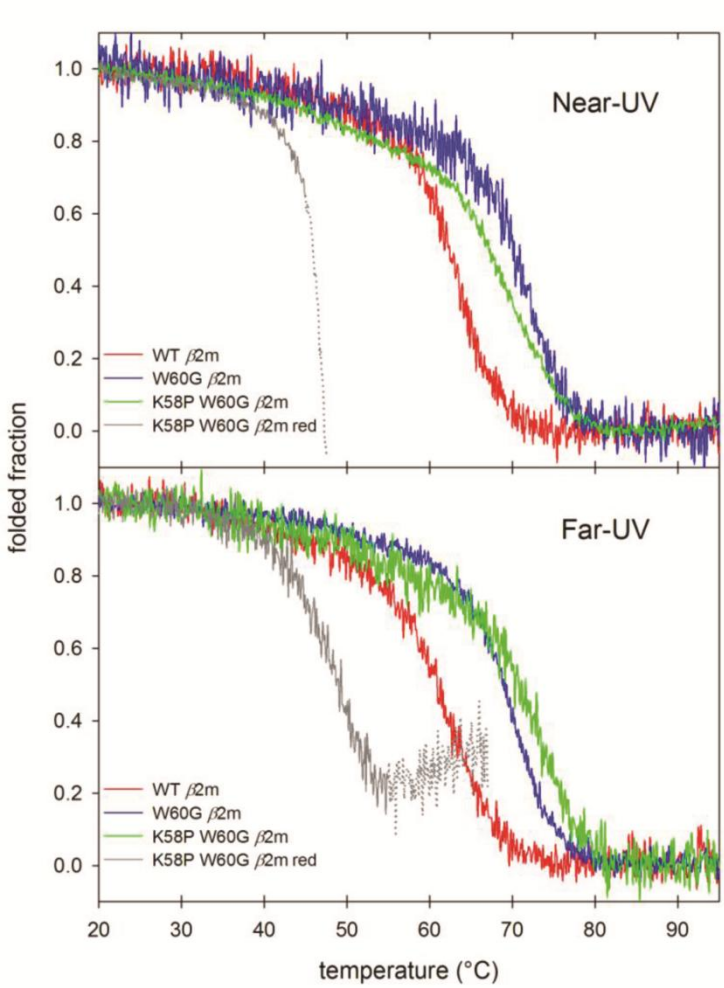

Figure 15. Thermal stability assessed by circular dichroism in Near-UV (panel above) and Far-UV (bottom panel), for w.t. (red), K58P-W60G (blue), K58P-W60G reduced form (gray) and W60G (green).

Moreover, Far-UV measurements show that the secondary structure of the K58P-W60G β2m mutant unfolds at T_m= 73.5 °C against the T_m= 62.4 °C and T_m= 69.8 °C of the w.t. and W60G β2m mutant respectively. Refolding kinetics was measured by intrinsic fluorescence and Far-UV circular dichroism. The intrinsic fluorescence revealed a rate constant of 1.6 s^{-1} for the w.t. and 10 s^{-1} for the K58P-

W60G β2m mutant. Moreover, the K58P-W60G β2m mutant profile displays the absence of the slow phase of folding, which is detectable in the w.t. β2m. The refolding kinetics measurements based on the secondary structure (λ= 233 nm) show two similar profiles between the K58P-W60G β2m mutant and the w.t. β2m. Moreover, the slow-phase of folding was not detectable for both K58P-W60G β2m mutant and w.t. β2m.

3.3.3 *Crystal structure of the K58P-W60G β2m mutant.*

K58P-W60G β2m mutant was dissolved in milli-Q water at a final concentration of 10 mg/ml and crystallized by hanging drop technique as described in the material and methods section of the Paper I. The X-ray structure of the K58P-W60G β2m mutant was determined to 1.25 Å resolution and the 100 amino acids were fitted in a very well-defined electron density. The mutated amino acids (Pro58 and Gly60) are clearly visible (Fig. 16 A).

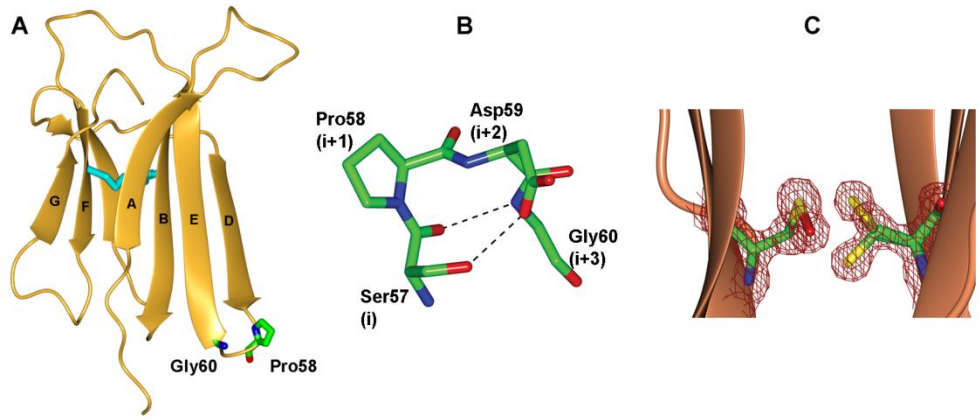

Figure 16. A) K58P-W60G structure showing the mutated residues (sticks). B) DE loop of the K58P-W60G showing hydrogen bonds (dashed line). C) Cys25 and Cys80 highlighted by electron density contoured at 1σ, showing the absence of the internal disulphide bond.

The asymmetric unit contains one molecule of K58P-W60G β2m mutant and the DE loop displayed a type I β-turn conformation as observed in the crystal structures of the β2m mutants in which the Trp60 was replaced by cysteine, valine or glycine. However, the K58P-W60G β2m mutant DE loop is formed by the most favored amino acids for a type I β-turn (Ser57-Pro58-Asp59-Gly60) due to their stereochemical properties [78]. Indeed, Ser57 (site i) is a polar residue that established a H-bond with the main chain nitrogen of the residue i+2; Pro58 is the ideal amino acid for the i+1 site, because of the restriction on the Φ angle to about -60°. At site i+3, glycine is the most favored residue because its flexibility allowed the completion of the β-turn and the beginning of the antiparallel E strand (Fig. 16 B). Moreover, the high resolution of the X-ray structure allow to identify alternative conformations of the aromatic residues Phe56 and Phe62 together with two distinct D-strand arrangements.

3.3.4 *Reduced K58P-W60G β2m mutant.*

Combining the information provided by crystallography and ESI-MS (see the results section of the Paper I), it becomes evident that the K58P-W60G β2m mutant is present in solution as a mix of the common disulphide oxidized species with a disulphide-reduced variant of the K58P-W60G β2m mutant. In order to measure the fraction of the disulphide-reduced molecules, K58P-W60G β2m mutant was dissolved in 4M GdHCl and the level of free cysteine was assessed by titration with 5,5'-dithiobis-(2-nitrobenzoic acid) (DTNB). The results showed that the 30% of the cysteines were reduced confirming that the 30% of the K58P-W60G β2m mutant molecules display a severed disulphide-bond. Subsequently, the fold stability of the reduced form was assessed by circular dichroism thermal stability. The K58P-W60G β2m mutant was unfolded and completely reduced with

dithiothreitol in the presence of GdHCl and then refolded (by removal of GdHCl) in the presence of dithiothreitol to prevent cysteine oxidation. The reduced K58P-W60G mutant was successfully refolded according to Ohhashi et al.[79]. The thermal stability of the reduced variant of the K58P-W60G mutant could not be determined because the precipitation of the sample occur before the completion of the spectra. However, the onset of the transition occur 15-20 °C lower than the Tm of the other β2m mutants allowing us to hypothesize that the Tm should fall below 50-55°C. Intriguingly, a closer analysis of the thermal unfolding of the K58P-W60G mutant monitored by Trp-fluorescence revealed that the first derivative has a first, although minor, minimum at 48 °C. This may well represent unfolding of the reduced K58P-W60G fraction (about 30%). On the other hand, the temperature ramps monitored by near- and far-UV CD detect only the unfolding of a major protein component (i.e. the disulphide-oxidised form), due to the lower sensibility (signal-to-noise ratio) of the CD signal compared to Trp-fluorescence.

3.3.5 *DE loop geometry affects the folding and the aggregation propensity of the β2m.*

The DE loop is a region of β2m that affects its aggregation propensity. Indeed, it has been reported to mediate protein-protein interactions in the H13F β2m mutant [61]. Moreover, D59P and W60G β2m mutants represent the two edges of the DE loop effects on the overall β2m thermodynamical stability; while D59P confers rigidity to the DE loop resulting in an increased amyloidogenicity and in a lower thermodynamical stability compared to the w.t., W60G relaxes the geometry of the DE loop which resulted in the opposite effect observed for D59P mutant. The double mutant K58P-W60G was designed to transform the DE loop into a perfect β-turn according to the Hutchinson et al. [78]. Data showed that the engineered β-turn increases the β2m thermodynamical stability compared to the w.t. insomuch as the

internal disulphide bond of β2m becomes not fundamental for the correct folding of the protein. Indeed, DTNB experiments assessed that nearly 30% of the purified K58P-W60G presented a reduced disulphide bond. These results reinforce the role of the DE loop in the β2m aggregation and the D-D strand interface previously reported strongly suggest an involvement of the DE loop in the early stages of β2m amyloidosis.

4. CONCLUSIONS AND PERSPECTIVES:

4.1 *A recurrent D-strand association interface is observed in β2m oligomers.*

The experiments here presented highlight the role of a surface of interaction mediated by the D-strands of two β2m molecules in the early stages of β2m amyloidosis. Indeed, DIMC20, DIMC50 and DIMC88 are amyloidogenic, while DIMC60 is not. In particular, DIMC20 and DIMC50 display a conserved D-D strand interface characterized at atomic resolution and moreover can trigger the w.t. β2m amyloid aggregation. Conversely, DIMC60, in which the D-D strand interface is impaired, resulted non-amyloidogenic and unable to catalyse the w.t. β2m amyloid formation. The residues involved in the D-D strand interface support a role for the BC loop and the DE loop for the early interactions. Given the biochemical and structural data, the D-D strand interface could be the target of drug design to impair the formation of β2m amyloid fibrils. Furthermore, DIMC88 X-ray structure could be important to determine if the D-D strand interface is conserved as suggested in the study here reported. Finally, β2m mutants affecting the residues involved in the D-D strand interface can be designed and their oligomerization properties characterized by ESI-MS and SEC in order to further investigate the role of the D-D strand interface. Moreover, the chemical shift investigation of the D-D strand interface residues in DIMC20 and DIMC50 could be monitored in a TFE buffer.

4.2 *DE loop geometry affects the overall stability of β2m.*

The K58P-W60G β2m mutant was designed to further characterize the role of the DE loop on the β2m fold stability and aggregation properties. K58P-W60G β2m mutant resulted more stable compared to the w.t. β2m in terms of thermal and chemical stability. Moreover, K58P-W60G β2m mutant lacks the slow-phase of folding and can reach the correct shape although the internal disulphide bond is reduced. The crystal structure of the K58P-W60G β2m mutant shows that the DE loop forms a perfect β-turn. Finally, the K58P-W60G β2m mutant does not form amyloid fibrils at neutral pH strengthening the link between the folding stability of β2m and its tendency to form amyloid fibrils. In order to further evaluate the role of the DE loop in the β2m folding stability, it could be interesting to produce the K58P-W60G-P32A β2m mutant. Indeed, Ala32 would adopt a constitutively *trans* orientation which in theory may cause a destabilization of the β2m folding. However, it can also be hypothesize that the DE loop, in a perfect β-turn conformation can protect the β2m folding.

5. REFERENCES

1. Chiti, F. & Dobson, C.M. Protein misfolding, functional amyloid, and human disease. *Annu Rev Biochem* **75**, 333-66 (2006).
2. Radford, S.E., Gosal, W.S. & Platt, G.W. Towards an understanding of the structural molecular mechanism of beta(2)-microglobulin amyloid formation in vitro. *Biochim Biophys Acta* **1753**, 51-63 (2005).
3. Harris, H.W. & Gill, T.J., 3rd. Expression of class I transplantation antigens. *Transplantation* **42**, 109-17 (1986).
4. Berggard, I. & Bearn, A.G. Isolation and properties of a low molecular weight beta-2-globulin occurring in human biological fluids. *J Biol Chem* **243**, 4095-103 (1968).
5. Miyata, T., Jadoul, M., Kurokawa, K. & Van Ypersele de Strihou, C. Beta-2 microglobulin in renal disease. *J Am Soc Nephrol* **9**, 1723-35 (1998).
6. Bernier, G.M. & Conrad, M.E. Catabolsm of human beta-2-microglobulin by the rat kidney. *Am J Physiol* **217**, 1359-62 (1969).
7. Floege, J. & Ehlerding, G. Beta-2-microglobulin-associated amyloidosis. *Nephron* **72**, 9-26 (1996).
8. Floege, J. & Ketteler, M. beta2-microglobulin-derived amyloidosis: an update. *Kidney Int Suppl* **78**, S164-71 (2001).
9. Morgan, C.J., Gelfand, M., Atreya, C. & Miranker, A.D. Kidney dialysis-associated amyloidosis: a molecular role for copper in fiber formation. *J Mol Biol* **309**, 339-45 (2001).
10. Okon, M., Bray, P. & Vucelic, D. 1H NMR assignments and secondary structure of human beta 2-microglobulin in solution. *Biochemistry* **31**, 8906-15 (1992).
11. Bryngelson JD, W.P. Intermediates and barrier crossing in a random energy model (with applications to protein folding). *J. Phys. Chem.* **93**, 13 (1989).
12. Gruebele, M. & Wolynes, P.G. Satisfying turns in folding transitions. *Nat Struct Biol* **5**, 662-5 (1998).
13. Hartl, F.U., Bracher, A. & Hayer-Hartl, M. Molecular chaperones in protein folding and proteostasis. *Nature* **475**, 324-32 (2011).
14. Chiti, F. et al. A partially structured species of beta 2-microglobulin is significantly populated under physiological conditions and involved in fibrillogenesis. *J Biol Chem* **276**, 46714-21 (2001).
15. Chiti, F. et al. Detection of two partially structured species in the folding process of the amyloidogenic protein beta 2-microglobulin. *J Mol Biol* **307**, 379-91 (2001).
16. Kameda, A. et al. Nuclear magnetic resonance characterization of the refolding intermediate of beta2-microglobulin trapped by non-native prolyl peptide bond. *J Mol Biol* **348**, 383-97 (2005).

17. Armen, R.S. & Daggett, V. Characterization of two distinct beta2-microglobulin unfolding intermediates that may lead to amyloid fibrils of different morphology. *Biochemistry* **44**, 16098-107 (2005).
18. Brandts, J.F., Halvorson, H.R. & Brennan, M. Consideration of the Possibility that the slow step in protein denaturation reactions is due to cis-trans isomerism of proline residues. *Biochemistry* **14**, 4953-63 (1975).
19. Elove, G.A., Chaffotte, A.F., Roder, H. & Goldberg, M.E. Early steps in cytochrome c folding probed by time-resolved circular dichroism and fluorescence spectroscopy. *Biochemistry* **31**, 6876-83 (1992).
20. Kiefhaber, T. & Schmid, F.X. Kinetic coupling between protein folding and prolyl isomerization. II. Folding of ribonuclease A and ribonuclease T1. *J Mol Biol* **224**, 231-40 (1992).
21. Schmid, F.X. Prolyl isomerase: enzymatic catalysis of slow protein-folding reactions. *Annu Rev Biophys Biomol Struct* **22**, 123-42 (1993).
22. Radzicka, A., Pedersen, L. & Wolfenden, R. Influences of solvent water on protein folding: free energies of solvation of cis and trans peptides are nearly identical. *Biochemistry* **27**, 4538-41 (1988).
23. Reimer, U., el Mokdad, N., Schutkowski, M. & Fischer, G. Intramolecular assistance of cis/trans isomerization of the histidine-proline moiety. *Biochemistry* **36**, 13802-8 (1997).
24. Reimer, U. et al. Side-chain effects on peptidyl-prolyl cis/trans isomerisation. *J Mol Biol* **279**, 449-60 (1998).
25. Eakin, C.M., Berman, A.J. & Miranker, A.D. A native to amyloidogenic transition regulated by a backbone trigger. *Nat Struct Mol Biol* **13**, 202-8 (2006).
26. Jahn, T.R., Parker, M.J., Homans, S.W. & Radford, S.E. Amyloid formation under physiological conditions proceeds via a native-like folding intermediate. *Nat Struct Mol Biol* **13**, 195-201 (2006).
27. Jahn, T.R., Tennent, G.A. & Radford, S.E. A common beta-sheet architecture underlies in vitro and in vivo beta2-microglobulin amyloid fibrils. *J Biol Chem* **283**, 17279-86 (2008).
28. McParland, V.J. et al. Partially unfolded states of beta(2)-microglobulin and amyloid formation in vitro. *Biochemistry* **39**, 8735-46 (2000).
29. Smith, A.M., Jahn, T.R., Ashcroft, A.E. & Radford, S.E. Direct observation of oligomeric species formed in the early stages of amyloid fibril formation using electrospray ionisation mass spectrometry. *J Mol Biol* **364**, 9-19 (2006).
30. Caughey, B. & Lansbury, P.T. Protofibrils, pores, fibrils, and neurodegeneration: separating the responsible protein aggregates from the innocent bystanders. *Annu Rev Neurosci* **26**, 267-98 (2003).
31. Antwi, K. et al. Cu(II) organizes beta-2-microglobulin oligomers but is released upon amyloid formation. *Protein Sci* **17**, 748-59 (2008).
32. White, H.E. et al. Globular tetramers of beta(2)-microglobulin assemble into elaborate amyloid fibrils. *J Mol Biol* **389**, 48-57 (2009).

33. Relini, A. et al. Collagen plays an active role in the aggregation of beta2-microglobulin under physiopathological conditions of dialysis-related amyloidosis. *J Biol Chem* **281**, 16521-9 (2006).
34. Relini, A. et al. Heparin strongly enhances the formation of beta2-microglobulin amyloid fibrils in the presence of type I collagen. *J Biol Chem* **283**, 4912-20 (2008).
35. Yamamoto, S. et al. Glycosaminoglycans enhance the trifluoroethanol-induced extension of beta 2-microglobulin-related amyloid fibrils at a neutral pH. *J Am Soc Nephrol* **15**, 126-33 (2004).
36. Eakin, C.M., Knight, J.D., Morgan, C.J., Gelfand, M.A. & Miranker, A.D. Formation of a copper specific binding site in non-native states of beta-2-microglobulin. *Biochemistry* **41**, 10646-56 (2002).
37. Yamaguchi, K., Naiki, H. & Goto, Y. Mechanism by which the amyloid-like fibrils of a beta 2-microglobulin fragment are induced by fluorine-substituted alcohols. *J Mol Biol* **363**, 279-88 (2006).
38. LeVine, H., 3rd. Thioflavine T interaction with synthetic Alzheimer's disease beta-amyloid peptides: detection of amyloid aggregation in solution. *Protein Sci* **2**, 404-10 (1993).
39. Puchtler, H., Sweat F., Levine M. On the binding of Congo Red by amyloid. *Journal of Histochemistry and cytochemistry*, 355-364 (1962).
40. Sunde, M. et al. Common core structure of amyloid fibrils by synchrotron X-ray diffraction. *J Mol Biol* **273**, 729-39 (1997).
41. Hoshino, M. et al. Mapping the core of the beta(2)-microglobulin amyloid fibril by H/D exchange. *Nat Struct Biol* **9**, 332-6 (2002).
42. Barbet-Massin, E. et al. Fibrillar vs crystalline full-length beta-2-microglobulin studied by high-resolution solid-state NMR spectroscopy. *J Am Chem Soc* **132**, 5556-7 (2010).
43. Debelouchina, G.T., Platt, G.W., Bayro, M.J., Radford, S.E. & Griffin, R.G. Intermolecular Alignment in beta(2)-Microglobulin Amyloid Fibrils. *J Am Chem Soc* (2010).
44. Debelouchina, G.T., Platt, G.W., Bayro, M.J., Radford, S.E. & Griffin, R.G. Magic angle spinning NMR analysis of beta2-microglobulin amyloid fibrils in two distinct morphologies. *J Am Chem Soc* **132**, 10414-23 (2010).
45. Paulsson, K.M. et al. Distinct differences in association of MHC class I with endoplasmic reticulum proteins in wild-type, and beta 2-microglobulin- and TAP-deficient cell lines. *Int Immunol* **13**, 1063-73 (2001).
46. Trinh, C.H., Smith, D.P., Kalverda, A.P., Phillips, S.E. & Radford, S.E. Crystal structure of monomeric human beta-2-microglobulin reveals clues to its amyloidogenic properties. *Proc Natl Acad Sci U S A* **99**, 9771-6 (2002).
47. Hong, D.P., Gozu, M., Hasegawa, K., Naiki, H. & Goto, Y. Conformation of beta 2-microglobulin amyloid fibrils analyzed by reduction of the disulfide bond. *J Biol Chem* **277**, 21554-60 (2002).

48. Kihara, M. et al. Conformation of amyloid fibrils of beta2-microglobulin probed by tryptophan mutagenesis. *J Biol Chem* **281**, 31061-9 (2006).
49. Bellotti, V. et al. Beta2-microglobulin can be refolded into a native state from ex vivo amyloid fibrils. *Eur J Biochem* **258**, 61-7 (1998).
50. Esposito, G. et al. Removal of the N-terminal hexapeptide from human beta2-microglobulin facilitates protein aggregation and fibril formation. *Protein Sci* **9**, 831-45 (2000).
51. Myers, S.L. et al. A systematic study of the effect of physiological factors on beta2-microglobulin amyloid formation at neutral pH. *Biochemistry* **45**, 2311-21 (2006).
52. Eichner, T., Kalverda, A.P., Thompson, G.S., Homans, S.W. & Radford, S.E. Conformational conversion during amyloid formation at atomic resolution. *Mol Cell* **41**, 161-72 (2011).
53. Esposito, G. et al. The controlling roles of Trp60 and Trp95 in beta2-microglobulin function, folding and amyloid aggregation properties. *J Mol Biol* **378**, 885-95 (2008).
54. Batuwangala, T. et al. The crystal structure of human CD1b with a bound bacterial glycolipid. *J Immunol* **172**, 2382-8 (2004).
55. Ricagno, S. et al. DE loop mutations affect beta-2 microglobulin stability and amyloid aggregation. *Biochem Biophys Res Commun* **377**, 146-50 (2008).
56. Santambrogio, C. et al. DE-loop mutations affect beta2 microglobulin stability, oligomerization, and the low-pH unfolded form. *Protein Sci* **19**, 1386-94 (2010).
57. Calabrese, M.F., Eakin, C.M., Wang, J.M. & Miranker, A.D. A regulatable switch mediates self-association in an immunoglobulin fold. *Nat Struct Mol Biol* (2008).
58. Esposito, G. et al. Solution structure of beta(2)-microglobulin and insights into fibrillogenesis. *Biochim Biophys Acta* **1753**, 76-84 (2005).
59. Jiang, L.F., Yao, T.M., Zhu, Z.L., Wang, C. & Ji, L.N. Impacts of Cd(II) on the conformation and self-aggregation of Alzheimer's tau fragment corresponding to the third repeat of microtubule-binding domain. *Biochim Biophys Acta* **1774**, 1414-21 (2007).
60. Uversky, V.N., Li, J. & Fink, A.L. Metal-triggered structural transformations, aggregation, and fibrillation of human alpha-synuclein. A possible molecular NK between Parkinson's disease and heavy metal exposure. *J Biol Chem* **276**, 44284-96 (2001).
61. Rana, A., Gnaneswari, D., Bansal, S. & Kundu, B. Prion metal interaction: is prion pathogenesis a cause or a consequence of metal imbalance? *Chem Biol Interact* **181**, 282-91 (2009).
62. Remko, M., Fitz, D. & Rode, B.M. Effect of metal ions (Li+, Na+, K+, Mg2+, Ca2+, Ni2+, Cu2+ and Zn2+) and water coordination on the structure and properties of L-histidine and zwitterionic L-histidine. *Amino Acids* **39**, 1309-19 (2010).
63. Mendoza, V.L. & Vachet, R.W. Probing protein structure by amino acid-specific covalent labeling and mass spectrometry. *Mass Spectrom Rev* **28**, 785-815 (2009).

64. Mendoza, V.L., Antwi, K., Baron-Rodriguez, M.A., Blanco, C. & Vachet, R.W. Structure of the preamyloid dimer of beta-2-microglobulin from covalent labeling and mass spectrometry. *Biochemistry* **49**, 1522-32 (2010).
65. Mendoza, V.L., Baron-Rodriguez, M.A., Blanco, C. & Vachet, R.W. Structural Insights into the Pre-Amyloid Tetramer of beta-2-Microglobulin from Covalent Labeling and Mass Spectrometry. *Biochemistry* **50**, 6711-6722 (2011).
66. Smith, D.P. et al. Deciphering drift time measurements from travelling wave ion mobility spectrometry-mass spectrometry studies. *Eur J Mass Spectrom (Chichester, Eng)* **15**, 113-30 (2009).
67. Smith, D.P., Woods, L.A., Radford, S.E. & Ashcroft, A.E. Structure and Dynamics of Oligomeric Intermediates in beta(2)-Microglobulin Self-Assembly. *Biophys J* **101**, 1238-47 (2011).
68. Domanska, K. et al. Atomic structure of a nanobody-trapped domain-swapped dimer of an amyloidogenic {beta}2-microglobulin variant. *Proc Natl Acad Sci U S A* **108**, 1314-9 (2011).
69. Ivanova, M.I., Sawaya, M.R., Gingery, M., Attinger, A. & Eisenberg, D. An amyloid-forming segment of beta2-microglobulin suggests a molecular model for the fibril. *Proc Natl Acad Sci U S A* **101**, 10584-9 (2004).
70. Liu, C., Sawaya, M.R. & Eisenberg, D. beta-microglobulin forms three-dimensional domain-swapped amyloid fibrils with disulfide linkages. *Nat Struct Mol Biol* **18**, 49-55 (2011).
71. Drueke, T.B. Beta2-microglobulin and amyloidosis. *Nephrol Dial Transplant* **15 Suppl 1**, 17-24 (2000).
72. Ricagno, S., Raimondi, S., Giorgetti, S., Bellotti, V. & Bolognesi, M. Human beta-2 microglobulin W60V mutant structure: Implications for stability and amyloid aggregation. *Biochem Biophys Res Commun* **380**, 543-7 (2009).
73. Prendergast, F.G., Meyer, M., Carlson, G.L., Iida, S. & Potter, J.D. Synthesis, spectral properties, and use of 6-acryloyl-2-dimethylaminonaphthalene (Acrylodan). A thiol-selective, polarity-sensitive fluorescent probe. *J Biol Chem* **258**, 7541-4 (1983).
74. Hutchinson, E.G. & Thornton, J.M. A revised set of potentials for beta-turn formation in proteins. *Protein Sci* **3**, 2207-16 (1994).
75. Ohhashi, Y. et al. The intrachain disulfide bond of beta(2)-microglobulin is not essential for the immunoglobulin fold at neutral pH, but is essential for amyloid fibril formation at acidic pH. *J Biochem* **131**, 45-52 (2002).

MANUSCRIPT I

A Recurrent D-strand Association Interface is Observed in β-2 microglobulin Oligomers

Matteo Colombo[1], Matteo de Rosa[1], Vittorio Bellotti[2], Stefano Ricagno[1] and Martino Bolognesi[1,3*]

[1] Dipartimento di Scienze Biomolecolari e Biotecnologie and CIMAINA, Università di Milano, Via Celoria 26, 20133 Milano, Italy.

[2] Dipartimento di Biochimica, Università di Pavia, Via Taramelli 3/b, 27100 Pavia, Italia. Laboratori di Biotecnologie IRCCS Fondazione Policlinico San Matteo, Pavia, Italy.

[3] Consiglio Nazionale delle Ricerche, Istituto di Biofisica, Via Celoria 26, 20133 Milano, Italy.

*to whom correspondence should be addressed:
Department of Biomolecular Sciences & Biotechnology
University of Milano
Via Celoria, 26
I-20133 Milano - Italy
phone: +39 02 50314893
fax: +39 02 50314895
e-mail: martino.bolognesi@unimi.it

Running title: β-2 microglobulin oligomeric interface.

Abbreviations

β2m, β-2 microglobulin; S20C, Ser20→Cys20 β2m mutant; E50C, Glu50→Cys50 β2m mutant; W60C, Trp60→Cys60 β2m mutant; DIMC20, S20C disulphide-

linked homodimer; DIMC50, E50C disulphide-linked homodimer; DIMC60, W60C disulphide-linked homodimer; ThT, Thioflavine assay; CR, Congo Red; TEM, Transmission Electron Microscopy; TFE, 2,2,2 trifluoroethanol; MHC-I, class I major histocompatibility complex; SEC, size exclusion chromatography; ESI-MS, electrospray ionization mass spectrometry; SDS, sodium dodecyl sulfate.

Keywords: β-2 microglobulin; β-2 microglobulin disulphide-linked homodimers; ***:*** β-2 microglobulin mutants; amyloidogenic oligomers; amyloid fibrils; dialysis related amyloidosis.

Subdivision: Structural Biology.

Summary.

β-2 microglobulin (β2m) is an amyloidogenic protein responsible for dialysis related amyloidosis in man. In the early stages of amyloid fibril formation, β2m associates into dimers and higher oligomers, but the structural details of such aggregates are poorly understood. To characterize the protein-protein interactions supporting formation of oligomers, three individual β2m cysteine mutants and their disulphide-linked homodimers (DIMC20, DIMC50, DIMC60) were prepared. Amyloid propensity, oligomerization state in solution and crystallogenesis were tested for each β2m homodimer: DIMC20 and DIMC50 display a mixture of tetrameric and dimeric species in solution, yield protein crystals and amyloid fibrils, while DIMC60 is dimeric in solution, does not form protein crystals nor amyloid fibrils. The X-ray structures of DIMC20 and DIMC50 show dimers of (disulphide-linked) dimers, yielding a tetrameric assembly where an association interface based on the interaction of β2m D-strands is conserved. Notably, DIMC20 and DIMC50 trigger amyloid formation in w.t. β2m in unseeded reactions. Thus, when the D-D strand interface is impaired by an intermolecular disulphide bond (as in DIMC60), formation of tetramers is hindered, the protein is not amyloidogenic and does not promote amyloid aggregation of w.t. β2m. Implications for β2m oligomerization are discussed.

INTRODUCTION

Amyloidosis is a generally pathological state in humans, characterized by the conversion of a correctly folded protein into insoluble highly organized fibrillar aggregates. It is at the roots of several protein misfolding diseases such as Alzheimer, Parkinson and Huntington diseases in man, and spongiform encephalopathy in cows [80]. β-2 microglobulin (β2m) is a 99-residue protein adopting an immunoglobulin-like fold, based on two facing β-sheets that are linked by a disulphide bond. β2m is the light chain of class I major histocompatibility complex (MHC-I) [81]. Under physiological conditions, β2m turnover takes place in the kidneys, where β2m is degraded. In case of renal failure, the degradation of β2m does not occur, and the protein accumulates in the blood increasing its concentration up to 50-fold, particularly in hemodialyzed patients [8]. When a high β2m blood level is retained over the years, the protein self-associates into amyloid fibrils [82], which accumulate in the joints, bones and tendons, where amyloid fibrils aggregation is favoured by type I collagene and glycosaminoglycans (GAGs), determining Dialysis Related Amyloidosis (DRA) [33].

β2m amyloid fibrils can be obtained *in vitro* using different approaches, such as the addition of metal cations like Cu^{2+} [9,36], or by addition of denaturing agents or organic co-solvents at neutral pH [35,37,43]. Among others, 2, 2, 2, trifluoethanol (TFE) is an organic solvent that promotes polar interactions between protein molecules favoring aggregation processes such as amyloidogenesis [37]. Notably, β2m amyloid fibrils obtained *in vitro* display polymorphic nature, often linked to the different physicochemical fibrillogenic conditions employed [83]. β2m conversion into mature amyloid fibrils requires the formation of partially folded species that aggregate into dimers, tetramers, higher order oligomers and eventually *nuclei*, which become the bases for fibril growth and elongation [1]. Interestingly, it was recently reported that the ΔN6-β2m variant can catalyze the w.t. β2m amyloid

formation [55] revealing that folded w.t. β2m can be converted into a partially-folded amyloidogenic species by bimolecular collisions with the ΔN6-β2m variant. Several recent studies focused on the early stages of amyloid fibril formation in order to characterize the structure of the protein oligomers. In particular, a β2m dimer was proposed as the first pre-amyloid aggregated species formed during fibrillogenesis [31,61,84], and its structure was investigated through X-ray crystallography, electrospray ionization mass spectrometry (ESI-MS), cryo-electron microscopy and molecular dynamics simulations [25,29,61,68,85]. The X-ray structure of the P32A β2m mutant crystallographic dimer showed a possible surface of interaction mediated by interactions of two antiparallel D-strands [25]. More recently, the hexameric structure of the non-amyloidogenic H13F β2m mutant highlighted two possible dimer interfaces, one that involves the D-strands of two adjacent H13F β2m chains, and one that is mediated by stacking of the ABED β-sheet of two β2m molecules [61]. A recent cryo-EM 3D-reconstruction of β2m amyloid fibrils grown at pH 2.5 stressed the hypothesis that the fibril unit blocks are built by globular tetramers, composed of dimers of dimers [32]. Besides, ESI-MS analysis of w.t. β2m at neutral pH under non-denaturing conditions revealed the presence of dimers, trimers and tetramers [60]. Interestingly, ESI-MS spectra of the W60G, W60V, D59P β2m mutants showed a decreased amount of oligomers, suggesting that the DE-loop (hit by the mutations) is involved in protein-protein interactions [60]. More recently, a solid-state NMR study compared samples of native and fibrillar β2m [46], suggesting that the native β2m fold is mostly included in the fibrils, in keeping with previous evidences [32,86]. Thus, β2m would not undergo major fold rearrangements upon fibril formation, the main differences between the native and fibrillar β2m being located in loop regions [46].

In the work here presented we produced three single-site β2m mutants where a Cys residue was individually engineered to replace Ser20, Glu50 and Trp60,

respectively. Covalent, disulphide-stabilized homodimers of each of the three single-site mutants were isolated, and their ability to form fibrils was investigated to assess whether the structural/topological constraints imposed by each engineered disulphide (differently located relative to β2m tertiary structure) would promote or inhibit fibrillogenesis. To shed light on the intermolecular interactions defining the assembly properties of the disulphide-linked homodimers, the X-ray structures of the E50C β2m mutant dimer (DIMC50) and of the S20C β2m mutant dimer (DIMC20) were determined. Our data may reconcile independent observations on other β2m oligomeric species, and in particular stress the role played by a specific interface for oligomer formation and amyloid aggregation. Such association interface is mediated by the interactions between the D strands of two adjacent β2m molecules and involves β2m residues previously identified as crucial for β2m amyloid aggregation.

RESULTS

Design of β2m-Cys mutants.

In order to explore the molecular mechanisms underlying formation of β2m amyloid fibrils, three β2m Cys-mutants (S20C, E50C, W60C) were produced and purified in a monomeric form. All the mutated residues are exposed to the solvent in the protein native fold [50]; the three mutation sites were chosen in order to map very different regions of β2m. In particular Ser20 is located on the AB loop, a region protruding from the core of the protein that has been shown to adopt different conformations [45,46,50]. Glu50 and Trp60 are located at the N- and C-termini of the D-strand, respectively; the D-strand is an edge strand that is involved in intermolecular interfaces in several crystal structures previously reported [25,61]. Recent reports highlight a crucial role of the neighboring DE loop (residues 57-60) in β2m fibrillogenesis [57,59,60].

Amyloid fibril formation of the monomeric species of β2m-Cys mutants.

The ability of the three β2m Cys-mutants to aggregate as amyloid fibrils at pH 7.4 in the presence of fibril seeds was assessed by ThT fluorescence, CR assay and TEM. Monomeric S20C and E50C β2m mutants display tendencies to form amyloid fibrils similar to w.t. β2m (Table I and Fig. 1B). On the other hand, W60C appears to be less prone to aggregation than w.t. β2m, in keeping with a previous report [59]. W.t. β2m and all the monomeric Cys-mutant species form amyloid fibrils with a diameter of ≈10 nm, morphologically similar as inspected by electron microscopy images (Fig 1A).

Aggregation properties of the β2m (disulphide-linked) homodimers.

Each of the three β2m Cys-mutants was used to produce the β2m disulphide-linked homodimers (DIMC20, DIMC50, DIMC60) through the procedures

described in the Material and Methods section. For the sake of clarity, in the following the terms "monomer", "dimer" and "tetramer" will always be relative to a single β2m chain, while DIMC20/50/60 will address the disulphide-linked homodimer formed by S20C/E50C/W60C mutants, respectively. Briefly, each monomeric β2m Cys-mutant was mixed with H_2O_2 in a molar ratio of 2:1 and incubated for 1h at room temperature. Each β2m mixture was then separated by size exclusion chromatography (SEC). The elution profiles of DIMC20 and DIMC50 showed varying relative abundance of dimeric and tetrameric species, while DIMC60 displayed only one peak corresponding to the dimer (Fig. 1C); the tetrameric species is particularly abundant in the DIMC20 elution profile. DIMC50 is mainly eluted as dimeric species, with minor tetramer components. The mass of the main eluted species was assigned using static light scattering confirming the dimeric/tetrameric oligomerisation state (see Table S1 in Supplementary materials).

To investigate the effects of the intermolecular disulphide bonds on β2m amyloid aggregation, fibrillogenesis tests for DIMC20, DIMC50 and DIMC60 were carried out using the same protocol used for the monomeric β2m Cys-mutants (pH 7.4, in the presence of 20% TFE and fibril seeds). DIMC20 and DIMC50 displayed a high ThT fluorescence signal after five days of incubation, higher than w.t. β2m and, moreover, displayed classical green birefringence after CR staining (see Table I, Fig. 1B and Fig. S3 in Supplementary materials). On the contrary, DIMC60 did not yield amyloid fibrils, showing a low ThT signal and a negative CR assay, even after months of incubation. In addition TEM images show the amyloid fibrils of DIMC20 and DIMC50 (Fig. 1A) while TEM images of DIMC60 samples do not reveal the presence of amyloid fibrils.

In order to assess that the intermolecular disulphide bond of each β2m mutant was indeed preserved in the aggregated materials, the amyloid fibrils of each homodimeric species were dissolved in 10% SDS and the samples examined

through SDS-PAGE. Under such conditions the amyloid fibrils of each β2m homodimeric mutant yielded a pure dimeric species, confirming the presence of the intermolecular disulphide in the β2m amyloid fibrils (see fig. S2 in Supplementary materials). Additionally, SDS-PAGE did not display any ladder pattern indicative of β2m oligomers of increasing size, contrary to what has recently been reported by Liu et al.[73], who showed oligomers of various sizes (monomer, dimer, trimer, tetramer etc.) that resulted from a domain-swapping aggregation mechanism.

Crystallization of the β2m homodimers.

All β2m homodimers were screened for crystallization using commercial kits such as HCS I & II, STURA/MACROSOL and JENA 1-4 [87-89]. DIMC20 crystals grew in Hepes 0.1 M pH 7.7, $CdSO_4$ 0.12 M, sodium acetate 2.4 M, at T=293 K, using a sitting-drop vapor diffusion setup and diffracted up to 2.45 Å resolution. DIMC50 crystals were obtained in imidazole-malate 0.2 M, pH 5.5, PEG 600 24% solution at T= 293 K using a sitting-drop vapor diffusion setup and diffracted up to 2.7 Å. In contrast, DIMC60 failed to form protein crystals under the same conditions screened for the other β2m homodimers.

X-ray crystal structure of DIMC50.

The structure of DIMC50 was refined at 2.7 Å resolution, with R-factor 23.4% and R-free 26.3% (see Table II). Each DIMC50 is formed by two chains of β2m E50C mutant linked by the expected disulphide bond between residues 50, as clearly shown by the electron density (see Fig. S1 in Supplementary materials). There are four DIMC50 moieties per asymmetric unit, assembled in two tight tetramers (Fig. 2A, showing only one tetramer). Each chain within a DIMC50 moiety displays electron density of good quality for residues 0-97, and a high degree of structural similarity (r. m. s. d of 0.46 Å over 98 Cα atoms). Moreover,

the four DIMC50 moieties and the two tetrameric assemblies show a high level of similarity, with an average r. m. s. d. of 0.78 Å over all the 196 Cα (DIMC50), and a r. m. s. d of 0.62 Å over all the 392 Cα (tetramer), respectively. The β2m chains of the DIMC50 crystal structure most closely resemble β2m in its MHC-I complex (PDB 3I6G, average over 98 Cα r. m. s. d 1.07 Å), which displays the same conformation of the AB loop (residues 13-21) and of the DE loop (residues 57-60). Moreover, in the middle of the D-strand, residue 53 hosts a β-bulge, which has been previously observed in β2m complexed in MHC-I, but not in isolated β2m (PDB 1LDS [50]). Finally, close inspection of the region around residue 50, and of the electron density in general, shows that neither the Cys mutation nor the formation of the covalent dimer modify globally or locally the β2m native fold, and no residue chemical modifications are present as a result of the H_2O_2 treatment.

The two β2m chains linked in the same DIMC50 moiety, contact each other over an area of ≈ 270 $Å^2$. Besides the S-S bond, the interface involves residues 45-52, which are located in the CD loop, and residues 67-69 that are located at the end of the E-strand. As mentioned above, two DIMC50 moieties tightly interact forming a tetramer of β2m chains. Two different non-covalent interaction surfaces in the tetramer cover 570 $Å^2$ and 150 A^2, respectively. The larger interface (hereafter called D-D strand interface) (Fig. 2B) is symmetric and involves the BC loop, the D-strand, the DE loop and the E-strand of the facing β2m chains (Table III). His31, Asp34, His51, Phe56 and Trp60 are the main residues involved in contacts at the association interface. In particular, His31 of one subunit establishes a hydrogen-bond with Asp34 of the adjacent subunit (see Fig. 2B). Moreover, Trp60 and Phe56 from one chain are located in an hydrophobic pocket built by Leu54, Leu64 and Tyr66, and are sandwiched between residues Asp34 and His51 of the adjacent subunit (Fig. 2B).

The smaller interface (hereafter called the phosphate interface) (Fig. 2C) is mediated by two β2m chains that are disposed in an anti-parallel orientation, where the main interactions are established by the A and the D strands. The interface hosts two phosphate ions located at its rims, held by the positive charges and H-bonds of Arg12 and His13 from one subunit, and by H-bonds from the backbone of Lys58 of the facing subunit, allowing stabilization of the tetramer (Fig. 2C).

X-ray crystal structure of DIMC20.

The structure of DIMC20 was refined at 2.45Å resolution with R-factor 22.6% and R-free 26.6 % (see Table II). Each DIMC20 is formed by two chains of the S20C β2m mutant linked by the expected disulphide bond (see Fig. S1 in Supplemetary materials). The asymmetric unit contains two DIMC20 moieties, yielding a tetrameric assembly of four β2m chains (Fig. 3A). Each DIMC20 displays clear electron density for the intermolecular disulphide bond, and for residues 0-99. Contrary to what has been observed in the DIMC50 structure, the two DIMC20 units building the β2m tetramer are not identical (r. m. s. d. 1.53 Å over 200 Cα pairs), and indeed display two somewhat different β2m chain conformations (r. m. s. d. 1.44 Å over 100 Cα pairs). The main difference between such two conformations is located in the D-strand: in one DIMC20 moiety each β2m chain displays the same D-strand conformation observed in β2m MHC-I (Fig. 3B, cyan), with a β-bulge at Asp53. In the other DIMC20 moiety, the D-strands (residues 51-56 in w.t. β2m) are interrupted by a less regular region between residues 52-55 (Fig. 3B, magenta). All the β2m chains in the DIMC20 crystal structure matched β2m from the MHC-I complex (PDB 3I6G, r.m.s.d. 0.9 Å and 1.6 Å over 100 Cα for each β2m chain configuration). The four β2m chains do not display any modification in the regions close to the mutation site, nor the intermolecular disulphide appears to affect the overall β2m fold. Similarly to what

reported for DIMC50, no electron density features are present that would suggest additional residue oxidations due to H_2O_2 treatment. The two β2m chains within one DIMC20 unit display a surface of interaction of ~400Å^2 that includes residues 12, 13 (A-strand), 18-22 (AB loop), 47 (CD loop), 52-54 (D-strand), 67-71 (E-strand). A residual electron density located among residues His13, Glu47, Glu69 was modeled as a Cd^{2+} ion; indeed, $CdSO_4$ was present in the crystallization buffer. Two DIMC20 moieties assemble into a tetramer, which embodies one non-covalent interface of 590 Å^2. Such interface occurs between two β2m chains that display different conformations of the D-strand, resulting in an asymmetric contact interface. However, such association interface closely resembles the D-D strand interface observed in the DIMC50 structure (hence hereafter both are referred as D-D strand interface) and it includes the BC loop, the D-strand, the DE loop and the E-strand (Table III). Notably, as observed for the DIMC50 D-D strand interface, His31, Asp34, His51, Phe56 and Trp60 are the residues providing the main association interactions. However, due to the two interface Cd^{2+} ions, the H-bond network between His31 and Asp34 is replaced by the coordination of a Cd^{2+} ion by His31 and Met0 of one subunit, and Asp34 of the neighboring subunit (Fig. 3C). The non-polar interactions observed in the D-D strand interface of the DIMC50 structure are also partly modified in the DIMC20 tetramer. Firstly, two Asp34 residues coordinate the Cd^{2+} ions; two Trp60 side chains are wedged in the same hydrophobic pocket built by Tyr66, Leu64 and Leu54, noted in DIMC50, however in the two chains the degree of insertion of residue Trp60 varies. Furthermore, in only one subunit Phe56 is stacked over Trp60 in the cavity, while in the other Phe56 is solvent exposed. Analogously, only one of the His51 side chains establishes intermolecular stacking interactions with Trp60 (as in DIMC50), while the second His51 residue is H-bonded to Lys58 of the neighboring molecule.

DIMC20 and DIMC50 promote w.t. β2m amyloid aggregation.

In order to shed light on the fibrillogenic properties of DIMC20 and DIMC50, unseeded fibrillogenesis tests were performed using solutions containing both DIMC20 (or DIMC50) and w.t. β2m, in a 1:3 ratio, respectively. As controls, unseeded reactions of w.t. β2m and of a DIMC60/w.t. β2m solution (1:3 ratio) were carried out under the same conditions. As shown in Fig. 5A, DIMC20 and DIMC50 were able to trigger amyloid formation in the absence of fibril seeds (see Table I), while the mixture of DIMC60/w.t. β2m and w.t. β2m alone solution did not aggregate into fibrils.

In order to check that the amyloid fibrils grown from the DIMC20/w.t. and DIMC50/w.t. solutions contained both the proper homodimer and w.t. β2m, the amyloid fibrils of each mixture were isolated, dissolved in 10% SDS and loaded on SDS-PAGE. In both cases, the samples were shown to contain both the disulphide-linked homodimer and w.t. (Fig. 5B). Thus, DIMC20 and DIMC50, as soluble species and, notably, in the absence of fibril seeds, proved active in promoting β2m amyloid aggregation, leading to fibrils of mixed (homodimer/w.t.) composition.

DISCUSSION

Three individual β2m cysteine mutants were designed, expressed and purified in a monomeric form. Each monomeric species was shown to aggregate into amyloid fibrils similarly to w.t. β2m, with the exception of the W60C β2m mutant that displayed lower propensity to aggregate, in agreement with previous published data [59]. We then produced disulphide-linked homodimers for each of the β2m cysteine mutants. Engineering of the intermolecular disulphide bonds was undertaken as a means to restrain intermolecular contacts in a controlled way, allowing us to explore the mechanisms of β2m association through analysis of the mutant aggregation properties, under native and amyloidogenic conditions.

The aggregation properties of the three homodimers were found to be remarkably distinct. The SEC elution profiles show that DIMC20 and DIMC50 behave as varying mixtures of dimeric and tetrameric species in solution, while DIMC60 is purely dimeric (Fig. 1C). Indeed, DIMC20 and DIMC50 crystal structures show that both homodimers assemble into tetramers in the crystals. Inspection of the crystal structures shows that despite the different locations of the intermolecular disulphide bonds in DIMC20 and DIMC50, their tetrameric species assemble through a largely conserved D-D strand interface (Figs. 2-3-4). In contrast, the formation of a disulphide bond at residue 60 would prevent tetrameric aggregation through the D-D strand interface; in agreement with such modeling considerations, DIMC60 does not assemble into higher species in solution. Related to these observations, DIMC20 and DIMC50 display similar amyloidogenic propensities, while DIMC60 amyloid formation appears totally hampered. Importantly, DIMC20 and DIMC50 soluble species trigger w.t. β2m amyloid fibril formation at neutral pH, even in the absence of fibril seeds that are normally required to promote aggregation of the w.t. protein. Conversely, DIMC60 soluble species resulted inactive in promoting w.t. β2m amyloid formation. These observations suggest that

DIMC20 and DIMC50 have an aggregation mechanism compatible with the aggregation of the w.t. protein and that the D-D strand interface shared by DIMC20 and DIMC50 can mediate the early steps of β2m amyloidogenesis. Interestingly, it has been reported that ΔN6-β2m (a naturally occurring β2m truncated version devoid of the first six residues) can catalyze w.t. β2m amyloid aggregation [55]; based on NMR evidences, it has been suggested that the dimeric interface of the ΔN6-β2m variant can be mediated by the BC loop and the DE loop [55]. In this context, the same regions are involved in the D-D strand interface here presented. Furthermore, the X-ray structure of the ΔN6-β2m variant (PDB 2X89) in its complex with a nanobody was reported as a dimer based on domain swapping [72]. The crystal asymmetric unit contains two ΔN6 β2m molecules that interact through a non-covalent interface encompassing the BC loop, the D-strand and the DE loop (see Table III). Although the non-covalent interface displayed by the two ΔN6-β2m molecules does not match the D-D strand interface here reported, it is notable that the main residues involved in the interface (His31, Asp34, Phe56 and Trp60) match those observed in the dimer here described.

The D-D strand interfaces observed in the crystal structures of DIMC20 and DIMC50 resemble closely the intermolecular association interface observed in the hexameric structure of the H13F β2m mutant (r. m. s. d. values of 3.3/2.0 Å calculated over the whole Cα backbones of the dimers built across the D-D strand interfaces of DIMC20 and DIMC50, respectively) (see Fig. 4A), which displays also a comparable contact area (DIMC20 and DIMC50 ~600 $Å^2$ *vs.* H13F mutant ~700 $Å^2$) [61]. Although some reorientation of the β2m molecules across the D-D strand interface is evident, it is striking that the main interactions at the D-D strand interfaces are closely conserved, and that the same quaternary assembly of two β2m chains is achieved. Thus, in keeping with all such observations, analysis of the data provided by our disulphide-linked dimers further suggests that the D-D strand

interface is a frequent association element for β2m molecules, compatible with maintenance of the protein native tertiary structure and with the formation of oligomers. Several previous reports have shown that the β2m amyloidogenic intermediate is native-like, and that such intermediate aggregates into early oligomeric species [25,55,68,84]. Moreover, a dimeric assembly has been repeatedly suggested as the building block for the first steps of aggregation [32,68].

Focusing on the D-D strand interface may help rationalize previous independent observations on residues His31, Asp34, His51, Phe56 and Trp60, held to be involved in β2m oligomer assembly. His31 was shown to be the primary binding site for Cu^{2+} [36], a process inducing formation of β2m amyloid fibrils *in vitro* and *in vivo* [9]. However, since the H31Y mutant is poorly amyloidogenic regardless of the presence of Cu^{2+} ions, a more general function for His31 for β2m aggregation was suggested [90]. Interestingly, the H31F mutant showed a residual affinity for Cu^{2+} indicating the involvement of His31 neighboring residues [36]; Asp34 is properly located to play such an auxiliary role in Cu^{2+} coordination and interestingly it is involved in the Cd^{2+} coordination in the DIMC20 D-D strand interface (Fig. 3). His51 is important for the stability of the D-D strand interface, being involved in stacking interactions with Phe56 (Figs. 2, 4) and in hydrogen bonding with Lys58 in the DIMC20 structure (Table III). It has been shown that the H51F, H51Y and H51A mutants display a diminished tendency to oligomerize in the presence of Cu^{2+} [91], suggesting that His51 may be involved in the formation of the early oligomers, and stressing the role played by this residue in the D-D strand interface here highlighted. Trp60 provides stacking interactions with Phe56 at the D-D strand interface and is located in the DE loop (residues 57-60), which was shown to play a prominent role in modulating amyloid aggregation propensity. Indeed, the substitution of Trp60 with Gly completely abolishes the amyloid propensity of β2m at pH 7.4 [57], while the W60V and W60C β2m mutants display decreased

amyloidogenic trends relative to w.t. β2m at pH 7.4 [59,76]. Trp60 is stabilized in the D-D strand interface by residues Leu54, Leu64 and Tyr66; accordingly, Platt *et al*. 2008 [92] showed the crucial role of the hydrophobic residues comprised in the 62-70 stretch for the nucleation phase of β2m amyloid fibrils.

For several amyloid related diseases, growing evidence indicates that protein oligomers of contained size are not only an obligate step towards the final deposition of amyloid fibrils, but may indeed represent the most cytotoxic species in the whole degenerative process [1]. The characterization of such oligomers is technically challenging, due to their transient nature and to a persistent lack of high resolution structural models. Such structural information is however crucial in order to devise any therapeutic means or intervention able to antagonize oligomerization. By designing artificial disulphide-linked β2m dimers, we forced β2m molecules to display their preferred interaction modes in a simplified molecular model amenable to characterization through high resolution structural analyses. While previous β2m oligomers reported were not amyloidogenic [25,61], DIMC20 and DIMC50 are highly amyloidogenic and, most importantly, solutions of DIMC20 and DIMC50 can trigger, in the absence of fibril seeds, w.t. β2m amyloid formation. On the other hand, the lack of fibril formation by DIMC60, where association through the D-D strand interface is hampered, points to a role played by this interface in promoting β2m aggregation. The results reported above not only highlight a conserved pattern of β2m intermolecular contacts, but are in remarkably good agreement with β2m intermolecular aggregation models earlier reported [29,84,93]. Under native or native-like conditions, β2m forms dimers that aggregate further into tetramers; β2m dimers have been suggested to be the building block of the mature fibrils [32]; moreover, the final β2m fold hosted in the mature fibrils appears to be compatible with the native structure [46]. In this context it is notable that the main residues building the D-D strand interface (His31, His51,

Phe56, Trp60, the C-terminal part of the D strand and the DE loop) have all been reported to be involved in intermolecular interactions stabilizing the mature fibrils [47,48].

MATERIALS AND METHODS

Mutagenesis, expression and purification.

β2m cysteine mutants (S20C, E50C, W60C) were produced using the QuikChangeTM site-directed mutagenesis kit supplied by Stratagene (La Jolla, CA) as previously described [57]. The following primers were used: for **S20C**, 5' CCA GCA GAG AAT GGA AAG TGT AAT TTC CTG AAT TGC TAT GTG 3'and 3' CAC ATA GCA ATT CAG GAA ATT ACA CTT TCC ATT CTC TGC TGG 5'. For **E50C**, 5' GGA GAG AGA ATT GAA AAA GTG TGC CAT TCA GAC TTG TCT TTC AGC 3' and 3' GCT GAA AGA CAA GTC TGA ATG GCA CAC TTT TTC AAT TCT CTC TCC 5'. For **W60C** 5' TTG TCT TTC AGC AAG GAC TGC TCT TTC TAT CTC TTG TAC 3' and 3' GTA CAA GAG ATA GAA AGA GCA GTC CTT GCT GAA AGA CAA 5'. The constructs were introduced in the BL21-DE3 *E. coli* strain. A methionine residue, present at the N-terminal position of all recombinant products, will be referred to as Met0. Expression and purification of monomeric w.t. and β2m Cys-mutants species were carried out as previously reported [53]. The buffers used for β2m extraction from *E.coli* cells and the buffer used for Size Exclusion Chromatography (SEC) contained 1mM β-mercaptoethanol to avoid the formation of intermolecular disulphide bridges.

Fibrillogenesis of β2m Cys-mutants.

Monomeric S20C, E50C, W60C and their isolated homodimeric species (DIMC20, DIMC50, DIMC60) were mixed with the fibrillogenesis buffer (sodium phosphate 50 mM pH 7.4, TFE 20%, NaCl 0.1M, and w.t. β2m seeds 2.5 μg/ml) at a final protein concentration of 100 μM, and incubated quiescently at 37 °C as previously reported [35].

In the unseeded reactions, DIMC20, DIMC50 and DIMC60 were individually mixed with w.t. β2m in a ratio of 1:3 in an unseeded fibrillogenesis buffer at a final concentration of 100 μM and incubated quiescently at 37 °C. An unseeded w.t. β2m mixture was used as a negative control. The amount of amyloid fibrils for each sample was quantified by Thioflavine T (ThT) [38] and Congo Red birefringence assay (CR assay) [39]. All the experiments were performed in triplicate.

Transmission Electron Microscopy (TEM).

Samples were diluted 1:20 in distilled water. 10μl were deposited on carbon-coated grids and allowed to stand for 10 minutes before water excess was dried with filter paper. Then samples were negatively stained using uranyl acetate 2% solution for 2-3 minutes. The staining solution was removed using filter paper and the samples were analysed using an EFTEM LEO 912AB TEM. The same procedure was adopted for w.t. β2m, for the monomeric β2m Cys-mutants and for their homodimeric species.

Production and purification of β2m Cys-homodimers (DIMC20, DIMC50 and DIMC60).

Monomeric β2m-Cys mutant solutions (1.67 mM) and H_2O_2 were mixed in a 2:1 molar ratio in sodium phosphate 0.25 M pH 8.0 at a final volume of 200 μl, and incubated 1h at room temperature. Each sample was loaded on a Superdex75 10/30 column and eluted with sodium phosphate 50mM, pH 8.0. The molecular mass correspondent to each peak was determined using a multi-angle light scattering device (DAWN HELEOS, Wyatt), provided with a fast photon counter (QELS) and a differential refractometer (Optilab rEX). The determination of the molecular masses was performed by ASTRA V software (Wyatt Technology) using dn/dc = 0.185 ml/g. The peaks corresponding to the tetrameric and dimeric species were

collected. β2m Cys-homodimers were desalted using Amicon centrifugal filter units (Millipore) cutoff 10 kDa, and lyophilized.

Crystallization and structure determination.

The lyophilized disulphide-linked dimer of the E50C β2m mutant (DIMC50) was dissolved in Milli-Q water at a final concentration of 9 mg/ml, and crystallized using an imidazole-malate 0.2 M, pH 5.5, PEG 600 24% solution (Stura crystal screen MD1-20, condition 2) at T=293 K, in a sitting-drop vapor diffusion setup. Crystals were flash-frozen using mother-liquor as cryoprotectant, and X-ray diffraction data were collected at the ID-14 4 beamline at 100 K, at the European Synchrotron Radiation Facility (ESRF, Grenoble). The lyophilized disulphide-linked dimer of the S20C β2m mutant (DIMC20) was dissolved in Milli-Q water at a final concentration of 6 mg/ml, and was crystallized in Hepes 0.1 M pH 7.7, $CdSO_4$ 0.12 M, sodium acetate 2.4 M, at T=293 K, using a sitting-drop vapor diffusion setup. Crystals were flash-frozen at 100 K under paraffin oil, and X-ray data collection was performed at the ID-29 beamline at 100 K at the European Synchrotron Radiation Facility (ESRF, Grenoble). DIMC20 and DIMC50 crystals diffracted up to 2.45 Å and 2.70 Å, respectively. Diffraction data were then processed with MOSFLM [94] and SCALA [95] for DIMC50, while DIMC20 diffraction data were processed using XDS [96] and SCALA [95]. Phases were obtained through molecular replacement (PHASER [97]) using the W60G β2m mutant (PDB 2Z9T) as search model for DIMC50, showing that eight chains of the E50C β2m mutant are hosted in the crystallographic asymmetric unit. Taking into account the intermolecular Cys50-Cys50' disulphide, this arrangement corresponds to four DIMC50 covalent dimers per asymmetric unit. BALBES [98] was instead used to perform the molecular replacement for DIMC20, based on the PDB coordinates of the MHC-I β2m component (PDB 2X4S) as search model. In this case, two DIMC20 covalent dimers were located in the asymmetric unit. Both crystal structures were refined using REFMAC5 [99]; translation-libration-screw motion determination (TLSMD) [100] was applied in both cases. Non Crystallographic

Symmetry (NCS) was applied to improve the electron density for both DIMC20 and DIMC50 [101]. Refinement of the metal ions was performed with autoBUSTER [102]. Model building and structure analysis were performed using COOT [103]. Data collection and refinement statistics are reported in table II.

ACCESSION NUMBERS:

Atomic coordinates and structure factors are available at the Protein Data Bank database under the accession codes 3TLR and 3TM6 for the structures of DIMC20 and DIMC50, respectively.

ACKNOWLEDGEMENTS

We thank Ms Nadia Santo (Centro Interdipartimentale di Microscopia Avanzata, University of Milano, Italy), Dr. Alberto Barbiroli (Department of AgriFood Molecular Sciences, Università degli Studi di Milano) and Dr. Mariarosa Gioria (Department of Biology; Laboratory of cellular and Molecular Biology of Reproduction; Università degli studi di Milano) for technical support. This work was supported by Fondazione Cariplo, Milano, Italy (NOBEL Project: Transcriptomics and Proteomics Approaches to Diseases of High Socio-medical Impact: a Technology Integrated Network), S.R. is recipient of a FIRB Grant “Futuro in Ricerca” from the Ministry of the University and Scientific Research of Italy (contract no. RBFR109EOS_002).

REFERENCES

1. Chiti, F. & Dobson, C.M. Protein misfolding, functional amyloid, and human disease. *Annu Rev Biochem* **75**, 333-66 (2006).
2. Radford, S.E., Gosal, W.S. & Platt, G.W. Towards an understanding of the structural molecular mechanism of beta(2)-microglobulin amyloid formation in vitro. *Biochim Biophys Acta* **1753**, 51-63 (2005).
3. Harris, H.W. & Gill, T.J., 3rd. Expression of class I transplantation antigens. *Transplantation* **42**, 109-17 (1986).
4. Berggard, I. & Bearn, A.G. Isolation and properties of a low molecular weight beta-2-globulin occurring in human biological fluids. *J Biol Chem* **243**, 4095-103 (1968).
5. Miyata, T., Jadoul, M., Kurokawa, K. & Van Ypersele de Strihou, C. Beta-2 microglobulin in renal disease. *J Am Soc Nephrol* **9**, 1723-35 (1998).
6. Bernier, G.M. & Conrad, M.E. Catabolsm of human beta-2-microglobulin by the rat kidney. *Am J Physiol* **217**, 1359-62 (1969).
7. Floege, J. & Ehlerding, G. Beta-2-microglobulin-associated amyloidosis. *Nephron* **72**, 9-26 (1996).
8. Floege, J. & Ketteler, M. beta2-microglobulin-derived amyloidosis: an update. *Kidney Int Suppl* **78**, S164-71 (2001).
9. Morgan, C.J., Gelfand, M., Atreya, C. & Miranker, A.D. Kidney dialysis-associated amyloidosis: a molecular role for copper in fiber formation. *J Mol Biol* **309**, 339-45 (2001).
10. Okon, M., Bray, P. & Vucelic, D. 1H NMR assignments and secondary structure of human beta 2-microglobulin in solution. *Biochemistry* **31**, 8906-15 (1992).
11. Bryngelson JD, W.P. Intermediates and barrier crossing in a random energy model (with applications to protein folding). *J. Phys. Chem.* **93**, 13 (1989).
12. Gruebele, M. & Wolynes, P.G. Satisfying turns in folding transitions. *Nat Struct Biol* **5**, 662-5 (1998).
13. Hartl, F.U., Bracher, A. & Hayer-Hartl, M. Molecular chaperones in protein folding and proteostasis. *Nature* **475**, 324-32 (2011).
14. Chiti, F. et al. A partially structured species of beta 2-microglobulin is significantly populated under physiological conditions and involved in fibrillogenesis. *J Biol Chem* **276**, 46714-21 (2001).
15. Chiti, F. et al. Detection of two partially structured species in the folding process of the amyloidogenic protein beta 2-microglobulin. *J Mol Biol* **307**, 379-91 (2001).
16. Kameda, A. et al. Nuclear magnetic resonance characterization of the refolding intermediate of beta2-microglobulin trapped by non-native prolyl peptide bond. *J Mol Biol* **348**, 383-97 (2005).
17. Armen, R.S. & Daggett, V. Characterization of two distinct beta2-microglobulin unfolding intermediates that may lead to amyloid fibrils of different morphology. *Biochemistry* **44**, 16098-107 (2005).

18. Brandts, J.F., Halvorson, H.R. & Brennan, M. Consideration of the Possibility that the slow step in protein denaturation reactions is due to cis-trans isomerism of proline residues. *Biochemistry* **14**, 4953-63 (1975).
19. Elove, G.A., Chaffotte, A.F., Roder, H. & Goldberg, M.E. Early steps in cytochrome c folding probed by time-resolved circular dichroism and fluorescence spectroscopy. *Biochemistry* **31**, 6876-83 (1992).
20. Kiefhaber, T. & Schmid, F.X. Kinetic coupling between protein folding and prolyl isomerization. II. Folding of ribonuclease A and ribonuclease T1. *J Mol Biol* **224**, 231-40 (1992).
21. Schmid, F.X. Prolyl isomerase: enzymatic catalysis of slow protein-folding reactions. *Annu Rev Biophys Biomol Struct* **22**, 123-42 (1993).
22. Radzicka, A., Pedersen, L. & Wolfenden, R. Influences of solvent water on protein folding: free energies of solvation of cis and trans peptides are nearly identical. *Biochemistry* **27**, 4538-41 (1988).
23. Reimer, U., el Mokdad, N., Schutkowski, M. & Fischer, G. Intramolecular assistance of cis/trans isomerization of the histidine-proline moiety. *Biochemistry* **36**, 13802-8 (1997).
24. Reimer, U. et al. Side-chain effects on peptidyl-prolyl cis/trans isomerisation. *J Mol Biol* **279**, 449-60 (1998).
25. Eakin, C.M., Berman, A.J. & Miranker, A.D. A native to amyloidogenic transition regulated by a backbone trigger. *Nat Struct Mol Biol* **13**, 202-8 (2006).
26. Jahn, T.R., Parker, M.J., Homans, S.W. & Radford, S.E. Amyloid formation under physiological conditions proceeds via a native-like folding intermediate. *Nat Struct Mol Biol* **13**, 195-201 (2006).
27. Jahn, T.R., Tennent, G.A. & Radford, S.E. A common beta-sheet architecture underlies in vitro and in vivo beta2-microglobulin amyloid fibrils. *J Biol Chem* **283**, 17279-86 (2008).
28. McParland, V.J. et al. Partially unfolded states of beta(2)-microglobulin and amyloid formation in vitro. *Biochemistry* **39**, 8735-46 (2000).
29. Smith, A.M., Jahn, T.R., Ashcroft, A.E. & Radford, S.E. Direct observation of oligomeric species formed in the early stages of amyloid fibril formation using electrospray ionisation mass spectrometry. *J Mol Biol* **364**, 9-19 (2006).
30. Caughey, B. & Lansbury, P.T. Protofibrils, pores, fibrils, and neurodegeneration: separating the responsible protein aggregates from the innocent bystanders. *Annu Rev Neurosci* **26**, 267-98 (2003).
31. Antwi, K. et al. Cu(II) organizes beta-2-microglobulin oligomers but is released upon amyloid formation. *Protein Sci* **17**, 748-59 (2008).
32. White, H.E. et al. Globular tetramers of beta(2)-microglobulin assemble into elaborate amyloid fibrils. *J Mol Biol* **389**, 48-57 (2009).
33. Relini, A. et al. Collagen plays an active role in the aggregation of beta2-microglobulin under physiopathological conditions of dialysis-related amyloidosis. *J Biol Chem* **281**, 16521-9 (2006).

34. Relini, A. et al. Heparin strongly enhances the formation of beta2-microglobulin amyloid fibrils in the presence of type I collagen. *J Biol Chem* **283**, 4912-20 (2008).
35. Yamamoto, S. et al. Glycosaminoglycans enhance the trifluoroethanol-induced extension of beta 2-microglobulin-related amyloid fibrils at a neutral pH. *J Am Soc Nephrol* **15**, 126-33 (2004).
36. Eakin, C.M., Knight, J.D., Morgan, C.J., Gelfand, M.A. & Miranker, A.D. Formation of a copper specific binding site in non-native states of beta-2-microglobulin. *Biochemistry* **41**, 10646-56 (2002).
37. Yamaguchi, K., Naiki, H. & Goto, Y. Mechanism by which the amyloid-like fibrils of a beta 2-microglobulin fragment are induced by fluorine-substituted alcohols. *J Mol Biol* **363**, 279-88 (2006).
38. LeVine, H., 3rd. Thioflavine T interaction with synthetic Alzheimer's disease beta-amyloid peptides: detection of amyloid aggregation in solution. *Protein Sci* **2**, 404-10 (1993).
39. Puchtler, H., Sweat F., Levine M. On the binding of Congo Red by amyloid. *Journal of Histochemistry and cytochemistry*, 355-364 (1962).
40. Kad, N.M. et al. Hierarchical assembly of beta2-microglobulin amyloid in vitro revealed by atomic force microscopy. *J Mol Biol* **330**, 785-97 (2003).
41. Ono, K. & Uchino, F. Formation of amyloid-like substance from beta-2-microglobulin in vitro. Role of serum amyloid P component: a preliminary study. *Nephron* **66**, 404-7 (1994).
42. Connors, L.H., Shirahama, T., Skinner, M., Fenves, A. & Cohen, A.S. In vitro formation of amyloid fibrils from intact beta 2-microglobulin. *Biochem Biophys Res Commun* **131**, 1063-8 (1985).
43. Yamamoto, S. et al. Low concentrations of sodium dodecyl sulfate induce the extension of beta 2-microglobulin-related amyloid fibrils at a neutral pH. *Biochemistry* **43**, 11075-82 (2004).
44. Sunde, M. et al. Common core structure of amyloid fibrils by synchrotron X-ray diffraction. *J Mol Biol* **273**, 729-39 (1997).
45. Hoshino, M. et al. Mapping the core of the beta(2)-microglobulin amyloid fibril by H/D exchange. *Nat Struct Biol* **9**, 332-6 (2002).
46. Barbet-Massin, E. et al. Fibrillar vs crystalline full-length beta-2-microglobulin studied by high-resolution solid-state NMR spectroscopy. *J Am Chem Soc* **132**, 5556-7 (2010).
47. Debelouchina, G.T., Platt, G.W., Bayro, M.J., Radford, S.E. & Griffin, R.G. Intermolecular Alignment in beta(2)-Microglobulin Amyloid Fibrils. *J Am Chem Soc* (2010).
48. Debelouchina, G.T., Platt, G.W., Bayro, M.J., Radford, S.E. & Griffin, R.G. Magic angle spinning NMR analysis of beta2-microglobulin amyloid fibrils in two distinct morphologies. *J Am Chem Soc* **132**, 10414-23 (2010).

49. Paulsson, K.M. et al. Distinct differences in association of MHC class I with endoplasmic reticulum proteins in wild-type, and beta 2-microglobulin- and TAP-deficient cell lines. *Int Immunol* **13**, 1063-73 (2001).
50. Trinh, C.H., Smith, D.P., Kalverda, A.P., Phillips, S.E. & Radford, S.E. Crystal structure of monomeric human beta-2-microglobulin reveals clues to its amyloidogenic properties. *Proc Natl Acad Sci U S A* **99**, 9771-6 (2002).
51. Hong, D.P., Gozu, M., Hasegawa, K., Naiki, H. & Goto, Y. Conformation of beta 2-microglobulin amyloid fibrils analyzed by reduction of the disulfide bond. *J Biol Chem* **277**, 21554-60 (2002).
52. Bellotti, V. et al. Beta2-microglobulin can be refolded into a native state from ex vivo amyloid fibrils. *Eur J Biochem* **258**, 61-7 (1998).
53. Esposito, G. et al. Removal of the N-terminal hexapeptide from human beta2-microglobulin facilitates protein aggregation and fibril formation. *Protein Sci* **9**, 831-45 (2000).
54. Myers, S.L. et al. A systematic study of the effect of physiological factors on beta2-microglobulin amyloid formation at neutral pH. *Biochemistry* **45**, 2311-21 (2006).
55. Eichner, T., Kalverda, A.P., Thompson, G.S., Homans, S.W. & Radford, S.E. Conformational conversion during amyloid formation at atomic resolution. *Mol Cell* **41**, 161-72 (2011).
56. Kihara, M. et al. Conformation of amyloid fibrils of beta2-microglobulin probed by tryptophan mutagenesis. *J Biol Chem* **281**, 31061-9 (2006).
57. Esposito, G. et al. The controlling roles of Trp60 and Trp95 in beta2-microglobulin function, folding and amyloid aggregation properties. *J Mol Biol* **378**, 885-95 (2008).
58. Batuwangala, T. et al. The crystal structure of human CD1b with a bound bacterial glycolipid. *J Immunol* **172**, 2382-8 (2004).
59. Ricagno, S. et al. DE loop mutations affect beta-2 microglobulin stability and amyloid aggregation. *Biochem Biophys Res Commun* **377**, 146-50 (2008).
60. Santambrogio, C. et al. DE-loop mutations affect beta2 microglobulin stability, oligomerization, and the low-pH unfolded form. *Protein Sci* **19**, 1386-94 (2010).
61. Calabrese, M.F., Eakin, C.M., Wang, J.M. & Miranker, A.D. A regulatable switch mediates self-association in an immunoglobulin fold. *Nat Struct Mol Biol* (2008).
62. Esposito, G. et al. Solution structure of beta(2)-microglobulin and insights into fibrillogenesis. *Biochim Biophys Acta* **1753**, 76-84 (2005).
63. Jiang, L.F., Yao, T.M., Zhu, Z.L., Wang, C. & Ji, L.N. Impacts of Cd(II) on the conformation and self-aggregation of Alzheimer's tau fragment corresponding to the third repeat of microtubule-binding domain. *Biochim Biophys Acta* **1774**, 1414-21 (2007).
64. Uversky, V.N., Li, J. & Fink, A.L. Metal-triggered structural transformations, aggregation, and fibrillation of human alpha-synuclein. A possible molecular NK

between Parkinson's disease and heavy metal exposure. *J Biol Chem* **276**, 44284-96 (2001).
65. Rana, A., Gnaneswari, D., Bansal, S. & Kundu, B. Prion metal interaction: is prion pathogenesis a cause or a consequence of metal imbalance? *Chem Biol Interact* **181**, 282-91 (2009).
66. Remko, M., Fitz, D. & Rode, B.M. Effect of metal ions (Li+, Na+, K+, Mg2+, Ca2+, Ni2+, Cu2+ and Zn2+) and water coordination on the structure and properties of L-histidine and zwitterionic L-histidine. *Amino Acids* **39**, 1309-19 (2010).
67. Mendoza, V.L. & Vachet, R.W. Probing protein structure by amino acid-specific covalent labeling and mass spectrometry. *Mass Spectrom Rev* **28**, 785-815 (2009).
68. Mendoza, V.L., Antwi, K., Baron-Rodriguez, M.A., Blanco, C. & Vachet, R.W. Structure of the preamyloid dimer of beta-2-microglobulin from covalent labeling and mass spectrometry. *Biochemistry* **49**, 1522-32 (2010).
69. Mendoza, V.L., Baron-Rodriguez, M.A., Blanco, C. & Vachet, R.W. Structural Insights into the Pre-Amyloid Tetramer of beta-2-Microglobulin from Covalent Labeling and Mass Spectrometry. *Biochemistry* **50**, 6711-6722 (2011).
70. Smith, D.P. et al. Deciphering drift time measurements from travelling wave ion mobility spectrometry-mass spectrometry studies. *Eur J Mass Spectrom (Chichester, Eng)* **15**, 113-30 (2009).
71. Smith, D.P., Woods, L.A., Radford, S.E. & Ashcroft, A.E. Structure and Dynamics of Oligomeric Intermediates in beta(2)-Microglobulin Self-Assembly. *Biophys J* **101**, 1238-47 (2011).
72. Domanska, K. et al. Atomic structure of a nanobody-trapped domain-swapped dimer of an amyloidogenic {beta}2-microglobulin variant. *Proc Natl Acad Sci U S A* **108**, 1314-9 (2011).
73. Liu, C., Sawaya, M.R. & Eisenberg, D. beta-microglobulin forms three-dimensional domain-swapped amyloid fibrils with disulfide linkages. *Nat Struct Mol Biol* **18**, 49-55 (2011).
74. Ivanova, M.I., Sawaya, M.R., Gingery, M., Attinger, A. & Eisenberg, D. An amyloid-forming segment of beta2-microglobulin suggests a molecular model for the fibril. *Proc Natl Acad Sci U S A* **101**, 10584-9 (2004).
75. Drueke, T.B. Beta2-microglobulin and amyloidosis. *Nephrol Dial Transplant* **15 Suppl 1**, 17-24 (2000).
76. Ricagno, S., Raimondi, S., Giorgetti, S., Bellotti, V. & Bolognesi, M. Human beta-2 microglobulin W60V mutant structure: Implications for stability and amyloid aggregation. *Biochem Biophys Res Commun* **380**, 543-7 (2009).
77. Prendergast, F.G., Meyer, M., Carlson, G.L., Iida, S. & Potter, J.D. Synthesis, spectral properties, and use of 6-acryloyl-2-dimethylaminonaphthalene (Acrylodan). A thiol-selective, polarity-sensitive fluorescent probe. *J Biol Chem* **258**, 7541-4 (1983).
78. Hutchinson, E.G. & Thornton, J.M. A revised set of potentials for beta-turn formation in proteins. *Protein Sci* **3**, 2207-16 (1994).

79. Ohhashi, Y. et al. The intrachain disulfide bond of beta(2)-microglobulin is not essential for the immunoglobulin fold at neutral pH, but is essential for amyloid fibril formation at acidic pH. *J Biochem* **131**, 45-52 (2002).
80. Merlini, G. & Bellotti, V. Molecular mechanisms of amyloidosis. *N Engl J Med* **349**, 583-96 (2003).
81. Porcelli, S.A. & Modlin, R.L. The CD1 system: antigen-presenting molecules for T cell recognition of lipids and glycolipids. *Annu Rev Immunol* **17**, 297-329 (1999).
82. Gejyo, F. et al. A new form of amyloid protein associated with chronic hemodialysis was identified as beta 2-microglobulin. *Biochem Biophys Res Commun* **129**, 701-6 (1985).
83. Kodali, R. & Wetzel, R. Polymorphism in the intermediates and products of amyloid assembly. *Curr Opin Struct Biol* **17**, 48-57 (2007).
84. Eakin, C.M., Attenello, F.J., Morgan, C.J. & Miranker, A.D. Oligomeric assembly of native-like precursors precedes amyloid formation by beta-2 microglobulin. *Biochemistry* **43**, 7808-15 (2004).
85. Fogolari, F. et al. Molecular dynamics simulation suggests possible interaction patterns at early steps of beta2-microglobulin aggregation. *Biophys J* **92**, 1673-81 (2007).
86. Yamaguchi, K. et al. Core and heterogeneity of beta2-microglobulin amyloid fibrils as revealed by H/D exchange. *J Mol Biol* **338**, 559-71 (2004).
87. Cudney, R., Patel, S., Weisgraber, K., Newhouse, Y. & McPherson, A. Screening and optimization strategies for macromolecular crystal growth. *Acta Crystallogr D Biol Crystallogr* **50**, 414-23 (1994).
88. Stura, E.A., Satterthwait, A.C., Calvo, J.C., Kaslow, D.C. & Wilson, I.A. Reverse screening. *Acta Crystallogr D Biol Crystallogr* **50**, 448-55 (1994).
89. Sugishima, M., Kitamori, Y., Noguchi, M., Kohchi, T. & Fukuyama, K. Crystal structure of red chlorophyll catabolite reductase: enlargement of the ferredoxin-dependent bilin reductase family. *J Mol Biol* **389**, 376-87 (2009).
90. Rosano, C. et al. beta2-microglobulin H31Y variant 3D structure highlights the protein natural propensity towards intermolecular aggregation. *J Mol Biol* **335**, 1051-64 (2004).
91. Blaho, D.V. & Miranker, A.D. Delineating the conformational elements responsible for Cu(2+)-induced oligomerization of beta-2 microglobulin. *Biochemistry* **48**, 6610-7 (2009).
92. Platt, G.W., Routledge, K.E., Homans, S.W. & Radford, S.E. Fibril growth kinetics reveal a region of beta2-microglobulin important for nucleation and elongation of aggregation. *J Mol Biol* **378**, 251-63 (2008).
93. Eichner, T. & Radford, S.E. A generic mechanism of beta2-microglobulin amyloid assembly at neutral pH involving a specific proline switch. *J Mol Biol* **386**, 1312-26 (2009).

94. Leslie, A.G.W. Recent changes to the MOSFLM package for processing film and image plate data. *Joint CCP4 + ESF-EACMB Newsletter on Protein Crystallography* (1992).
95. CCP4. The CCP4 suite: programs for protein crystallography. *Acta Crystallogr D Biol Crystallogr* **50**, 760-3 (1994).
96. Kabsch, W. Xds. *Acta Crystallogr D Biol Crystallogr* **66**, 125-32 (2010).
97. McCoy, A.J. et al. Phaser crystallographic software. *J. Appl. Cryst.* **40**, 658-74 (2007).
98. Long, F., Vagin, A.A., Young, P. & Murshudov, G.N. BALBES: a molecular-replacement pipeline. *Acta Crystallogr D Biol Crystallogr* **64**, 125-32 (2008).
99. Murshudov, G.N., Vagin, A.A. & Dodson, E.J. Refinement of macromolecular structures by the maximum-likelihood method. *Acta Crystallogr D Biol Crystallogr* **53**, 240-55 (1997).
100. Painter, J. & Merritt, E.A. Optimal description of a protein structure in terms of multiple groups undergoing TLS motion. *Acta Crystallogr D Biol Crystallogr* **62**, 439-50 (2006).
101. Kleywegt, G.J. Use of non-crystallographic symmetry in protein structure refinement. *Acta Crystallogr D Biol Crystallogr* **52**, 842-57 (1996).
102. Bricogne G, B.E., Brandl M, Flensburg C, Keller P, Paciorek P, & Roversi P, S.A., Smart O, Vonrhein C, Womack T. BUSTER
version 2.9. Cambridge, United Kingdom: Global Phasing Ltd. (2010).
103. Emsley, P. & Cowtan, K. Coot: model-building tools for molecular graphics. *Acta Crystallogr D Biol Crystallogr* **60**, 2126-32 (2004).

Table I. CR assay for each β2m mutant.

β-2m variant	CR assay scale: +++ > ++ > +
w.t.	+++
S20C	++
E50C	++
W60C	+
DIMC50	++
DIMC20	+++
DIMC60	-
DIMC20/w.t.	++
DIMC50/w.t.	++

Table II. Data collection and refinement statistics for β2m DIMC20 and DIMC50 homodimers.
Values in parenthesis are for the highest resolution shell.

Structure	DIMC20	DIMC50
Beam line	ID29 (ESRF)	ID14-3 (ESRF)
Space Group	Orthorhombic $P2_12_12_1$	Monoclinic $P2_1$
Unit Cell Constants (Å, º)	a= 29.9 b= 98.2 c=142.4	a= 90.1 b= 56.3 c=96.4 β= 115.7°
Resolution (Å)	47.4-2.45 (2.58-2.45)	20-2.7 (2.85-2.70)
R merge[a] (%)	9.0 (53.2)	11.9 (41.8)
I/σI	8.4 (2.0)	5.6 (2.4)
Completeness (%)	97.2 (98.9)	95.6 (97.4)
Redundancy	3.1 (3.2)	2.8 (2.8)
Unique Reflections	15721 (2285)	23049 (3416)
R work[b] (%)	22.6	23.4
R-free[b] (%)	26.6	26.3
Number of atoms:	3439	6729
Protein	3347	6552
Water	80	112
Heteroatoms	12	65
Ramachandran plot:		
Most favoured region	372 (94.9 %)	754 (97.8 %)
Allowed region	15 (3.8%)	17 (2.2%)
Outliers	5 (1.2 %)	0

[a] R merge = $\Sigma_{hkl} | I_{hkl} - < I_{hkl} > | / \Sigma_{hkl} | I_{hkl} |$ where I is the observed intensity and < I > is the average intensity.

[b] R work = $\Sigma_{hkl}||Fo|-|Fc||/\Sigma_{hkl}|Fo|$ for all data except 5% (DIMC20) and 10% (DIMC50) which were used for Rfree calculation.

Table III. Residues involved in the D-D strand intermolecular association interface of β2m dimeric species: DIMC20, DIMC50, H13F, ΔN6β2m.

	DIMC20	DIMC50	H13F	ΔN6-swapped dimer
N-ter	Met0 (H)	/	/	/
BC loop	His31(Cd), Asp34 (HCd) Ile35(W)	His31(H), Asp34 (HW)	His31(H), Asp34 (HW), Ile35 (H)	His31 (W), Asp34 (W)
D strand	His51(HW), Leu54(W) Phe56 (W)	His51(W) Leu54 (H), Phe56 (W)	His51 (HW), Asp53 (H), Leu54 (H), Ser55 (H), Phe56 (HW)	Leu54(W) Phe56 (W)
DE loop	Trp60 (W), Lys58 (HS)	Trp60 (W)	Trp60 (HW)	Trp60 (W)
E strand	Phe62 (W), Leu64 (W), Tyr66 (W)	Phe62 (W), Leu64 (W), Tyr66 (W)	Leu64 (W), Tyr66 (W)	/

W= van der Waals contacts, H= Hydrogen-bonding, Cd= cadmium coordination.

Figure legends:

Figure 1. Aggregation of β2m Cys-mutants. **A)** TEM images of amyloid fibrils at pH 7.4 of w.t. β2m, S20C/E50C/W60C β2m monomeric mutants (left column), and of DIMC20/DIMC50 β2m homodimers (right column). DIMC60 does not yield amyloid fibrils. Scale bars represent 200 nm. **B)** ThT fluorescence intensity values (arbitrary units) measured at pH 7.4 on fibrils of w.t. β2m, S20C/E50C/W60C β2m monomeric mutants, and of DIMC20/DIMC50 β2m homodimers. DIMC60 does not yield amyloid fibrils. **C)** Size-exclusion chromatography profiles of w.t. β2m (dash-dot line), DIMC20 (dashed line), DIMC50 (dot line), and DIMC60 (solid line); labels on each peak indicate the estimated oligomerization state (4x, tetramer *i.e.* two interacting covalent dimers; 2x, a disulphide-linked dimer; 1x, monomer).

Figure 2. Ribbons representations of the DIMC50 tetramer and its interfaces. **A)** The DIMC50 tetramer is composed of two DIMC50 moieties (cyan and gold, respectively). **B)** D-D strand interface highlighted by an orange circle. The side chains of Asp34, Trp60, Phe56, His51 are shown as stick models. Trp60 is inserted in the hydrophobic pocket built by Leu54, Leu64 and Tyr66. Asp34-His31 hydrogen bonding is shown by a dashed line. **C)** Phosphate interface highlighted by an orange circle showing the hydrogen bonding scheme of one phosphate ion (magenta) with Lys58 backbone of the gold subunit, and with Arg12 and His13 of the cyan subunit.

Figure 3. Ribbon representations of the DIMC20 tetramer and its D-D strand interface. **(A)** The tetramer is formed by two DIMC20 moieties highlighted in cyan and magenta, stabilized by cadmium ions shown as grey spheres. **B)** The D-D strand interface hosting two cadmium ions (grey spheres), and a water molecule (red). In **C)** the residues that coordinate the Cd^{2+} ions (grey) are represented as sticks. A network of hydrogen bonds linking His31and Met0 of one chain with

Asp34 of a facing subunit and one water molecule (red) surround the Cd^{2+} ion. Trp60 is inserted in the hydrophobic pocket built by Leu54, Leu64 and Tyr66, while Phe56 is partly exposed to the solvent.

Figure 4. Superposition of D-D strand interfaces. **A)** Stereo view of the β2m dimers built across the D-D strand interface as observed in the crystal structures of DIMC20 (magenta), DIMC50 (light blue), and of the hexameric H13F mutant (green). For clarity, out of the three superimposed monomeric chains used for the comparison (lower part of the figure), only the DIMC50 backbone is shown as ribbon (light blue). As a reference, three Glu16 residues are drawn as stick models. **B)** Superposition of the residues involved in the D-D strand interface represented as stick (DIMC50 light blue, DIMC20 magenta, H13F β2m green).

Figure 5. DIMC20 and DIMC50 triggers the w.t. β2m amyloid formation. **A)** Kinetics of the amyloid fibrils formation of the following unseeded reactions: w.t. β2m (■) and the mixtures of DIMC20/w.t. β2m (1:3 ratio) (▼), DIMC50/w.t. β2m (1:3 ratio) (▲), DIMC60/w.t. β2m (1:3 ratio) (●). Bars represent standard deviations. **B)** SDS-PAGE showing soluble w.t. β2m (lane 1), then solubilised samples of amyloid fibrils of the DIMC20-w.t. β2m mixture (lane 2), amyloid fibrils of the DIMC50-w.t. β2m (lane 3), amyloid fibrils of w.t. β2m (lane 4), amyloid fibrils of DIMC20 (lane 5), amyloid fibrils of DIMC50 (lane 6).

Figure 1

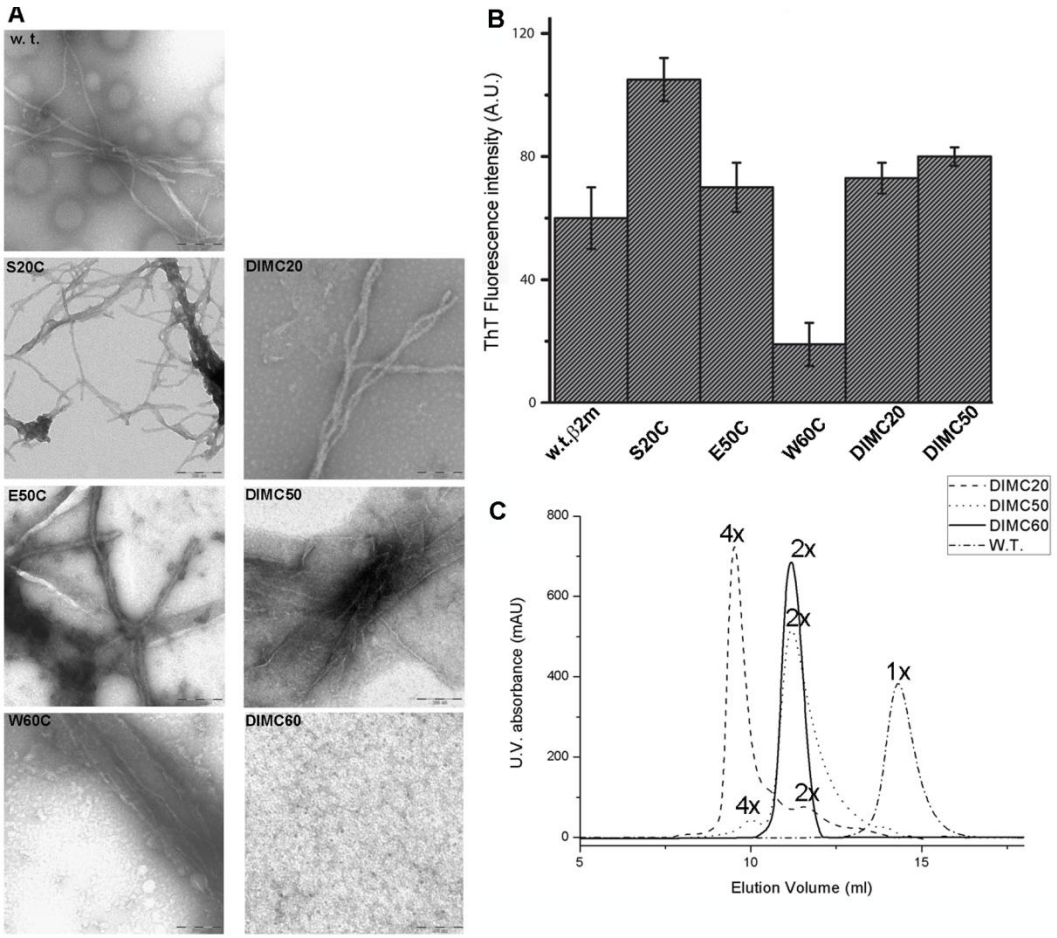
A
w. t.
S20C
DIMC20
E50C
DIMC50
W60C
DIMC60
B
ThT Fluorescence intensity (A.U.)
120
80
40
0
w.t.β2m
S20C
E50C
W60C
DIMC20
DIMC50
C
DIMC20
DIMC50
DIMC60
W.T.
U.V. absorbance (mAU)
800
600
400
200
0
4x
2x
2x
1x
4x
2x
5
10
15
Elution Volume (ml)

Figure 2

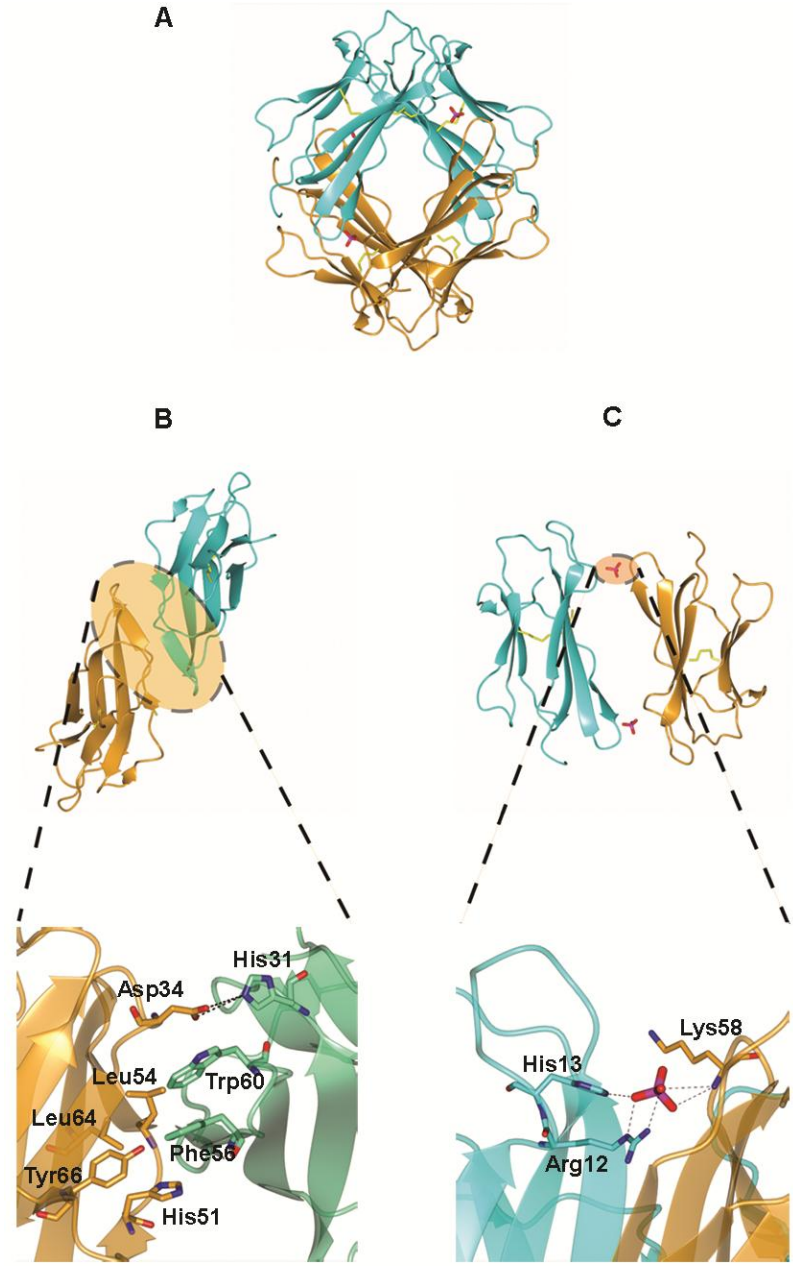
A
B
C
His31
Asp34
Leu54
Trp60
Leu64
Phe56
Tyr66
His51
Lys58
His13
Arg12

Figure 3

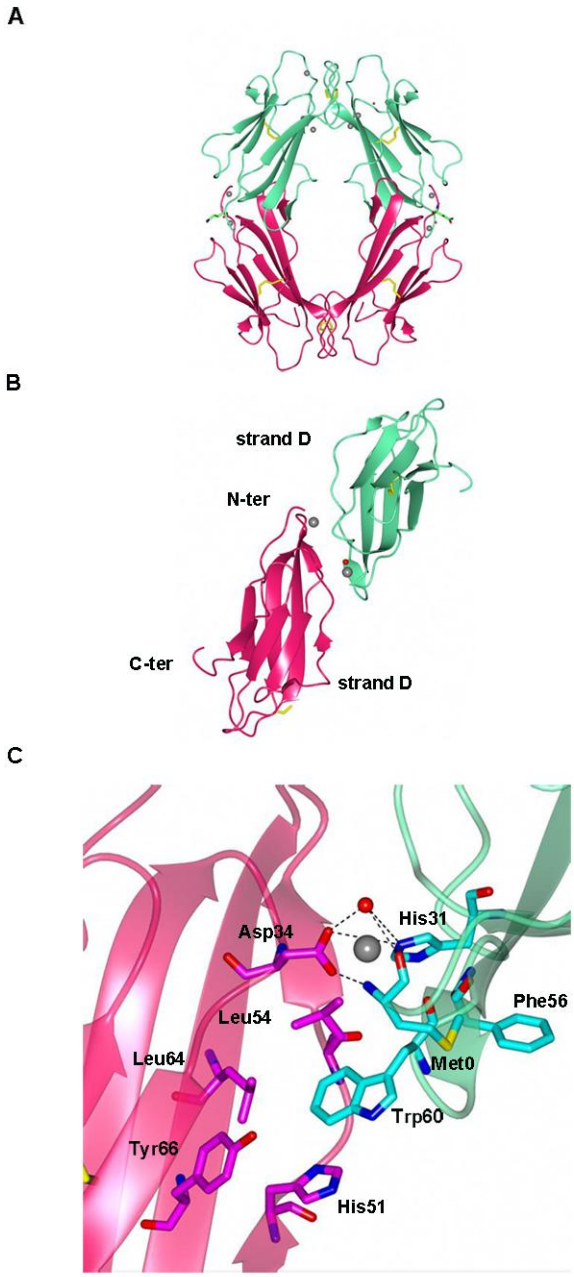
A
B
strand D
N-ter
C-ter
strand D
C
Asp34
His31
Phe56
Leu54
Leu64
Met0
Trp60
Tyr66
His51

Figure 4

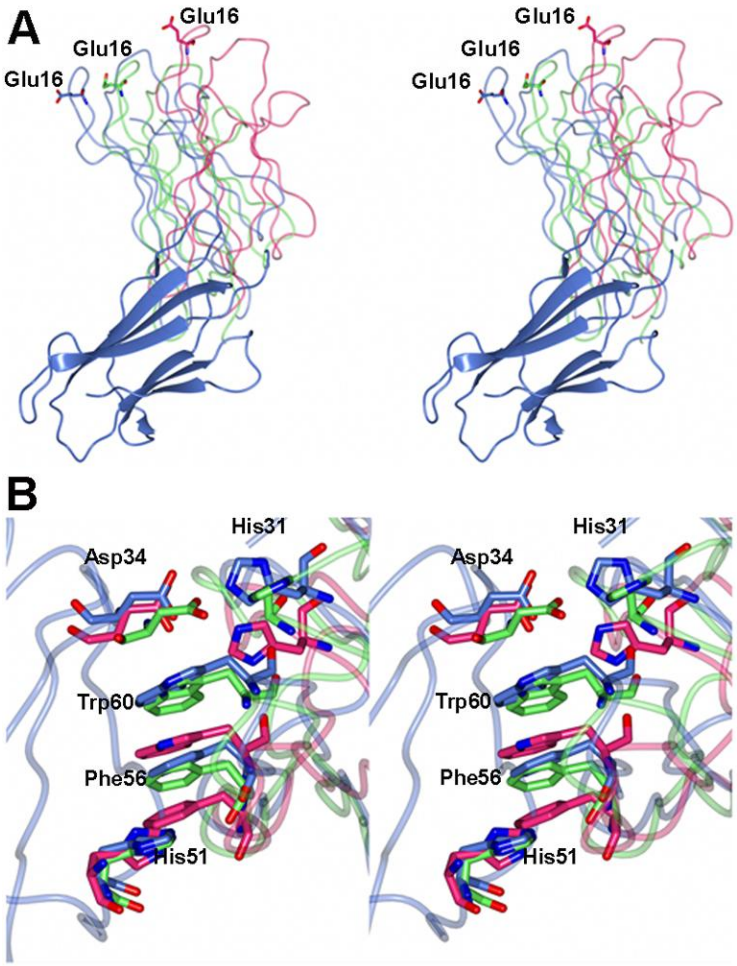
A
Glu16
Glu16
Glu16
Glu16
Glu16
Glu16
B
His31
Asp34
Trp60
Phe56
His51
His31
Asp34
Trp60
Phe56
His51

Figure 5

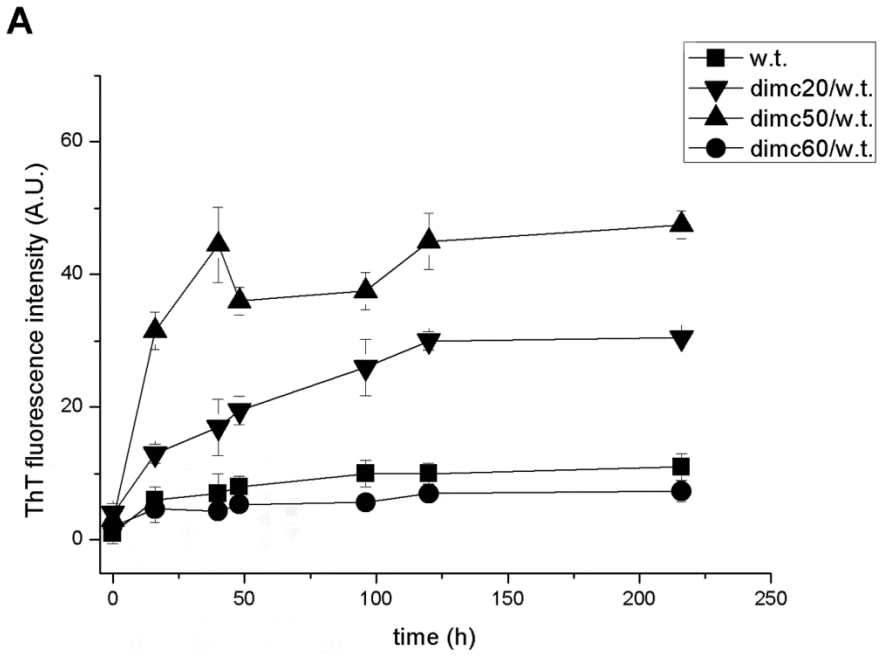
A
w.t.
dimc20/w.t.
dimc50/w.t.
dimc60/w.t.
ThT fluorescence intensity (A.U.)
time (h)
0
20
40
60
0
50
100
150
200
250

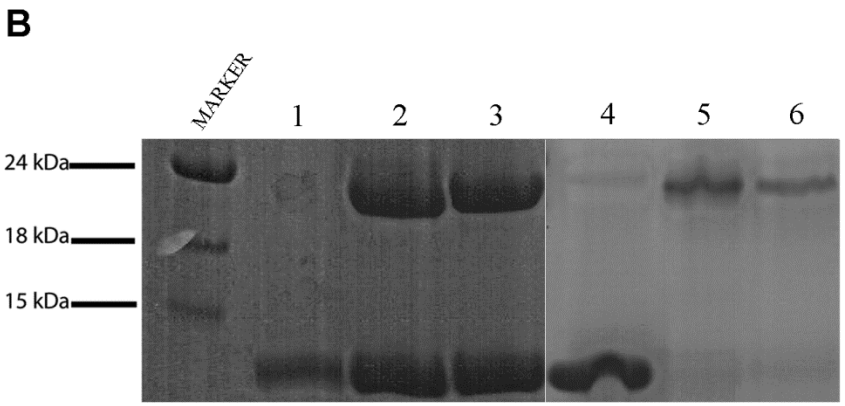
B
MARKER
1
2
3
4
5
6
24 kDa
18 kDa
15 kDa

Supplementary Material:

A Recurrent D-strand Association Interface is Observed in β-2 microglobulin Oligomers

Matteo Colombo[1], Matteo de Rosa[1], Vittorio Bellotti[2], Stefano Ricagno[1] and Martino Bolognesi[1,3*]

[1] Dipartimento di Scienze Biomolecolari e Biotecnologie and CIMAINA, Università di Milano, Via Celoria 26, 20133 Milano, Italy.

[2] Dipartimento di Biochimica, Università di Pavia, Via Taramelli 3/b, 27100 Pavia, Italia. Laboratori di Biotecnologie IRCCS Fondazione Policlinico San Matteo, Pavia, Italy.

[3] Consiglio Nazionale delle Ricerche, Istituto di Biofisica, Via Celoria 26, 20133 Milano, Italy.

Table S1. Mass values of the eluted SEC species determined by static light scattering.

Oligomeric species	DIMC20 molecular mass (Da)	DIMC50 molecular mass (Da)	DIMC60 molecular mass (Da)
2X (dimer)	/	30190±150	24290±95
4X (tetramer)	47760±140	/	/

Molecular masses corresponding to the main elution peaks reported in Fig. 1C, assigned by Static Light Scattering (SLS). The dimeric species and tetrameric species of the DIMC20 and DIMC50, respectively, although visible from the SEC elution profiles were not measured by SLS because their amount was below the level of detection. The mass of the DIMC50 was slightly overestimated likely due to a minor tetrameric component coeluted with the dimeric species. DIMC60 is purely dimeric and display a mass value correspondent to a dimeric form of β2m.

Fig. S1

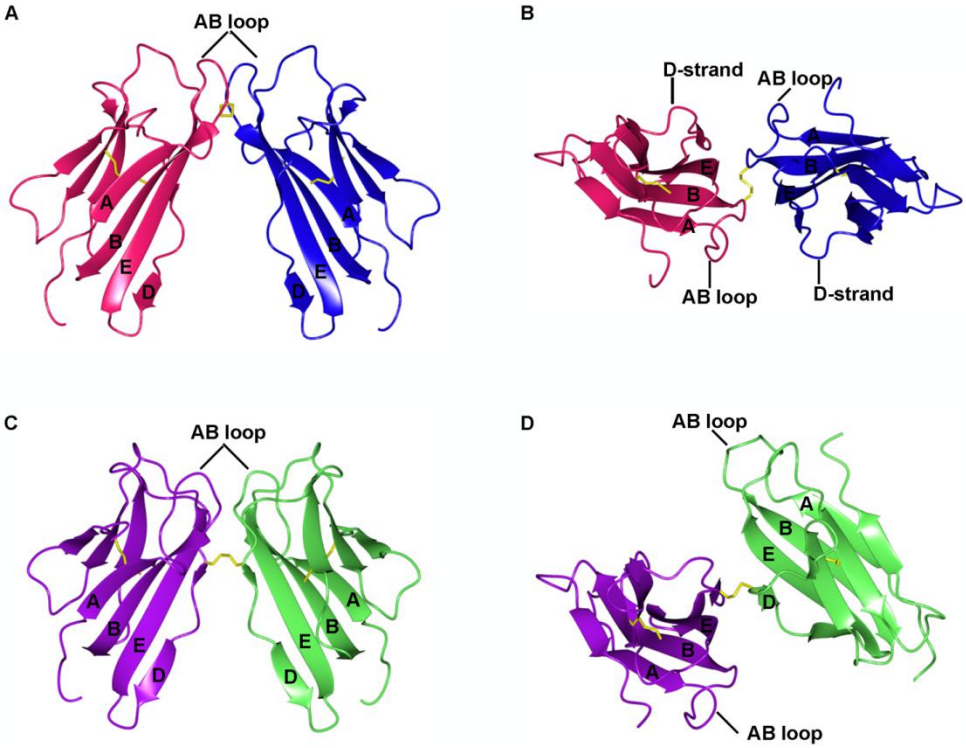

Fig. S1. Disulphide bonds are in yellow. **A)** Front-view of the disulphide-linked homodimer of the DIMC20 formed by two β2m chains (magenta and blue). **B)** Side-view (90° rotation considering the parallel axis of the intermolecular disulphide bond) of the two β2m chains forming DIMC20. **C)** Front-View of the disulphide-linked homodimer of the DIMC50 formed by two β2m chains (violet and cyan). **D)** Side-View (90° rotation considering the parallel axis of the intermolecular disulphide bond) of the two β2m chains forming DIMC50. It is notable the different position of the engineered intermolecular disulphide between DIMC20 and DIMC50.

Fig. S2

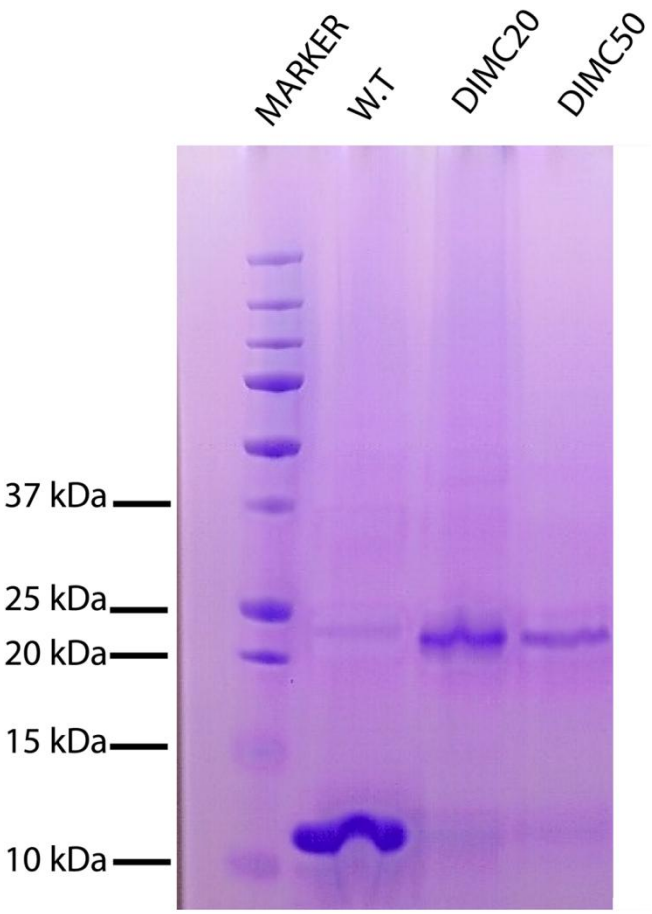

Fig. S2. SDS-PAGE of the SDS-dissolved amyloid fibrils of the w.t. β2m, DIMC20 and DIMC50 grown at pH 7.4, TFE 20% in the presence of w.t. β2m fibril seeds. Amyloid fibrils of the w.t. β2m, DIMC20 and DIMC50 were centrifugated at 10000 rpm for 10 min. The supernatant was discarded and 10% SDS was added to the amyloid fibrils. Each sample was incubated for 10 min at room temperature and loaded on a SDS-PAGE. The gel showed that the intermolecular disulphide of both DIMC20 and DIMC50 was not impaired during the amyloid fibril formation.

Fig. S3

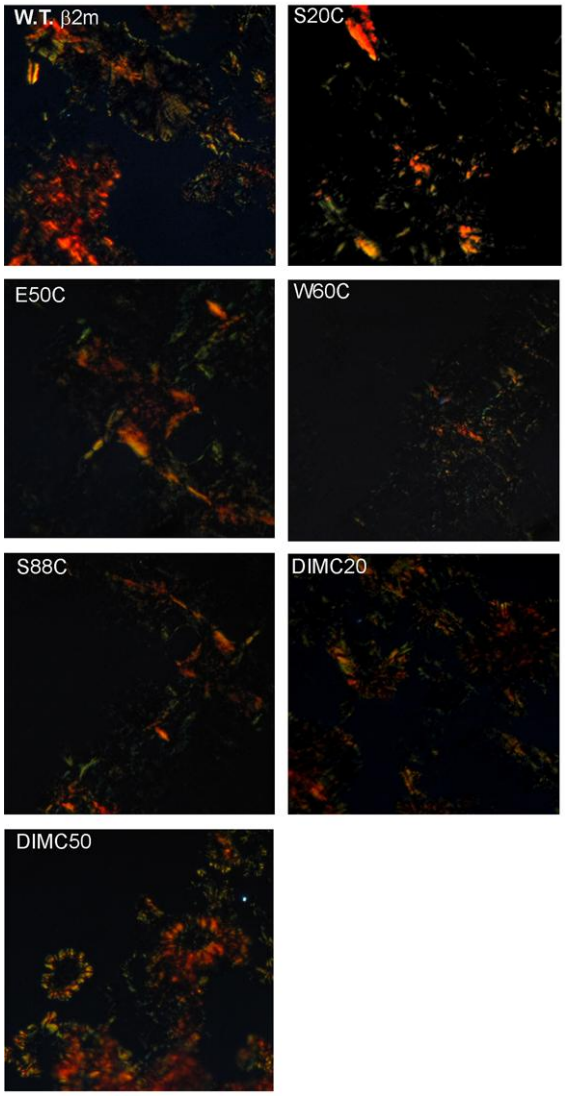

Fig. S3. Amyloid fibrils of w.t. β2m/S20C/E50C/W60C/S88C and of the DIMC20/DIMC50 display the typical amyloid green-red birefringence when stained by Congo Red.

PAPER I

J. Biochem. 2011;150(1):39–47 doi:10.1093/jb/mvr034

JB THE JOURNAL OF BIOCHEMISTRY

The effects of an ideal β-turn on β-2 microglobulin fold stability

Received January 14, 2011; accepted February 27, 2011; published online March 11, 2011

Matteo Colombo[1], Stefano Ricagno[1], Alberto Barbiroli[2], Carlo Santambrogio[3], Sofia Giorgetti[4,5], Sara Raimondi[4,5], Francesco Bonomi[2], Rita Grandori[3], Vittorio Bellotti[4,5] and Martino Bolognesi[1,*]

[1]Dipartimento di Scienze Biomolecolari e Biotecnologie, CNR-INFM and CIMAINA, Università di Milano, Via Celoria 26, 20133 Milan, Italy; [2]Dipartimento di Scienze Molecolari Agroalimentari, Sezione di Biochimica, Università di Milano, Via Celoria 2, 20133 Milan, Italy; [3]Dipartimento di Biotecnologie e Bioscienze, Università di Milano-Bicocca, Piazza della Scienza 2, 20126 Milan, Italy; [4]Dipartimento di Biochimica, Università di Pavia, Via Taramelli 3/b, 27100 Pavia, Italy; and [5]Laboratori di Biotecnologie IRCCS Fondazione Policlinico San Matteo, Pavia, Italy

*Martino Bolognesi, Department of Biomolecular Sciences & Biotechnology, University of Milano, Via Celoria, 26, I-20133 Milano, Italy. Tel: +39 02 50314893, Fax: +39 02 50314895, email: martino.bolognesi@unimi.it

Accession numbers: K58P-W60G β2m atomic coordinates and structure factors were deposited in the Protein Data Bank (code 3IB4).

Beta-2 microglobulin (β2m) is the light chain of Class I major histocompatibility complex (MHC-I) complex. β2m is an intrinsically amyloidogenic protein capable of forming amyloid fibrils *in vitro* and *in vivo*. β2m displays the typical immunoglobulin-like fold with a disulphide bridge (Cys25–Cys80) cross-linking the two β-sheets. Engineering of the loop comprised between β-strands D and E has shown that mutations in this region affect protein structure, fold stability, folding kinetics and amyloid aggregation properties. Such overall effects have been related to the DE loop backbone structure, which presents a strained conformation in the wild-type (wt) protein, and a type I β-turn in the W60G mutant. Here, we report a biophysical and structural characterization of the K58P-W60G β2m mutant, where a Pro residue has been introduced in the type I β-turn $i+1$ position. The K58P-W60G mutant shows improved chemical and temperature stability and faster folding relative to wt β2m. The crystal structure (1.25 Å resolution) shows that the Cys25–Cys80 disulphide bridge is unexpectedly severed, in agreement with electrospray ionization–mass spectrometry (ESI–MS) spectra that indicate that a fraction of the purified protein lacks the internal disulphide bond. These observations suggest a stabilizing role for Pro58, and stress a crucial role for the DE loop in determining β2m biophysical properties.

Keywords: Beta-2-microglobulin/dialysis-related amyloidosis/fold stability/crystal structure/disulphide bond.

Abbreviations: β2m, β2 microglobulin; CD, circular dichroism; C_m, melting concentration; CR, Congo Red; CSD, charge-state distribution; DTT, dithiothreitol; DTNB, 5,5′-dithiobis-(2-nitrobenzoic acid); DRA, dialysis-related amyloidosis; ESI–MS, electrospray ionization–mass spectrometry; K58P-W60G, β2 microglobulin Asp58→Pro58 and Trp60→Gly60 double mutant; MHC-I, Class I major histocompatibility complex; SDS, sodium dodecyl sulphate; T_m, melting temperature; TFE, trifluoroethanol; ThT, Thioflavin T; wt, wild-type.

Amyloidosis, the *in vivo* deposition of protein fibril material, is linked to specific protein misfolding diseases, often leading to neurodegeneration, such as Alzheimer disease in man and spongiform encephalopathy in cow (*1*). Formation of amyloid plaques arises from the aggregation of partially or totally unfolded protein molecules into elongated protein fibrils, known as amyloid fibrils, characterized by a typical cross-β structure (*2*), and by high mechanical and chemical resistance (*1*). Among recognized amyloidogenic proteins, β-2 microglobulin (β2m) has been considered and used as a model for studies on folding, aggregation and amyloid fibril formation (*3*), being directly responsible for the disease known as dialysis-related amyloidosis (DRA). β2m is the light chain of Class I major histocompatibility complex (MHC-I) and CD1 (*4*). β2m is a 99 residues protein endowed with a typical immunoglobulin fold, where two facing β-sheets, one containing strands ABDE and the other containing strands CFG, are linked by a core disulphide bond between Cys-25 (strand B) and Cys-80 (strand F). Under physiological conditions, β2m dissociated from MHC-I heavy chain is released in serum and transported to the kidneys where it is degraded. In patients with renal failure, β2m cannot be removed from blood circulation and its concentration increases up to 50-fold (*5*). When such high concentration level is retained for years, β2m aggregates into amyloid fibrils, leading to DRA (*6*). β2m fibrils can also be formed *in vitro* under chemically controlled conditions, such as acidic pH (2.5), or neutral pH in the presence of trifluoroethanol (TFE) or sodium dodecyl sulphate (SDS) (*7*).

Although a general mechanism of amyloid fibril formation has not yet been completely defined for β2m, some specific regions of the molecule have been shown to be critical for aggregation. The analysis of amyloid plaques extracted from DRA patients has shown the presence of the ΔN6 β2m variant, which is characterized by the absence of the N-terminal hexapeptide (*8*). Recently, a P5G mutant has been shown

to be prone to aggregation similarly to ΔN6 β2m (*9*). Furthermore, an important role has been assessed for the β2m Pro32 residue that shows a *cis*-peptide bond in wild-type (wt) β2m. In the P32A β2m mutant, the amide group of Ala32, has a *trans* conformation, determining a total abrogation of the lag phase observed for the formation of amyloid fibrils in the wt protein (*10*). It has also been reported that, under acidic conditions, substitution of the aromatic residues in the 62–70 sequence stretch with Ala, results in a decreased fibril elongation rate and an increased fibrillogenesis lag time (*11*), suggesting that this hydrophobic region is important for the fibril nucleation mechanism.

The aggregation properties of wt and mutant β2m have also been investigated by electrospray ionization–mass spectrometry (ESI–MS) and ion mobility. Three species of β2m have been identified (native, partially unfolded and acid unfolded), whose distribution depends on pH and mutations (*12–15*). Recently, the β2m loop between the D and E strands, which comprises residues 57–60, has been shown to be critical for β2m amyloid propensity (*16*). In particular, Trp60 is a strongly conserved residue among vertebrates due to its crucial role in the association of β2m with the heavy chain in the MHC-I complex (*16*). The substitution of the conserved residue Trp60 with Gly totally abrogates the amyloidogenic process under mild conditions, and results in an increased fold stability compared to wt β2m (*16*, *17*). The W60G mutant shows a distinct behaviour also under denaturing conditions, where it shows kinetics of disulphide reduction slower than wt β2m. The crystal structure of the W60G mutant shows that all residues of the DE loop fall in the favoured regions of the Ramachandran plot, suggesting that the mutation to Gly confers higher overall stability to β2m, thanks to its unique conformational properties that help release stereochemical strain of the DE loop (*16*). Conversely, the mutation of Asp59 to Pro leads to a more strained DE loop, resulting in diminished thermal stability and increased propensity to form amyloid fibrils compared to wt β2m (*18*). Comparative analysis of the DE loop conformations shows that wt β2m and the D59P mutant display an irregular DE loop, while the W60G, W60V and W60C mutants host a regular β-turn (*19*). All such data suggest that increased stability of the DE loop may translate into β2m variants of increased overall stability. In this respect, we notice that the W60G mutant lacks a Pro residue in position 58 to reach the most favourite residue distribution for a type I β-turn in the DE loop (*20*).

Here, we report on the double substitution of β2m residues Lys58 with Pro and Trp60 with Gly. Our aim was to produce a β2m variant endowed with the most stable type I β-turn in the DE loop, and to analyse the effects of the double mutation on β2m overall properties. To this purpose, the isolated K58P-W60G mutant has been characterized by means of fluorescence, circular dichroism (CD), crystallography and mass spectrometry analyses. Furthermore, the K58P-W60G mutant amyloidogenic propensity was assessed at low and neutral pH values. The results here reported show that regularization of the protein conformation in the DE loop leads to stabilization of the whole β2m structure.

Materials and Methods

Mutagenesis, expression and purification

Mutagenesis of Lys58 to Pro was performed using the QuickChangeTM site-directed mutagenesis kit (Stratagene, La Jolla, CA, USA) starting from the plasmid of the W60G mutant (*16*). The following primers were used: for K58P, 5′-TCA GAC TTG TCT TTC AGC CCG GAC GGG TCT TTC TAT CTC TTG-3′ and 3′-CAA GAG ATA GAA AGA CCC GTC CGG GCT GAA AGA CAA GTC TGA-5′. The construct was introduced in the BL21-DE3 *Escherichia coli* strain. A methionine residue, present at the N-terminal position of all recombinant products, will be referred to as Met0. Expression and purification of wt and β2m K58P-W60G species were carried out as previously reported (*8*).

Thermal and chemical unfolding

In all the temperature ramps here described, β2m was in 50 mM sodium phosphate pH 7.4. The protein concentration was 1.4 mg/ml (cell path 1 cm) or 0.1 mg/ml (cell path 0.1 cm) for measurements in the near- and far-UV regions, respectively. The temperature increment was set to 50°C/h (0.83°C/min). β2m temperature unfolding from 20°C to 95°C has been simultaneously followed by intrinsic Trp fluorescence and by near-UV CD signals on a Jasco J-810 spectropolarimeter, equipped with a Peltier device and fluorescence detector. Wavelength was set at 293 nm to follow simultaneously the variation of molar ellipticity and to excite tryptophan. Emitted fluorescence was detected at 350 nm. The Trp-fluorescence of β2m variants bearing or not Trp60 is comparable since, as previously shown, the Trp60 fluorescence is almost totally quenched by the solvent (*21*). Temperature unfolding of β2m secondary structure has been monitored by far-UV CD at 202 nm.

Stopped-flow refolding

Kinetics of tertiary structure refolding was monitored by Trp-fluorescence for wt β2 microglobulin (β2m) and W60G β2m using a Bio-Logic SFM-300 stopped-flow fluorimeter, with an excitation wavelength of 295 nm and monitoring the total fluorescence emission change at 320 nm. All the experiments were performed at 303 K in 10 mM sodium phosphate buffer, pH 7.4, at 0.02 mg/ml final protein concentration. The refolding experiments were performed by a 10-fold dilution of unfolded protein samples (0.2 mg/ml in 4 M GdHCl).

Kinetics of the secondary structure recovery was studied by stopped-flow CD using a BioLogic SFM-20 stopped-flow system fitted to a Jasco J-810 spectropolarimeter. The protein (20 μl of 0.2 mg/ml in 4 M GdHCl) was mixed with 480 μl of buffer (sodium phosphate 50 mM pH 7.4) in 100 ms (dead time 10.8 ms). Data traces were recorded at 233 nm through a 2-mm cell path and fitted using a first-order rate equation by means of SigmaPlot 2001 software.

Crystallization and structure determination

The K58P-W60G β2m mutant was crystallized using the hanging-drop vapour diffusion technique under the following conditions: protein solution at a concentration of 10 mg/ml, sodium acetate 0.1 M pH 5.5, ammonium acetate 0.2 M, PEG4000 22%, glycerol 20%. Crystals of the mutant protein grew in few days at 20°C.

X-ray diffraction data were collected on flash-frozen crystals using the crystallization mother-liquor as cryoprotectant, at 100 K, at the beamline ID1-4 1 (the European Synchrotron Radiation Facility, ESRF, Grenoble, France). The K58P-W60G crystals diffracted to 1.25 Å resolution. Diffraction data were processed with MOSFLM (*22*) and SCALA (*23*). Phases were obtained by molecular replacement using MOLREP (*24*) and the W60G β2m mutant atomic coordinates (PDB code 2VB5) as search model. The refinement process was performed with REFMAC5, riding hydrogen atoms and anisotropic B factors have been applied at the end of the refinement (*25*). Model building, structure analysis and Kleywegt plot were carried out using COOT (*26*) (see Table II).

ESI–MS

A hybrid quadrupole-time-of-flight instrument (QSTAR Elite, Applied Biosystems, Foster City, CA, USA) was employed for ESI–MS analysis, using a nanospray source and metal-coated borosilicate capillaries with medium-length emitter tip of 1-μm internal diameter (Proxeon, Odense, Denmark). The following instrumental settings were applied: declustering potential 80 V; ion spray voltage 1.1–1.2 kV; curtain gas 20 PSI. Samples were sprayed at room temperature. Samples were prepared as equimolar mixtures of wt β2m and K58P-W60G mutant (5 μM each) in 10 mM ammonium acetate (Sigma Aldrich, St Louis, MO, USA), adjusting the pH to 7.4 or 2.5 with ammonium hydroxide (Sigma Aldrich, St Louis, MO, USA) or formic acid (Merck KGaA, Darmstadt, Germany), respectively.

Amyloid fibril formation at pH 7.4 and 2.5

β2m (100 μM) was incubated at 37°C in 50 mM phosphate buffer,100 mM NaCl, pH 7.4, in the presence of 20% (v/v) TFE (*7*). β2m fibril seeds (20 μg/ml) were added to the samples. To form amyloid fibrils at acidic pH, β2m (100 μM) was incubated at 37°C in 50 mM Na–citrate and 100 mM NaCl, pH 2.5, in the presence of 20 μg/ml of β2m fibril seeds (*27*). Quantification of amyloid formation was performed with ThT according to Ref. (*28*). ThT (SIGMA) concentration was 10 μM in 50 mM glycine–NaOH buffer, pH 8.5. A VARIAN Cary Eclipse spectrofluorimeter was used for the measurements, with excitation at 445 nm and emission collected at 480 nm, with slits set at 5 nm and high voltage. The measurements are the average of three independent experiments.

Results

Fold stability and folding kinetics

K58P-W60G β2m mutant conformational stability, determined by guanidium-hydrochloride equilibrium unfolding, shows an increased chemical stability with respect to wt β2m (melting concentration, $C_{m\ K58P\text{-}W60G} = 2.7$ M GdHCl versus $C_{m\ wt} = 1.7$ M GdHCl), while $\Delta G°(H_2O)$ is 7.6 kcal mol^{-1} for the K58P-W60G mutant and 5.5 kcal mol^{-1} for wt β2m; β2m chemical unfolding has been followed by Trp fluorescence (Fig. 1A). Furthermore, in order to obtain an independent assessment of the K58P-W60G β2m stability, thermal unfolding was monitored by CD (near- and far UV) (Fig. 1B) and by intrinsic fluorescence. Near-UV CD and Trp-fluorescence approaches show that the K58P-W60G β2m mutant displays distinctly higher tertiary structure stability relative to wt β2m, comparable to that achieved by the W60G mutant (Table I). Interestingly, far-UV CD analysis reveals that the K58P-W60G mutant has a melting temperature, $T_m = 73.5$°C, thus a thermal stability higher than both the W60G mutant and the wt protein ($T_{mW60G} = 69.8$°C and $T_{m\ wt} = 62.4$°C) (*17*) (Table I).

Refolding kinetics were monitored by intrinsic fluorescence (Fig. 2A and B). In the K58P-W60G mutant, the rate constant of the folding fast phase shifts from 1.6 s^{-1} for wt β2m to 10 s^{-1} for the mutant. The plateau is reached after 5 s for the mutant (versus 20 min required for wt β2m). Therefore, the slow phase of folding, observed for wt β2m, is not detectable in the double mutant, similarly to what has been previously reported for the W60G mutant (*16*).

In order to compare the folding process of wt β2m and the K58P-W60G β2m mutant based on secondary structure, refolding kinetics were monitored by CD at $\lambda = 233$ nm. As shown in Fig. 2C, the profiles for the two β2m variants are indistinguishable. It is noteworthy that the slow phase, which is observed in wt β2m folding by Trp-fluorescence, is absent in both wt and mutant β2m when refolding is monitored by far-UV CD.

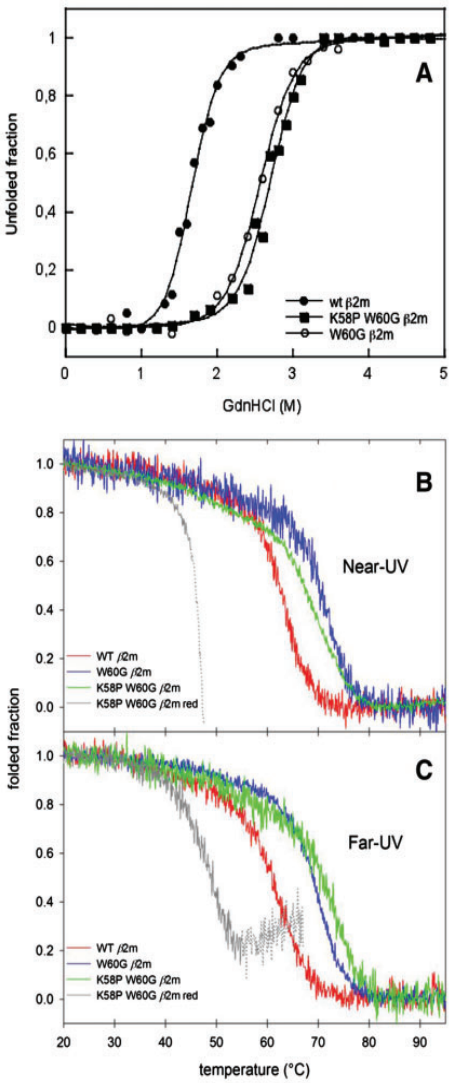

Fig. 1 Thermal and chemical fold stability of the K58P-W60G β2m mutant. (A) Unfolding titration curves as a function of denaturant (GdHCl) concentration for wt β2m, W60G and K58P-W60G mutants. The fraction of unfolded protein is reported on the *y*-axis. (B and C) Temperature dependence of circular dichroism signal, in near-UV (B) and far-UV (C) for w.t. β2m (red), K58P-W60G mutant (blue), reduced K58P-W60G (grey) and W60G mutant (green).

Crystal structure of K58P-W60G β2m mutant

The crystal structure of the K58P-W60G β2m mutant was solved and refined at 1.25 Å resolution, with R_{work} of 14.4% and R_{free} of 17.2% (Fig. 3A and Table II). All the 100 amino acids are clearly traced in the electron density, which is of excellent quality, clearly defining the mutated Pro58 and Gly60 residues. As for the other β2m mutants affecting residue 60 (*16*, *18*, *19*) in the K58P-W60G mutant the DE loop matches the

Table I. Summary of chemical and thermal unfolding results for β2m variants.

	Cm (GdHCl)	ΔG° (H_2O) kcal mol^{-1}	T_m (Near-UV) (°C)	T_m (Trp-fluorescence) (°C)	T_m (Far-UV) (°C)
wt β2m[a]	1.7 M	5.5	63.8	64.1	62.4
W60G mutant[a]	2.5 M	6.6	71.6	71.7	69.8
K58P-W60G mutant	2.7 M	7.6	69.9	73.0	73.5

[a]Melting temperatures taken from Santambrogio *et al.* (*17*).

canonical conformation of a type-I β turn. According to Hutchinson *et al.*, specific residues are preferred for each of the four positions of a type-I β turn, due to their stereochemical properties. At the β turn site *i* (corresponding to residue 57 in the K58P-W60G structure; Fig. 3B) a polar residue (typically Asp, Ser, Cys and His), which can establish a H-bond with the main chain nitrogen of the $i+2$ residue, is preferred. At site $i+1$, a Pro residue is favoured because of the restriction on the Φ angle to about $-60°$. At site $i+2$ Asp, Arg, Ser and Thr are preferred. Finally, at site $i+3$ Gly is the most favoured residue, since it helps the polypeptide chain return to an anti-parallel β-structure after completion of the turn (*20*). The K58P-W60G mutant, with its amino acid sequence 57-SPDG-60, thus displays the most favoured residues at each of the four sites. Moreover, residues Ser57 and Asp59, together with Ser61 (the first residue after the β turn), help stabilizing an overall compact structure in the 57–61 sequence stretch (Fig. 3B).

Relative to the other β2m mutants of known 3D structure, K58P-W60G shows a higher degree of alternative residue conformations. In particular, thanks the high resolution achieved, alternative conformations were observed for the aromatic residue cluster of Phe56 and Phe62. Moreover, the polypeptide backbone in the D strand was found in two similar but distinct conformations. Notably, the very high-resolution structure (1.13 Å) of wt β2m does not display any of such alternative conformations (*29*).

Unexpectedly, the disulphide bond between Cys25 and Cys80, which usually locks the two β2m β-sheets, was found severed in the crystal structure of the K58P-W60G mutant. To our knowledge, this is the first β2m structure where such a reduced disulphide bond is observed. Cys80 shows extra side chain density indicative of an oxidized species; the extra density was modelled as a sulphenic acid (i.e. –OH group bound to the thiol group; Fig. 3C). On the other side of the severed disulphide, Cys25 side chain is observed in three alternative conformations. The structures obtained from several crystals, grown from different purification batches, all show the same pattern of reduction. Given the known effects that X-rays may exert on proteins [reviewed in (*30*)], rupture of the disulphide bond can be (partly of fully) linked to the X-ray diffraction experiments run on a high-intensity synchrotron source. Nevertheless, the behaviour observed here, unprecedented for β2m, suggests that the disulphide bond in the K58P-W60G mutant is more labile to radiation damage than in wt and in the other previously described DE β2m mutants. However, radiation damage may be not the only factor, since several lines of evidence suggest that part of the protein is already reduced before crystallization (see below).

Unfolding and reduction monitored by ESI–MS

Figure 4 shows the nano-ESI–MS spectrum of an equimolar mixture of K58P-W60G mutant and wt β2m under non-denaturing conditions. The signals of the two proteins are clearly distinguishable due to their different masses. Both proteins are folded, as indicated by the narrow charge-state distribution (CSD) showing only the 8^+ and 7^+ ions. Mass deconvolution yields the values of $11{,}860 \pm 0.5$ Da for the wt protein, and $11{,}700 \pm 0.5$ Da for the mutant, in excellent agreement with the calculated mass for the proteins containing an oxidized disulphide (11,860.28 and 11,700.06 Da, respectively). By lowering the pH (Fig. 4B), the CSDs are shifted towards higher *z*-values, consistent with acid-induced protein denaturation taking place under such conditions. However, the main charge state of the wt protein is 11^+, while that of the mutant is 13^+, indicating more extensive unfolding in the latter. Interestingly, mass deconvolution performed only on the high-charge peaks of the mutant yields the mass of the disulphide-reduced protein ($11{,}702.06 \pm 0.5$ Da). These data indicate that part of the mutant protein is already in the reduced state in the absence of reducing agents. Such component is masked by the oxidized protein under mild ESI conditions, since both oxidized and reduced proteins populate the same charge states. However, it becomes detectable at low pH because protein unfolding can proceed more extensively in the reduced protein, leading to higher charge states than the unfolded protein with an intact disulphide. Thus, the highest charge state is dramatically enriched in the contribution of the reduced component and the 2-Da mass shift can be detected. No evidence of oxygen addition (i.e. formation of a sulphenic centre at Cys80) is found in the ESI–MS data, suggesting that the modification observed in the crystal structure is merely an artefact due to X-ray radiation damage.

Reduced K58P-W60G β2m mutant

Combining the information provided by crystallography and ESI–MS, we propose that in solution the K58P-W60G mutant may coexist as two species: the common disulphide-oxidized form and a reduced variant where the disulphide bond between Cys25 and Cys80 is absent. In order to verify such hypothesis, the K58P-W60G mutant protein was unfolded in 4 M GdHCl and the level of free cysteine was assessed by

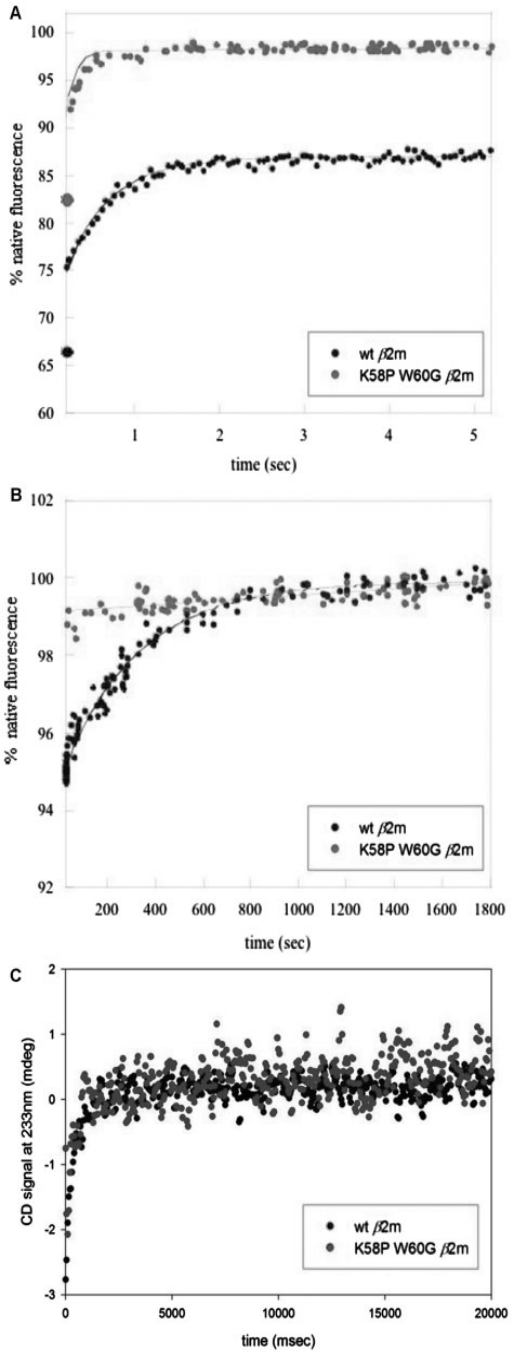

Fig. 2 Refolding kinetics of the K58P-W60G β2m mutant. (A and B) Intrinsic fluorescence curves of wt β2m (black) and of the K58P-W60G mutant (grey), monitoring the fast-phase and the slow-phase of folding. (C) CD far-UV folding curves of wt β2m (black) and of the K58P-W60G mutant (grey).

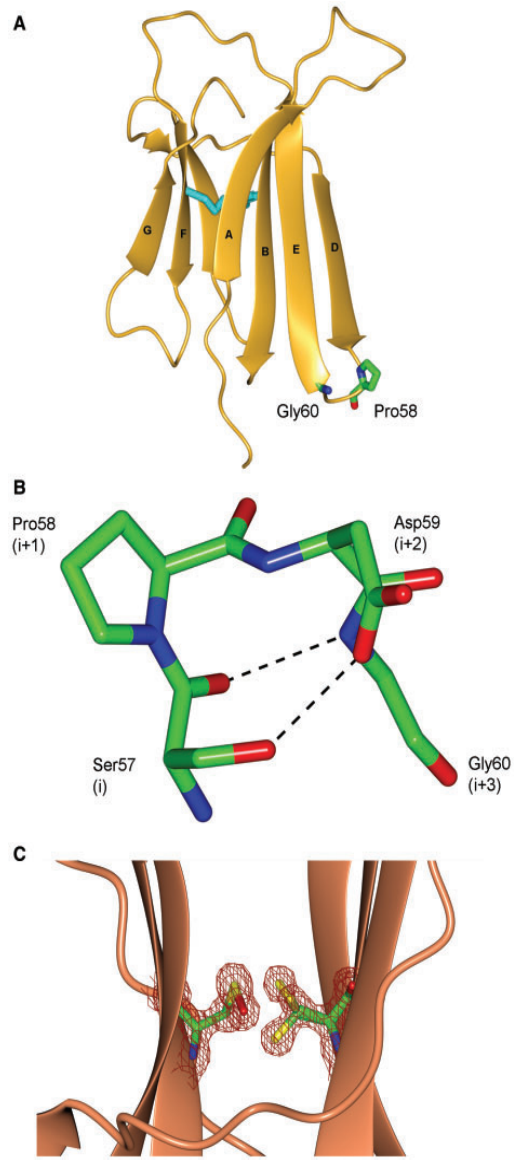

Fig. 3 Crystal structure of the K58P-W60G β2m mutant. (A) Cartoon representation of the crystal structure of the K58P-W60G mutant. Strands are labelled according to the convention for β2m. Residues Cys25, Cys80 and the mutated Pro58 and Gly60 are shown as stick models. (B) Stick model of the K58P-W60G mutant DE loop. Residues are labelled according to Hutchinson *et al.* type I β-turn definition. H-bonds are shown by dotted lines; the H-bond linking Ser57 OG (i) and the peptidic N of Asp59 ($i+2$) is weak (3.43 Å) and has not been drawn. In addition to those shown in the figure, H-bonds ($\leq$3.0 Å) stabilizing the β-turn region are observed between: the peptidic N atom of Ser57 and the carbonyl O of Ser61 ($i+4$), Ser57 OG atom and the peptidic N of Ser61, the carboxylate of Asp59 and Ser61 OG. (C) The $2F_O - F_C$ electron density map of the severed disulphide bond in K58P-W60G, contoured at 1.0 σ, highlights the triple conformation of Cys25 and the oxidized Cys80 sulphenic centre (both represented as stick models).

titration with 5,5′-dithiobis-(2-nitrobenzoic acid) (DTNB). The titration confirmed that ~30% of the cysteines are in the reduced state (data not shown), indicating that in 30% of the β2m molecules present in solution the disulphide bond is severed. Subsequently, the ability of the reduced K58P-W60G mutant to fold to a wt-native structure was assessed. The mutant protein was unfolded and completely reduced by dithiothreitol (DTT) in the presence of GdHCl, and then refolded (by removal of GdHCl) in

the presence of DTT to prevent cysteine oxidation. The reduced K58P-W60G mutant was successfully refolded according to Ohhashi *et al.* (*31*) and the thermal stability of the reduced protein was monitored by CD (Fig. 1B). These observations are in keeping with previous results on the role of the disulphide bonds in immunoglobulin fold stability (*32*). A proper unfolding Tm could not be directly measured, since the reduced K58P-W60G mutant shows a distinct propensity to precipitate before the end of the transition (also at the low concentration used in the far-UV region). However, the onset of transition occurs at least 15–20°C lower than observed for the other mutants (Fig. 1B), allowing us to hypothesize that the T_m should fall below 50–55°C.

Intriguingly, a closer analysis of the thermal unfolding of the K58P-W60G mutant monitored by Trp-fluorescence revealed that the first derivative has a first, although minor, minimum at 48°C (Supplementary Fig. S1). This may well represent unfolding of the reduced K58P-W60G fraction (~30%). On the other hand, the temperature ramps monitored by near- and far-UV CD detect only the unfolding of a major protein component (i.e. the disulphide-oxidized form), due to the lower sensibility (signal-to-noise ratio) of the CD signal compared with Trp-fluorescence.

Table II. Data collection and refinement statistics for β2m K58P-W60G.

Beam line	ESRF ID14-1
Space group	Monoclinic C2
Unit cell constants (Å, °)	$a = 76.35$, $b = 28.58$, $c = 60.73$, $\beta = 132.9°$
Resolution (Å)	19.0–1.25 (1.32–1.25)
R_{merge}[a] (%)	10.0 (69.2)
$I/\sigma I$	15.5 (3.2)
Completeness (%)	99.6 (97.2)
Redundancy	10 (8.7)
Unique reflections	26776 (3812)
Refinement	
R_{work}[b] (%)	14.4
R_{free} (%)	17.2
Number of atoms	
Protein (Avg. B-factor, A^2)	935 (10.0)
Water (Avg. B-factor, A^2)	132 (21.0)
Ramachandran plot	
Most favoured region	99 (99%)
Allowed region	1 (1%)

Values in parentheses are for the highest resolution shell.
[a] $R_{merge} = \Sigma|I - \langle I \rangle| / \Sigma|I|$ where I is the observed intensity and $\langle I \rangle$ is the average intensity.
[b] $R_{work} = \Sigma_{hkl}||F_o| - |F_c||/\Sigma_{hkl}|F_o|$ for all data except 5% which were used for R_{free} calculation.

Amyloid fibril formation

The K58P-W60G mutant propensity to form amyloid fibrils was analysed either at pH 7.4 in the presence of 20% TFE, or at pH 2.5, in both cases with small-controlled additions of wt β2m fibril seeds. Under both conditions, a wt β2m control fibrillogenesis was performed. The data at pH 7.4 show that, after 1 week of incubation at 37°C, wt β2m forms amyloid fibrils, bind thioflavin T (ThT) and is positive to Congo Red (CR) staining, while the K58P-W60G mutant does not bind ThT (Fig. 5) and displays a negative CR assay (data not shown). On the contrary, at pH 2.5, both wt β2m and the K58P-W60G mutant are prone to aggregation, as shown by ThT and CR assays, with a higher fibril yield for the K58P-W60G mutant relative to wt β2m. Such distinct behaviour is similar to what has been observed for the W60G β2m mutant (*16*).

Discussion

Recent studies have focused the attention on the crucial role(s) played by Pro residues on β2m fold and stability. The Pro5 to Gly mutation results in the accumulation of an amyloidogenic intermediate with

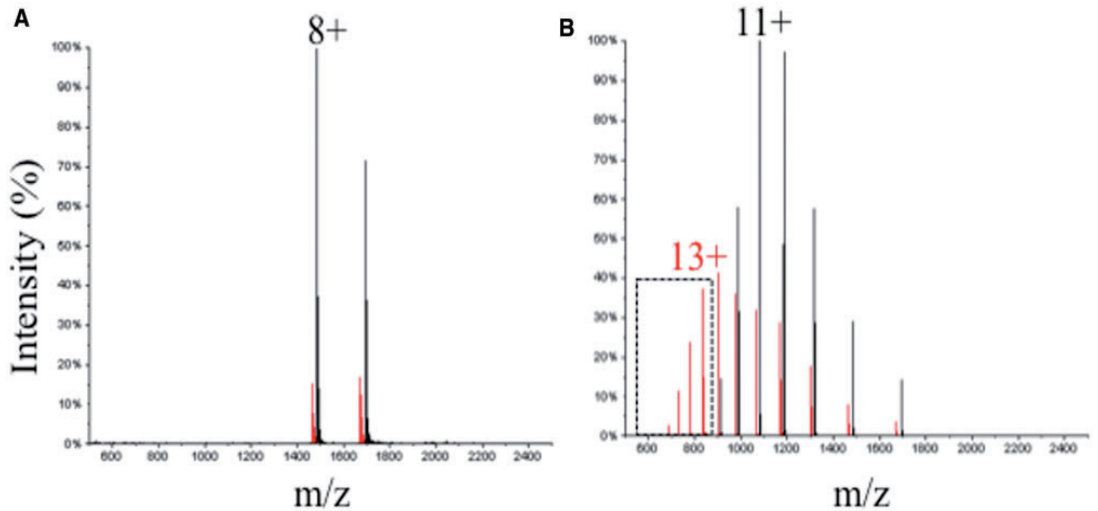

Fig. 4 Fold stability of reduced and oxidized K58P-W60G β2m mutant monitored by ESI-MS. Nano-ESI–MS spectra of an equimolar (5 μM) mixture of wt β2m (black) and K58P-W60G mutant (red) in 10 mM ammonium acetate, pH 7.4 (A) or pH 2.5 (B). The instrument interface was set at room temperature. The most intense charge state of each component is labelled by the corresponding charge state. Peaks in the dashed boxes correspond to the fully reduced mutant protein (11 702 Da).

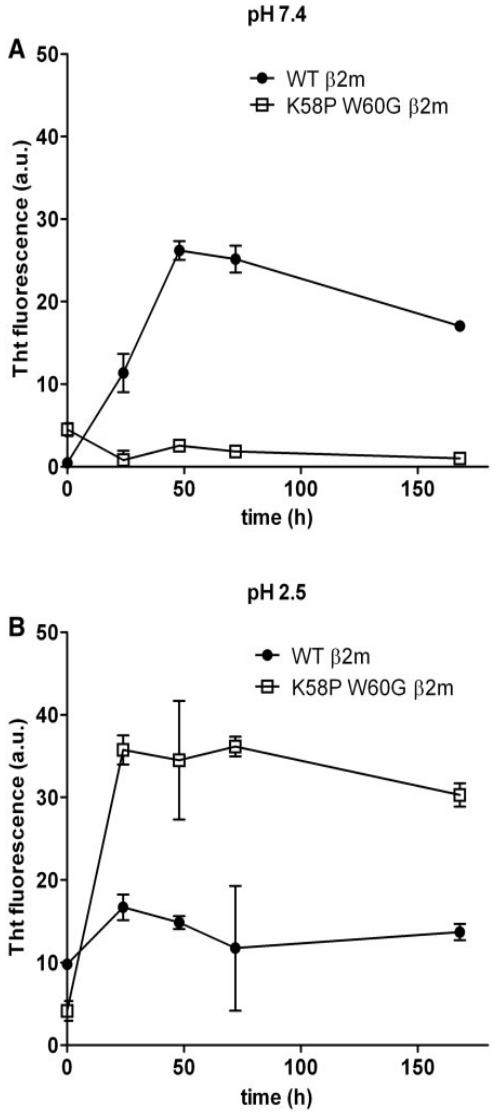

Fig. 5 Kinetics of fibril formation for wt β2m and for K58P-W60G mutant, at pH 7.4 and pH 2.5, monitored by fluorescence using ThT binding assay. Wt β2m and K58P-W60G were incubated at 37°C and diluted to 100 μM concentration in a buffer containing 50 mM Na phosphate and 100 mM NaCl, pH 7.4 in the presence of 20% TFE (v/v) and 2.5 μg/ml wt β2m fibril seeds. wt β2m and K58P-W60G were incubated at 37°C and diluted to a final 100 μM concentration in a buffer containing Na–citrate 50 and 100 mM NaCl, pH 2.5 in the presence of 2.5 μg/ml wt β2m fibril seeds.

lower structural compactness than observed for the native protein, causing a higher propensity to aggregate for the P5G mutant than for wt β2m (*9*). Mutations of Pro32 also lead to β2m variants with non-native fold and with different amyloidogenic properties compared with the wt protein (*10*, *33*, *34*). Both Pro5 and Pro32 are located in loops, where they likely help holding the entire protein in the compact native fold. On the other hand, we have recently prepared a β2m DE loop mutant introducing a Pro residue in position 59 (*18*). The presence of a proline in the DE loop does not affect the overall protein fold, however it increases the loop geometrical strain, lowering β2m fold stability and markedly enhancing its amyloidogenic propensity (*17*, *18*). These three examples show how 'native Pro' residues are carefully located in order to increase the stability of loops, and, in general, of the β-sandwich structure, while not adding strain to β2m backbone geometry.

In a recent work, the Trp60 to Gly mutation was shown to give rise to a regular β-turn conformation in the DE loop region (*16*). The work reported here introduced the Lys58 to Pro mutation (in addition to the Trp60 to Gly mutation) in order to mimic the effect of a 'native Pro' residue, e.g. to serve as a 'lock' of a loop, and to stabilize the overall protein conformation by building an ideal type-I β-turn. Complementary biophysical and structural techniques have been used to characterize the double mutant. As a first result, we confirm that the DE loop indeed adopts the ideal type I β-turn conformation (Fig. 3B), with Pro58 occupying position $i+1$ of the turn. Thermal and chemical unfolding indicates that the K58P-W60G mutant has a distinctly higher conformational stability than wt β2m (Fig. 1). Folding experiments show that the K58P-W60G mutant folds faster than the wt protein, and that the folding slow phase is absent (Fig. 2). Additionally, the double mutation leads to a variant that does not form amyloid under the standard conditions at pH 7.4 with 20% TFE.

The comparison between the K58P-W60G and the W60G mutant shows subtle yet interesting differences. The K58P-W60G mutant displays fold stability, as well as folding kinetics, comparable to the W60G mutant [this work and (*16*)], and the two protein structures are virtually identical (0.34 Å r.m.s.d. over 99 Cα pairs). The K58P-W60G and the W60G mutants display very similar propensities towards amyloid aggregation. However, an unexpected difference is that while the W60G mutant, as all other β2m variants characterized to date, shows a completely oxidized (intact) Cys25–Cys80 disulphide, the purified K58P-W60G mutant is a mixture of oxidized (~70%) and reduced (~30%) molecules, the latter lacking the stabilizing effects of the disulphide. Notably, in the K58P-W60G mutant crystal structure the disulphide bond is fully severed. Considering that no structural changes appear to affect the protein backbone of the mutant, thus its protein packing capability in the crystal lattice, likely both oxidized and reduced forms coexist in the crystals, even before exposure to X-rays. Complete rupture of the disulphide bond is an effect of radiation damage that is particularly visible in the case of the K58P-W60G mutant. Indeed ESI–MS analysis, DTNB titrations and protein unfolding monitored by Trp-fluorescence (Fig. 4 and Supplementary Fig. S1) show that a sizeable fraction of the purified protein is reduced, lacking an intact disulphide bond. Such an observation would be in keeping with a peculiar behaviour occasionally observed at the end of the mutant protein purification, whereby the purified K58P-W60G mutant formed an ensemble of SDS-resistant oligomers, which may correspond to covalent association of β2m molecules through intermolecular disulphide bonds (Supplementary Fig. S2B).

In our laboratory all β2m mutants are purified under denaturing conditions and subsequently refolded according to a standard protocol (*8*). After the refolding step, ion exchange chromatography is used to separate the protein population endowed with the correct surface charges (i.e. properly folded). It is also known that the disulphide bond is crucial for β2m to achieve a correct fold, and is formed in the fast-phase of the folding. Indeed, in our hands all the previously purified β2m variants displayed an oxidized disulphide, suggesting that the disulphide-reduced molecules either fail the refolding step or are discarded through the ion exchange chromatography step. Interestingly, while all β2m variants show some precipitate during the folding procedure (often the amount of precipitate relates to the variant stability), upon refolding of the K58P-W60G mutant almost no precipitate has been observed, suggesting that the K58P-W60G mutant may have a remarkable folding efficiency and that the disulphide-reduced form that achieves a proper fold can efficiently mimic the native oxidized variant. The disulphide-reduced K58P-W60G β2m mutant molecules are soluble and stable in solution, can crystallize, and do not display higher aggregation forms in size exclusion chromatography (data not shown). Such a novel behaviour may be related to stabilization encoded by the DE loop mutations, being specific for the K58P-W60G mutant and distinct from the W60G mutant, where disulphide-reduced properly folded molecules have not been observed.

Previously characterized β2m mutants show that modifying the DE loop backbone geometry deeply affects β2m stability and amyloid propensity (*16–19*). The evidences here reported additionally stress the structural role of the DE loop in β2m folding and stability; particularly, in the case of the K58P-W60G double mutation, the DE loop properties appear to affect not only fold stability but also the folding pathway. In apparent contrast with what has been reported for wt β2m, in the K58P-W60G mutant the disulphide bond is not as crucial for β2m folding, and the DE loop can promote folding independently of the disulphide bond redox state.

Supplementary Data

Supplementary Data are available at *JB* Online.

Acknowledgements

We are grateful to Prof. G. Merlini (IRCCS Policlinico San Matteo, Pavia, Italy) for helpful discussion and continuous support.

Funding

Fondazione Cariplo, Milano, Italy (N.O.B.E.L. Project: Transcriptomics and Proteomics Approaches to Diseases of High Sociomedical Impact: A Technology Integrated Network), from the Italian MIUR (FIRB contract RBLA03B3KC_005), from the EU grant EURAMY, by FAR (Fondo Ateneo per la Ricerca) to R.G.

Conflict of interest

None declared.

References

1. Merlini, G. and Bellotti, V. (2003) Molecular mechanisms of amyloidosis. *N. Engl. J. Med.* **349**, 583–596
2. Sunde, M., Serpell, L.C., Bartlam, M., Fraser, P.E., Pepys, M.B., and Blake, C.C. (1997) Common core structure of amyloid fibrils by synchrotron X-ray diffraction. *J. Mol. Biol.* **273**, 729–739
3. Kad, N.M., Myers, S.L., Smith, D.P., Smith, D.A., Radford, S.E., and Thomson, N.H. (2003) Hierarchical assembly of beta2-microglobulin amyloid in vitro revealed by atomic force microscopy. *J. Mol. Biol.* **330**, 785–797
4. Porcelli, S.A. and Modlin, R.L. (1999) The CD1 system: antigen-presenting molecules for T cell recognition of lipids and glycolipids. *Annu. Rev. Immunol.* **17**, 297–329
5. Floege, J. and Ketteler, M. (2001) beta2-microglobulin-derived amyloidosis: an update. *Kidney Int. Suppl.* **78**, S164–S171
6. Gejyo, F., Yamada, T., Odani, S., Nakagawa, Y., Arakawa, M., Kunitomo, T., Kataoka, H., Suzuki, M., Hirasawa, Y., Shirahama, T., Cohen, A.S., and Schimd, K. (1985) A new form of amyloid protein associated with chronic hemodialysis was identified as beta 2-microglobulin. *Biochem. Biophys. Res. Commun.* **129**, 701–706
7. Yamamoto, S., Yamaguchi, I., Hasegawa, K., Tsutsumi, S., Goto, Y., Gejyo, F., and Naiki, H. (2004) Glycosaminoglycans enhance the trifluoroethanol-induced extension of beta 2-microglobulin-related amyloid fibrils at a neutral pH. *J. Am. Soc. Nephrol.* **15**, 126–133
8. Esposito, G., Michelutti, R., Verdone, G., Viglino, P., Hernandez, H., Robinson, C.V., Amoresano, A., Dal Piaz, F., Monti, M., Pucci, P., Mangione, P., Stoppini, M., Merlini, G., Ferri, G., and Bellotti, V. (2000) Removal of the N-terminal hexapeptide from human beta2-microglobulin facilitates protein aggregation and fibril formation. *Protein Sci.* **9**, 831–845
9. Eichner, T. and Radford, S.E. (2009) A generic mechanism of beta2-microglobulin amyloid assembly at neutral pH involving a specific proline switch. *J. Mol. Biol.* **386**, 1312–1326
10. Eakin, C.M., Berman, A.J., and Miranker, A.D. (2006) A native to amyloidogenic transition regulated by a backbone trigger. *Nat. Struct. Mol. Biol.* **13**, 202–208
11. Platt, G.W., Routledge, K.E., Homans, S.W., and Radford, S.E. (2008) Fibril growth kinetics reveal a region of beta2-microglobulin important for nucleation and elongation of aggregation. *J. Mol. Biol.* **378**, 251–263
12. Borysik, A.J., Radford, S.E., and Ashcroft, A.E. (2004) Co-populated conformational ensembles of beta2-microglobulin uncovered quantitatively by electrospray ionization mass spectrometry. *J. Biol. Chem.* **279**, 27069–27077
13. Mendoza, V.L., Antwi, K., Baron-Rodriguez, M.A., Blanco, C., and Vachet, R.W. (2010) Structure of the preamyloid dimer of beta-2-microglobulin from covalent labeling and mass spectrometry. *Biochemistry* **49**, 1522–1532
14. Smith, D.P., Giles, K., Bateman, R.H., Radford, S.E., and Ashcroft, A.E. (2007) Monitoring copopulated conformational states during protein folding events using electrospray ionization-ion mobility spectrometry-mass spectrometry. *J. Am. Soc. Mass Spectrom.* **18**, 2180–2190
15. Smith, D.P., Radford, S.E., and Ashcroft, A.E. (2010) Elongated oligomers in beta2-microglobulin amyloid

assembly revealed by ion mobility spectrometry-mass spectrometry. *Proc. Natl. Acad. Sci. USA* **107**, 6794–6798
16. Esposito, G., Ricagno, S., Corazza, A., Rennella, E., Gumral, D., Mimmi, M.C., Betto, E., Pucillo, C.E., Fogolari, F., Viglino, P., Raimondi, S., Giorgetti, S., Bolognesi, B., Merlini, G., Stoppini, M., Bolognesi, M., and Bellotti, V. (2008) The controlling roles of Trp60 and Trp95 in beta2-microglobulin function, folding and amyloid aggregation properties. *J. Mol. Biol.* **378**, 885–895
17. Santambrogio, C., Ricagno, S., Colombo, M., Barbiroli, A., Bonomi, F., Bellotti, V., Bolognesi, M., and Grandori, R. (2010) DE-loop mutations affect beta2 microglobulin stability, oligomerization, and the low-pH unfolded form. *Protein Sci.* **19**, 1386–1394
18. Ricagno, S., Colombo, M., de Rosa, M., Sangiovanni, E., Giorgetti, S., Raimondi, S., Bellotti, V., and Bolognesi, M. (2008) DE loop mutations affect beta-2 microglobulin stability and amyloid aggregation. *Biochem. Biophys. Res. Commun.* **377**, 146–150
19. Ricagno, S., Raimondi, S., Giorgetti, S., Bellotti, V., and Bolognesi, M. (2009) Human beta-2 microglobulin W60V mutant structure: Implications for stability and amyloid aggregation. *Biochem. Biophys. Res. Commun.* **380**, 543–547
20. Hutchinson, E.G. and Thornton, J.M. (1994) A revised set of potentials for beta-turn formation in proteins. *Protein Sci.* **3**, 2207–2216
21. Kihara, M., Chatani, E., Iwata, K., Yamamoto, K., Matsuura, T., Nakagawa, A., Naiki, H., and Goto, Y. (2006) Conformation of amyloid fibrils of beta2-microglobulin probed by tryptophan mutagenesis. *J. Biol. Chem.* **281**, 31061–31069
22. Leslie, A.G.W. (1992) Recent changes to the MOSFLM package for processing film and image plate data. *Joint CCP4 + ESF-EACMB Newsletter on Protein Crystallography*
23. CCP4. (1994) The CCP4 suite: programs for protein crystallography. *Acta Crystallogr.* **50**, 760–763
24. Vagin, A.A. and Teplyakov, A. (1997) MOLREP: an automated program for molecular replacement. *J. Appl. Crystallogr.* **30**, 1022–1025
25. Murshudov, G.N., Vagin, A.A., and Dodson, E.J. (1997) Refinement of macromolecular structures by the maximum-likelihood method. *Acta Crystallogr.* **53**, 240–255
26. Emsley, P. and Cowtan, K. (2004) Coot: model-building tools for molecular graphics. *Acta Crystallogr.* **60**, 2126–2132
27. Naiki, H., Haschimoto, N., Suzuki, S., Rimura, H., Nakakuki, K., and Gejyo, F. (1997) Establishment of a kinetic model of dialysis-related amyloid fibril extension in vitro. *AMYLOID: Int. Exp. Clin. Invest.* **4**, 223–232
28. LeVine, H. III (1993) Thioflavine T interaction with synthetic Alzheimer's disease beta-amyloid peptides: detection of amyloid aggregation in solution. *Protein Sci.* **2**, 404–410
29. Iwata, K., Matsuura, T., Sakurai, K., Nakagawa, A., and Goto, Y. (2007) High-resolution Crystal Structure of beta2-Microglobulin Formed at pH 7.0. *J. Biochem.* **142**, 413–419
30. Garman, E.F. (2010) Radiation damage in macromolecular crystallography: what is it and why should we care? *Acta Crystallogr.* **66**, 339–351
31. Ohhashi, Y., Hagihara, Y., Kozhukh, G., Hoshino, M., Hasegawa, K., Yamaguchi, I., Naiki, H., and Goto, Y. (2002) The intrachain disulfide bond of beta(2)-microglobulin is not essential for the immunoglobulin fold at neutral pH, but is essential for amyloid fibril formation at acidic pH. *J. Biochem.* **131**, 45–52
32. Goto, Y. and Hamaguchi, K. (1979) The role of the intrachain disulfide bond in the conformation and stability of the constant fragment of the immunoglobulin light chain. *J. Biochem.* **86**, 1433–1441
33. Jahn, T.R., Parker, M.J., Homans, S.W., and Radford, S.E. (2006) Amyloid formation under physiological conditions proceeds via a native-like folding intermediate. *Nat. Struct. Mol. Biol.* **13**, 195–201
34. Sakata, M., Chatani, E., Kameda, A., Sakurai, K., Naiki, H., and Goto, Y. (2008) Kinetic coupling of folding and prolyl isomerization of beta2-microglobulin studied by mutational analysis. *J. Mol. Biol.* **382**, 1242–1255

8. ACKNOWLEDGEMENTS

Vorrei ringraziare tutti i membri del laboratorio per avermi accolto calorosamente nell'ambiente… certo con la mia simpatia era difficile aspettarsi il contrario. Grazie **Martino**, che mi hai dato la possibilità di lavorare con te imparando le basi del "mestiere" di ricercatore. Grazie **Stefano**, che mi hai seguito in questi tre anni facendomi appassionare alla cristallografia e che mi hai aiutato a scegliere la strada della ricerca anche dopo il dottorato. Grazie **Michi e Fede**, per la vostra allegria e per il ccp4 weekend 2010, davvero divertente... ma tutti ci ricordiamo la famosa domanda di **Michi**. Senza parlare del SIB o del congresso a Parma. Grazie **Marco** per avermi insegnato la cristallografia, perlomeno come punto di partenza. Grazie **Mario** per la tua disponibilità quando ho avuto dei problemi con il mio progetto. Grazie **Louise**, per la tua disciplina, fondamentale per mantenere il laboratorio in buono stato. Grazie **Patricia,** per avermi fatto parlare di nuovo francese.
Ora vorrei ringraziare chi mi è stato vicino in questi anni al di fuori del mio lavoro e mi riferisco a **Mamma e Papà,** a **Max** per i concerti, i film, il viaggio a Grenoble e perché sei mio fratello. Grazie **Boba**, per avermi sempre sostenuto, per la tua dolcezza, la tua schiettezza e la chitarra che mi hai regalato. Ora vorrei ringraziare e salutare tutti i miei amici, in particolare **Parra, Ska, il Duro, Giga, Zupo** per le belle serate e il tempo passato insieme. Vi auguro ogni bene. Ringrazio infine la **musica e Gesù Cristo**.